OUKA
The University of Osaka
Institutional Knowledge Archive

| | |
|---|---|
| Title | Novel Regulators of piRNA-Mediated Genome Defense in Drosophila |
| Author(s) | 一色, 和奏 |
| Citation | 大阪大学, 2026, 博士論文 |
| Version Type | VoR |
| URL | https://doi.org/10.18910/105608 |
| rights | |
| Note | |

*The University of Osaka Institutional Knowledge Archive : OUKA*

https://ir.library.osaka-u.ac.jp/

The University of Osaka

# Novel Regulators of piRNA-Mediated Genome Defense in *Drosophila*

**Ph.D. Thesis**

**Wakana Isshiki**

**March 2026**

**The University of Osaka**

**Graduate School of Frontier Biosciences**

# Acknowledgements

I would like to express my deepest gratitude to all those who have supported me throughout my doctoral research.

First and foremost, I am profoundly grateful to my supervisor, Professor Toshie Kai, for her invaluable guidance and unwavering support throughout my research. Her patience, encouragement, and willingness to discuss my research at any time have been instrumental in shaping both this work and my development as a scientist. I could not have asked for a better mentor. I would like to extend my sincere thanks to Associate Professor Taichiro Iki, for his insightful guidance on experimental techniques and manuscript preparation. His expertise and advice have greatly enhanced the quality of my research. I am deeply thankful to Assistant Professor Shinichi Kawaguchi for always being available to answer my questions and for providing valuable perspectives on my research. I would also like to express my gratitude to Professor Tetsuro Hirose and Professor Fumiyo Ikeda for their valuable advice, stimulating discussions, and for generously providing materials that were essential to this research. I would also like to acknowledge Dr. Hilo Yen, a research fellow in our laboratory, for his support in my research and for his dedicated efforts in maintaining our laboratory facilities.

My appreciation goes to the laboratory support staff for their assistance with laboratory maintenance and administrative matters, which allowed me to focus on my research. I am grateful to all members of the Kai laboratory for the daily discussions, helpful advice, and casual conversations that made the laboratory a stimulating and enjoyable environment.

I would like to thank the staff of the Graduate School of Frontier Biosciences for their management and maintenance of the shared research facilities. I am also grateful for the opportunity to participate in the WISE program ‘Transdisciplinary Program for Biomedical Entrepreneurship and Innovation’, which provided valuable educational experiences and support throughout my doctoral studies.

I am grateful to the Japan Society for the Promotion of Sciences (JSPS) for JSPS Research Fellowship for Young Scientists (DC1) and a Grant-in-Aid for JSPS Fellowship (23KJ1521) from April 2023 to March 2026.

Finally, I wish to express my heartfelt gratitude to my family for their constant support and understanding throughout my doctoral studies. I am also grateful to my axolotl and to my beloved dog, whose companionship sustained me through the most challenging times.

March 2026

Wakana Isshiki

# Abstract

Transposable elements (TEs) threaten genome integrity, particularly in germline cells where mutations are heritable. The PIWI-interacting RNA (piRNA) pathway defends against TE mobilization, but the complete regulatory network remains incompletely understood. This thesis characterizes two regulatory mechanisms in piRNA-directed TE silencing in *Drosophila melanogaster* germline. First, I functionally characterized Kumo, a protein containing a RING domain and five Tudor domains. I demonstrated that Kumo functions as a RING-type E3 ubiquitin ligase essential for transposon suppression. I also found out that RING domain is required for Kumo localization to nuage and its silencing activity. *In vitro* assays confirmed E3 ligase activity, and *in vivo* experiments revealed that Kumo undergoes auto-ubiquitination. This establishes ubiquitination as a critical regulatory layer in the piRNA pathway. Second, using proximity-dependent biotin labeling of PIWI proteins, I identified Set1, a histone H3K4 methyltransferase, as a proximity factor of Piwi. Set1 depletion causes dramatic derepression of telomeric transposons (*HeT-A*, *TART*, *TAHRE*) that maintain *Drosophila* telomeres. Set1 is specifically required for producing piRNAs targeting these transposons and functions through both catalytic activity-dependent and -independent mechanisms. Chromatin profiling revealed that Set1 cooperates with Piwi to maintain a unique bivalent chromatin state at subtelomeric piRNA clusters, characterized by co-occurring H3K4me2/3 and H3K9me3 marks. Collectively, this thesis demonstrates that piRNA-mediated genome defense employs multilayered regulation through cytoplasmic protein modification and chromatin control.

# Table of Contents

**Acknowledgements** ····· **II**
**Abstract** ····· **IV**
**Table of Contents** ····· **V**
**List of Figures and Tables** ····· **VIII**
**0. General Introduction** ····· **1**
0.1 *Drosophila melanogaster* ····· 1
0.1.1 *Drosophila* ovary ····· 1
0.1.2 Ovarian germline cells ····· 2
0.1.3 Ovarian somatic cells (follicle cells) ····· 3
0.2 Transposable elements ····· 4
0.2.1 Origins and classification of TEs ····· 4
0.2.2 TEs in *Drosophila* ····· 6
0.3 piRNA pathway ····· 7
0.3.1 piRNA overview ····· 7
0.3.2 precursor transcription ····· 9
0.3.3 piRNA processing in follicle cell ····· 10
0.3.3.1 Precursor processing in Yb body ····· 10
0.3.3.2 Phasing on mitochondrial outer membrane ····· 11
0.3.3.3 Nuclear translocation and transposon silencing of piRISC ····· 12
0.3.4 piRNA processing in germline cell ····· 12
**1. Functional characterization of Kumo as a RING-type E3 ubiquitin ligase essential for transposon silencing** ····· **18**
1.1 Introduction ····· 18
1.1.1 Known function of Kumo ····· 18
1.1.2 Ubiquitination ····· 19
1.1.3 Overview of this chapter ····· 21
1.2 Results ····· 22
1.2.1 Kumo possesses a conserved RING domain ····· 22
1.2.2 The intact RING domain is essential for nuage localization of Kumo ····· 26
1.2.3 The RING domain of Kumo is essential for transposon suppression ····· 27
1.2.4 Kumo possesses E3 ubiquitin ligase activity *in vitro* ····· 28
1.2.5 Kumo undergoes auto-ubiquitination *in vivo* ····· 30
1.3 Discussion ····· 32

1.3.1 Auto-ubiquitination and RING domain-dependent functions of Kumo ··· 32
1.3.2 Protein modifications and Kumo's role in the piRNA pathway ····· 34
**2. Proximity proteomics reveals Set1 as a key regulator of piRNA-directed TE silencing ····· 37**
2.1 Introduction ····· 37
2.1.1 Challenges in identifying piRNA pathway components ····· 37
2.1.2 Proximity-dependent biotin labelling as a tool for studying protein interactions ····· 37
2.1.3 Set1 and COMPASS complex: conserved regulators of transcription ····· 38
2.1.4 Diversity of piRNA cluster transcription mechanisms ····· 40
2.1.5 Overview of this chapter ····· 41
2.2 Results ····· 42
2.2.1 Labelling of PIWI proximity factors and purification from germline cells 42
2.2.2 Characterization of germline PIWI proximity proteomes ····· 46
2.2.3 Screening of PIWI proximity factors involved in piRNA production and TE silencing ····· 48
2.2.4 Set1 and Hrb27C control distinct TE families in germline cells ····· 51
2.2.5 Set1 localizes to germline nuclei and physically interacts with Piwi ····· 54
2.2.6 Catalytic activity-dependent and -independent functions of Set1 repress TEs ····· 56
2.2.7 Set1 is crucial in producing piRNAs targeting *HTT* families ····· 57
2.2.8 Set1 maintains chromatin status at subtelomeric piRNA cluster loci ····· 60
2.3 Discussion ····· 63
2.3.1 Hrb27C emerged as a functionally relevant partner of Aub ····· 63
2.3.2 Set1 is crucial for piRNA-directed silencing of telomeric TEs ····· 63
2.3.3 Developmental timing of Set1 function and the specification of subtelomeric piRNA clusters ····· 65
2.3.4 Catalytic activity-dependent and -independent functions of Set1 in TE silencing ····· 67
2.3.5 Conclusions and future perspectives ····· 68
**3. Materials and Methods ····· 70**
3.1 Fly husbandry ····· 70
3.2 Generation of plasmids and fly stocks ····· 72
3.3 Structure prediction using AlphaFold ····· 74
3.4 Sequence alignment ····· 75
3.5 Immunostaining and image acquisition ····· 75

3.6 *In vitro* ubiquitination assay ····· 76
3.7 Co-Immunoprecipitation ····· 77
3.8 Western blotting and biotinylated protein detection ····· 78
3.9 TurboID proximity labeling and streptavidin pulldown ····· 79
3.10 Mass spectrometry and proteomics analysis ····· 80
3.11 Reverse transcription and qPCR analysis ····· 80
3.12 Transcriptome analysis ····· 81
3.13 Crosslink Co-Immunoprecipitation ····· 82
3.14 Small RNA deep sequencing and analysis ····· 82
3.15 CUT&Tag ····· 84
**4. References ····· 86**
**5. Publication and Contributions ····· 104**

# List of Figures and Tables

**Chapter 0: General Introduction**
**Figure 0.1** Structure of *Drosophila* ovary 1
**Figure 0.2** Classification of transposable elements and overview of piRNA pathway 5
**Figure 0.3** *HTT* transposons and telomere maintenance in *Drosophila* 6
**Figure 0.4** piRNA pathways in follicle cells and nurse cells 10
**Table 0.1** piRNA pathway components in *Drosophila* ovary 15

**Chapter 1: Functional characterization of Kumo**
**Figure 1.1** Domain structure and structural prediction of Kumo 22
**Figure 1.2** Sequence alignment of N-ter region of Kumo across species 24
**Figure 1.3** Sequence alignment of N-ter region of Kumo in *Drosophila* species 25
**Figure 1.4** RING domain mutant Kumo dispersed in cytoplasm 27
**Figure 1.5** *HeT-A* transposon repression was not recovered in Kumo$^{C5}$ rescue ovary 28
**Figure 1.6** *In vitro ubiquitination assay reveals ubiquitination activity of Kumo* 29
**Figure 1.7** Localization of TUBE-fusion Kumo proteins 30
**Figure 1.8** Detection of Kumo auto-ubiquitination by Western blot 31

**Chapter 2: Proximity proteomics and Set1 characterization**
**Figure 2.1** Optimization of germline PIWI proximity labelling and purification 43
**Figure 2.2** PIWI proximity biotin labelling in germline stem cell-like cells (GSCLCs) 45
**Figure 2.3** Proximity proteome of PIWI proteins in germline cells 46
**Table 2.1** Known piRNA pathway components identified in PIWI proximity proteomes 47
**Figure 2.4** Germline knockdown (GLKD) screening of PIWI proximity factors 50
**Figure 2.5** Effect of GLKD on TE transcript levels in non-GSCLC and GSCLC ovaries 52
**Figure 2.6** Set1 colocalizes and physically interacts with Piwi 54
**Figure 2.7** Effects of Set1 and COMPASS components on TE repression 56
**Figure 2.8** Effect of *set1*-GLKD on piRNA pathway components 58
**Figure 2.9** Deep sequencing analysis of *set1*-GLKD ovary 59
**Figure 2.10** Effect of *set1*- and *piwi*-GLKD on chromatin status in piRNA cluster loci 61

**Chapter 3: Materials and Methods**
**Table 3.1** Fly lines used in this study 70

**Table 3.2** Primer list for plasmid construction 73
**Table 3.3** Amino acid sequence for AlphaFold prediction 74
**Table 3.4** Primer list for qPCR 80

# 0. General Introduction

## 0.1 *Drosophila melanogaster*

### 0.1.1 *Drosophila* ovary

*Drosophila melanogaster* serves as a model organism for developmental biology and genetics research. Its short generation time and well-established genetic tools, including the Gal4/UAS system and CRISPR/Cas9 technology, provide powerful experimental advantages (del Valle Rodríguez et al., 2012).

The *Drosophila* ovary consists of approximately 16-18 ovarioles bundled together (Figure 0.1) (Kahney et al., 2019). Each ovariole contains a germarium at its anterior tip, which contains 2-3 germline stem cells (GSCs). These GSCs are maintained in their stem cell state by surrounding niche cells, including cap cells and terminal filament cells (Xie & Spradling, 2000). Posterior to the germarium, egg chambers at different developmental stages are arranged in a chain-like fashion. Oogenesis is classified into 14 distinct stages (Bastock & St Johnston, 2008), and a single ovariole simultaneously contains egg chambers at various developmental stages. This feature

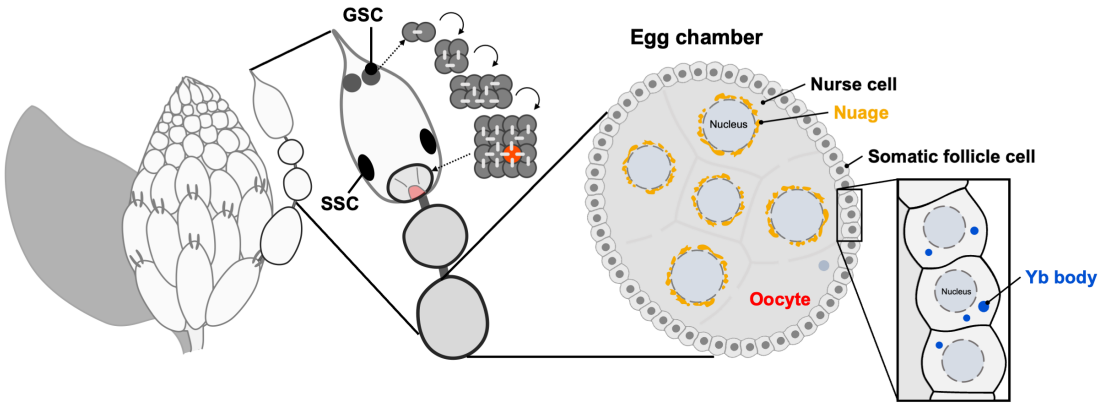



**Figure 0.1 Structure of *Drosophila* ovary**
GSC; germline stem cell, SSC; somatic (follicle) stem cell

makes the *Drosophila* ovary a model system for studying germline development, stem cell maintenance, and transposon control mechanisms, which are the focus of this study.

### 0.1.2 Ovarian germline cells

GSCs maintain their stem cell identity by adhering to niche cells. Signals from the niche, through the Dpp signaling pathway (Harris & Ashe, 2011), promote GSC self-renewal and suppress differentiation. GSCs undergo asymmetric division: the daughter cell that remains in contact with the niche retains stem cell properties, while the daughter cell displaced from the niche initiates differentiation. This differentiating cell is called a cystoblast and is characterized by the induced expression of the transcription factor *bag of marbles* (*bam*) (McKearin & Spradling, 1990). *bam* further activates downstream genes required for differentiation, committing the cell to the oogenesis. Within the germarium, the cystoblast undergoes four rounds of incomplete cell division to form a cyst consisting of 16 germline cells (Bastock & St Johnston, 2008). During this division process, cytokinesis remains incomplete, and daughter cells stay connected via cytoplasmic bridges called ring canals (Grieder et al., 2000). Upon completion of division into 16 cells, one of the cells migrates toward the distal side of the germarium and becomes the oocyte (Bastock & St Johnston, 2008). The remaining 15 cells differentiate as nurse cells. The 16-cell cyst becomes enveloped by somatic follicle cells (described below) to form an egg chamber, which then buds off from the germarium.

Throughout oogenesis, the oocyte and nurse cells exhibit distinct characteristics. The oocyte nucleus arrests in meiotic prophase I and remains largely transcriptionally inactive until fertilization (Page & Orr-Weaver, 1997; Von Stetina & Orr-Weaver, 2011). In contrast, nurse cell nuclei undergo endocycles—DNA replication without cell division—leading to polyploidization (Dej & Spradling, 1999). Eventually, the nucleus

occupies most of the nurse cell volume. These polyploid nuclei are highly transcriptionally active, producing massive amounts of mRNAs and proteins required for oocyte development. mRNAs and proteins synthesized in nurse cells are transported to the oocyte through ring canals (Theurkauf & Hazelrigg, 1998). Because nurse cells are highly transcriptionally active, transposons utilize this environment for their own proliferation. Transposons are actively amplified in nurse cells and subsequently transferred to the oocyte (L. Wang et al., 2018). If the transposon control fails, the resulting genome instability impairs oogenesis and causes sterility. Therefore, transposon repression in germline cells is essential for maintaining genome stability and fertility.

### 0.1.3 Ovarian somatic cells (follicle cells)

Follicle cells, the somatic cells of the ovary, have an independent origin from germline cells. Follicle stem cells are in the middle region of the germarium (region 2a/2b) (Figure 0.1) (Nystul & Spradling, 2007). Daughter cells derived from these stem cells proliferate and envelop the germline cyst, forming a monolayer epithelium. The primary function of follicle cells is to produce protective structures such as the chorion (eggshell) (Cavaliere et al., 2008). During late oogenesis, follicle cells undergo apoptosis (Nezis et al., 2002). Thus, their genomic information is not transmitted to the next generation. For this reason, transposons are generally considered to be less active in somatic cells.

However, in *Drosophila melanogaster*, specific transposons become activated in follicle cells when their controls are disrupted. Retrotransposons belonging to the gypsy family exhibit particularly high transcriptional activity in follicle cells (Touret et al., 2014). This demonstrates that transposon repression system is required not only in germline cells but also in somatic follicle cells. The types of transposons that become

activated differ between germline and somatic cells, implying the requirement of cell type-specific strategies for transposon control.

## 0.2 Transposable elements

### 0.2.1 Origins and classification of TEs

Transposable elements (TEs) are DNA sequences capable of moving within the genome and constitute a major portion of genomes in many organisms. TEs are ancient mobile genetic elements whose origins trace back to the early stages of eukaryotic evolution; some classes share evolutionary relationships with infectious viruses (Hayward & Gilbert, 2022; Kazazian, 2004). The diversity of TEs across eukaryotes reflects their long-standing co-evolution with host genomes. Approximately 45% of the human genome consists of TE-derived sequences (Deniz et al., 2019; C. R. L. Huang et al., 2012), the majority of which are fossilized TEs that have accumulated mutations and lost their transposition capability over evolutionary time. However, some TE families retain activity and can cause genome instability and disease (C. R. L. Huang et al., 2012). In *Drosophila melanogaster*, TEs account for approximately 20% of the genome (Deniz et al., 2019; C. R. L. Huang et al., 2012), and many TE families in *Drosophila* remain transcriptionally active and continue to pose a threat to genome integrity.

TEs are classified into two major classes based on their transposition mechanism (Figure 0.2 A: TE classes) (Deniz et al., 2019; C. R. L. Huang et al., 2012). Class I TEs (retrotransposons) transpose via an RNA intermediate. They are first transcribed from DNA to RNA, then reverse-transcribed back to DNA by reverse transcriptase and finally inserted into a different genomic location (copy-and-paste mechanism). Class I is further subdivided into LTR retrotransposons, which possess Long Terminal Repeats (LTRs), and non-LTR retrotransposons (including LINEs and SINEs), which lack LTRs. Class II TEs

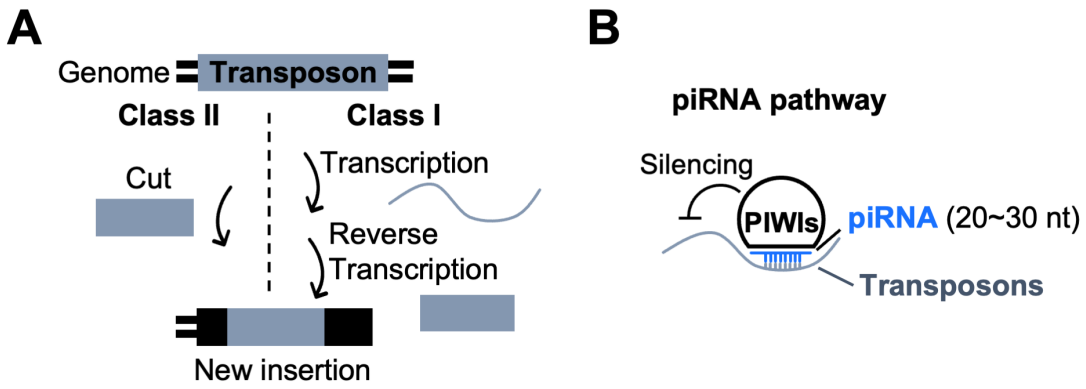



**Figure 0.2 Classification of transposable elements and overview of piRNA pathway**

(DNA transposons) transpose via a DNA intermediate. Transposase enzymes recognize inverted terminal repeats at both ends of the TE, excise the TE sequence from the genome, and insert it into a different location via a cut-and-paste mechanism. Class II TEs do not inherently increase copy number, although amplification is possible depending on replication timing.

TEs have both harmful and beneficial effects on host genomes. On the harmful side, TE insertions disrupt genes and alter regulatory regions, representing a major source of mutations (Hancks & Kazazian, 2016). Germline cells require particularly stringent transposon control because any mutations arising in these cells are heritable. When transposon activity causes excessive genomic damage in the germline, it results in infertility. On the beneficial side, TEs have served as drivers of adaptive evolution by generating novel genes, evolving gene regulatory regions, and mediating chromosomal rearrangements (Schrader & Schmitz, 2019). Due to this dual nature, host organisms have evolved strategies to appropriately control TEs rather than eliminate them. Particularly in animal germline cells, sophisticated TE suppression mechanisms, the piRNA pathway, have evolved.

### 0.2.2 TEs in *Drosophila*

The *Drosophila* genome harbors diverse TE families from both Class I and Class II. Remarkably, *Drosophila* provides a unique example where TEs have been co-opted to perform an essential host function. Most eukaryotes maintain telomere sequences at chromosome ends using an enzyme called telomerase, but *Drosophila* and some other insects have lost the telomerase gene during evolution (Casacuberta, 2017; Cui et al., 2021). Instead, *Drosophila* maintains telomeres using three specialized non-LTR retrotransposon families: *HeT-A*, *TART*, and *TAHRE* (collectively termed *HTT*) (Figure 0.3 A, B). *HTT* elements possess the unique property of specifically transposing to telomeric regions. The reverse transcriptase of *HTT* is thought to recognize chromosome

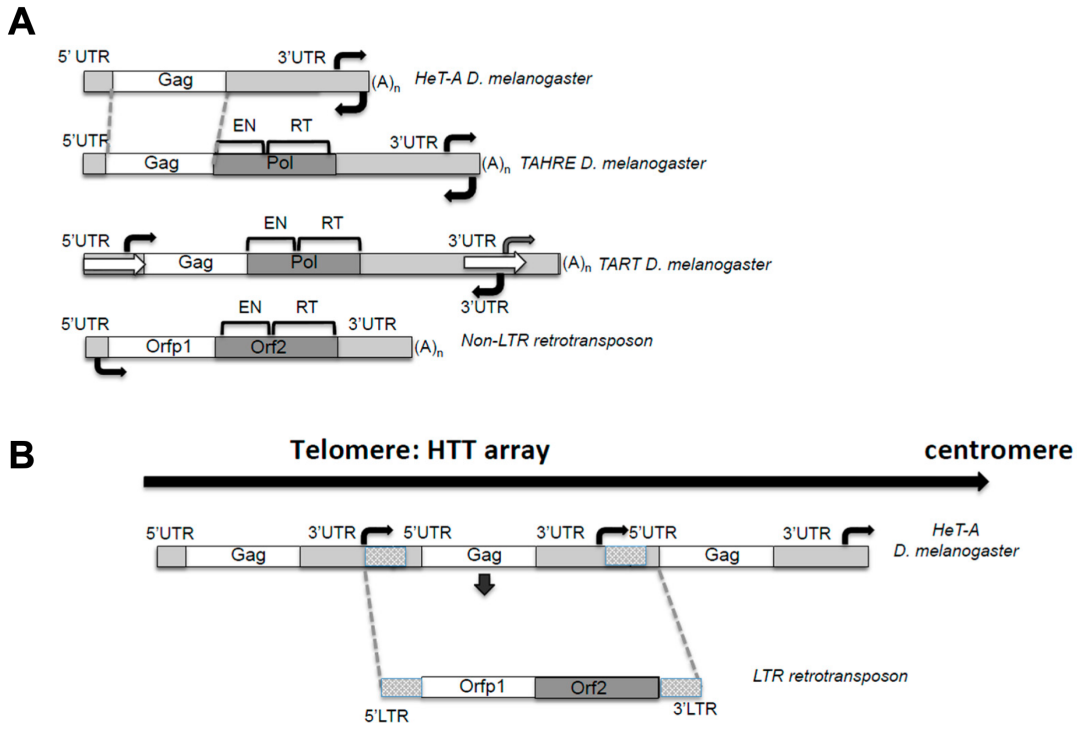



**Figure 0.3 *HTT* transposons and telomere maintenance in *Drosophila***

(A) Structural comparison of *HTT* family members and canonical non-LTR retrotransposons. *HeT-A*, *TAHRE*, and *TART* are specialized non-LTR retrotransposons that maintain *Drosophila* telomeres. (B) Organization of *HTT* elements at *Drosophila* telomeres. *HTT* elements are arranged in head-to-tail arrays at chromosome ends, with their 3' UTRs facing toward centromeres and 5' ends oriented toward chromosomal ends. Adapted from (Casacuberta, 2017)

ends and preferentially insert at these sites (Casacuberta, 2017; Pardue & DeBaryshe, 2011). During chromosome replication, linear DNA ends of chromosome cannot be fully replicated (the end-replication problem), causing gradual chromosome shortening. *HTT* transposition adds new sequences to chromosome ends, compensating for this shortening and maintaining chromosome stability. Unlike the other retrotransposons, *HTT* elements possess promoters at their 3' ends (Radion et al., 2017). Furthermore, *HTT* elements are arranged in head-to-tail arrays at telomeric regions (Casacuberta, 2017), with multiple *HTT* copies arrayed consecutively. This characteristic allows transcription to initiate the downstream *HTT* copies by 3' promoter even when the 5' end is lost due to chromosome replication. This arrangement allows telomere maintenance function to continue.

Thus, *HTT* elements are not merely parasitic TEs but rather factors that have co-evolved with the host to perform the essential function of telomere maintenance. However, complete derepression of *HTT* would allow indiscriminate transposition to non-telomeric genomic regions, potentially causing gene disruption and chromosomal instability. Therefore, *HTT* must be controlled under a delicate balance: maintaining sufficient activity for telomere maintenance while suppressing excessive mobilization.

## 0.3 piRNA pathway

### 0.3.1 piRNA overview

The piRNA (PIWI-interacting RNA) pathway is widely conserved in animal germline cells as a defense mechanism against genomic invasion by transposons (Figure 0.2 B) (X. Wang et al., 2023). piRNAs are a class of small RNA molecules, along with microRNAs (miRNAs) and small interfering RNAs (siRNAs), and are 23-30 nucleotides in length. The defining feature of piRNAs is that they possess sequences complementary to transposon sequences, enabling specific targeting of TE-derived mRNAs. piRNAs

function by binding to PIWI clade proteins, which belong to the Argonaute superfamily (Brennecke et al., 2007). PIWI-piRNA complexes (piRNA-induced silencing complexes, piRISCs) use piRNAs as guides to recognize transposon mRNAs and execute silencing at either the transcriptional or post-transcriptional level. *Drosophila melanogaster* possesses three PIWI family proteins; Piwi, Aubergine (Aub), and Argonaute 3 (Ago3). Piwi functions in the nucleus and mediates transcriptional silencing (Le Thomas et al., 2013; Onishi et al., 2020; Sienski et al., 2012). In contrast, Aub and Ago3 localize to a cytoplasmic structure called nuage and mediate post-transcriptional silencing and piRNA amplification (Sato et al., 2015; W. Wang et al., 2015; Webster et al., 2015).

The piRNA pathway consists of three major stages. The first stage is piRNA precursor transcription, in which long precursor RNAs are transcribed from genomic regions called piRNA clusters. The second stage is piRNA precursor processing, in which mature piRNAs are generated from precursor RNAs and loaded onto PIWI proteins. The third stage is transposon silencing, in which PIWI-piRNA complexes recognize transposon mRNAs and suppress them. Each of these stages involves several proteins and is governed by precisely controlled molecular mechanisms. Significantly, the piRNA pathway mechanisms differ partially between somatic cells (follicle cells) and germline cells (nurse cells) in *Drosophila*. In somatic cells, only Piwi functions and transcriptionally repress transposons (Qi et al., 2011; Saito et al., 2010). In germline cells, all three PIWI proteins function, and more complex piRNA biogenesis and transposon repression mechanisms exist (A. K. Lim & Kai, 2007; Webster et al., 2015). This cell type-specific diversity is thought to reflect adaptation to the types of transposons activated in each cell type and the physiological characteristics of each cell.

In the following sections, I describe the mechanisms of piRNA precursor transcription (0.3.2), piRNA biogenesis in somatic cells (0.3.3), and piRNA biogenesis in germline cells (0.3.4) in detail.

### 0.3.2 precursor transcription

piRNAs are primarily transcribed from genomic regions called piRNA clusters, where fragmented transposon sequences have accumulated (Brennecke et al., 2007; Klattenhoff et al., 2009; van Lopik et al., 2023). These clusters function as a molecular record of past transposon invasions and provide sequence information for recognizing transposons currently present in the genome. Long precursor RNAs spanning tens of kilobases are transcribed from piRNA clusters, which are subsequently exported to cytoplasm to generate individual piRNAs. piRNA clusters are classified into several types based on their transcription patterns. Uni-strand clusters are transcribed from only one direction and generate piRNAs directly complementary to transposons. The *flamenco* cluster functioning in follicle cells is a representative example (Pelisson et al., 1994; Rivera et al., 2025; van Lopik et al., 2023). In contrast, dual-strand clusters are transcribed from both strands and generate both sense and antisense piRNAs. Dual-strand clusters mostly function in germline cells (Klattenhoff et al., 2009; C. Li et al., 2009; Mohn et al., 2014). In addition to these canonical clusters, subtelomeric piRNA clusters represent a specialized class. Cluster 3 at the 4th chromosome end and cluster 22 at the X chromosome end are particularly enriched with *HTT*-derived fragments (Iyer et al., 2023; C. Li et al., 2009). piRNA precursors transcribed from these clusters serve as the major source of antisense piRNAs targeting *HTT*, functioning as a surveillance mechanism to prevent excessive *HTT* activation while permitting controlled activity for telomere maintenance.

### 0.3.3 piRNA processing in follicle cell

In follicle cells, piRNA precursor processing occurs sequentially at two distinct cytoplasmic structures: the Yb body and the mitochondrial outer membrane. Following maturation, Piwi-piRNA complexes translocate to the nucleus to achieve transcriptional silencing of transposons. This pathway involves only Piwi among the PIWI family proteins. Below, I describe each stage in detail.

#### 0.3.3.1 Precursor processing in Yb body

After transcription, piRNA precursor RNAs are spliced and transported to the cytoplasmic Yb body (Figure 0.4 A) (Qi et al., 2011; Saito et al., 2010). Yb body is a non-membranous structure specific to follicle cells. Yb is an RNA-binding protein with a helicase domain that recognizes and binds to the hairpin secondary structures of piRNA precursors (Murota et al., 2014; Szakmary et al., 2009). In addition to Yb, the Yb body contains factors such as Armitage (Armi), Sister of Yb (SoYb), and Vreteno (Vret) (Handler et al., 2011; Munafò et al., 2019; Saito et al., 2010). Armi and SoYb possess

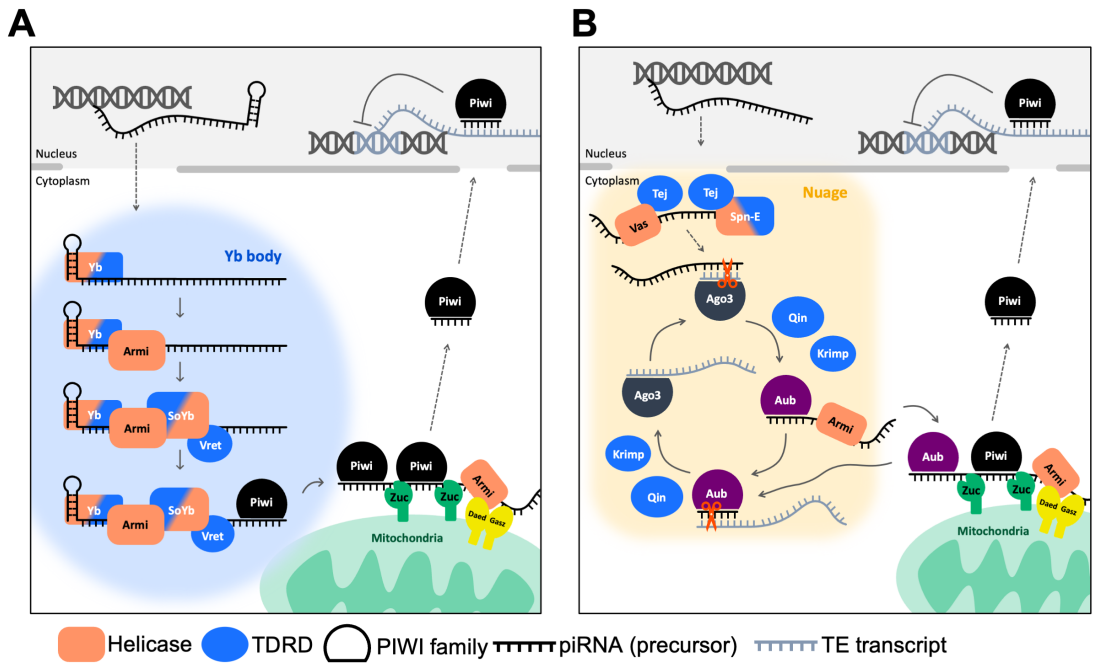



**Figure 0.4 piRNA pathways in follicle cells and nurse cells**

Schematics of piRNA pathway in somatic follicle cells (A) and germline cells (B).

RNA helicase domains and are thought to contribute to unwinding the secondary structures of piRNA precursors and facilitating proper conformational changes (Handler et al., 2011; Saito et al., 2010). Yb, SoYb, and Vret contain Tudor domains, which are known to recognize methylated arginine residues (Handler et al., 2011). Since PIWI proteins undergo arginine methylation, Tudor domain proteins are thought to mediate interactions with PIWI. Although Vret's molecular function is not fully understood, it has been shown to be required for piRNA precursor processing (Handler et al., 2011). Piwi associates with piRNA precursors bound by these factors in the Yb body. At this stage, the precursor RNAs are prepared for transfer to the mitochondrial outer membrane.

#### 0.3.3.2 Phasing on mitochondrial outer membrane

piRNA precursors are transferred from the Yb body to the adjacent mitochondrial outer membrane. This transfer is mediated by interactions between Armi and the Daed/Gasz complex, which localizes to the mitochondrial outer membrane (Ge et al., 2019; Munafò et al., 2019). Zucchini (Zuc), an endonuclease localized on the mitochondrial outer membrane, cleaves piRNA precursors successively (Han et al., 2015; Ipsaro et al., 2012; Koga et al., 2024; Mohn et al., 2015; Pane et al., 2007). This continuous cleavage is called "phasing," whereby multiple piRNAs are generated sequentially from a single precursor. Although Zuc shows no sequence specificity *in vitro*, the 5' ends of phased piRNAs generated *in vivo* frequently begin with uracil (U) residues (1U bias) (Brennecke et al., 2007; Gunawardane et al., 2007). This 1U bias is thought to arise from selective binding affinity of Piwi for piRNAs beginning with U (Stein et al., 2019). In other words, while Zuc cleaves relatively indiscriminately, Piwi preferentially loads U-starting fragments among the generated fragments, resulting in the accumulation of a piRNA population with 1U bias. Cleaved piRNA fragments undergo 3' end trimming and methylation while

bound to Piwi, becoming mature piRNAs (Feltzin et al., 2015; Hayashi et al., 2016; Saito et al., 2007; H. Wang et al., 2015).

#### 0.3.3.3 Nuclear translocation and transposon silencing of piRISC

Mature piRNA-Piwi complexes (piRISCs) translocate to the nucleus. piRNA binding induces conformational changes in Piwi, exposing its nuclear localization signal (NLS) and enabling transport to nucleus (Yashiro et al., 2018). Following nuclear import, piRISCs bind to nascent transposon transcripts (Dönertas et al., 2013; Fabry et al., 2019; Le Thomas et al., 2013; Ohtani et al., 2013; Zhao et al., 2019). Unlike Aub and Ago3, *Drosophila* Piwi has lost its endonuclease activity (slicer activity) (Darricarrère et al., 2013; Yamaguchi et al., 2020). Instead, Piwi functions as a core bound to nascent transcripts, recruiting other proteins. Specifically, it recruits the H3K9 methyltransferase SetDB1/Eggless (Egg) and its cofactor Panoramix (Panx), introducing H3K9me3 marks at transposon loci and promoting heterochromatin formation (Sienski et al., 2015; Y. Yu et al., 2015). This heterochromatinization suppresses transposon transcription, achieving persistent silencing.

### 0.3.4 piRNA processing in germline cell

piRNA biogenesis in germline cells (nurse cells) is more complex compared to the follicle cell pathway, with all three PIWI proteins functioning. In germline cells, a non-membranous structure with high electron density called nuage forms on the cytoplasmic side of the nuclear envelope (Eddy, 1976; A. K. Lim & Kai, 2007; Lin et al., 2023), serving as the central site for piRNA amplification and transposon silencing cycle called "ping-pong cycle" (Figure 0.4 B).

piRNA precursor RNAs transcribed from piRNA clusters is transported from the nucleus to cytoplasmic nuage. This transport requires the RNA-binding protein Nxf3, in

addition to RNA helicases Spindle-E (Spn-E) and Vasa (Vas), and the Tudor domain protein Tejas (Tej) (Kneuss et al., 2019; Lin et al., 2023). Spn-E and Vas possess RNA helicase domains and are thought to bind piRNA precursors. Tej belongs to the TDRD (Tudor domain-containing) protein family and contains domains that interact with Spn-E and Vas. These factors work cooperatively to facilitate the translocation of piRNA precursors to nuage and retain them within nuage (Lin et al., 2023).

piRNA precursors translocated to nuage bind to Aub and Armi. Subsequently, like follicle cells, precursor RNAs are transferred to the mitochondrial outer membrane (Ge et al., 2019). Zuc on the mitochondrial outer membrane cleaves precursor RNAs successively (phasing), generating multiple piRNAs. Both Aub and Piwi receive phased piRNAs. Phased piRNAs bound to Aub undergo 3' trimming (by Nibbler (Nib)) and methylation (by Hen1), become mature, and translocate back to nuage (Feltzin et al., 2015; Saito et al., 2007; H. Wang et al., 2015). In contrast, phased piRNAs bound to Piwi translocate to the nucleus and mediate transcriptional repression and heterochromatin formation, similar to the somatic piRNA pathway.

Mature Aub-piRNA complexes localized in nuage bind to transposon mRNAs and cleave them via their endonuclease activity (slicer activity) (Gunawardane et al., 2007). The 3' fragment generated by cleavage is received by Ago3, another PIWI family protein. In this step, the Tudor domain protein Krimper (Krimp) plays a crucial role (Sato et al., 2015; Webster et al., 2015). Krimp functions as a scaffold protein in nuage, and through its Tudor domain, interacts with both Aub and Ago3. This brings Aub and Ago3 into spatial proximity, enabling Ago3 to efficiently receive transposon mRNA fragments cleaved by Aub (Webster et al., 2015). The transposon mRNA fragment received by Ago3 undergoes trimming and methylation to become a mature piRNA. This piRNA is in the

sense orientation relative to transposon mRNA, meaning it is complementary to the piRNA cluster precursor (antisense). The Ago3-piRNA complex binds to piRNA precursors and again cleaves between the 10th and 11th nucleotides. The 3' fragment of this cleavage product is received by Aub and becomes a new antisense piRNA. This cycle, in which Aub and Ago3 reciprocally cleave targets and utilize the cleavage products as piRNAs for the other protein, is called the "ping-pong cycle" (Brennecke et al., 2007; Gunawardane et al., 2007). The ping-pong cycle is an efficient mechanism that simultaneously achieves transposon mRNA degradation and piRNA amplification. By accelerating the ping-pong cycle in response to actively transcribed transposons, effective suppression is achieved.

piRNAs generated through the ping-pong cycle possess characteristic sequence biases. Aub, like Piwi in follicle cells, selectively binds piRNAs beginning with uracil (U) at the 5' end (1U bias) (Brennecke et al., 2007). Cleavage by Aub occurs between the nucleotides complementary to the 10th and 11th nucleotides of the guide piRNA. Therefore, the 5' end of the cleavage fragment corresponds to the position opposite the 10th nucleotide of the Aub-piRNA. As a result, piRNAs loaded onto Ago3 tend to have adenine (A) at the 10th position (10A bias) (Brennecke et al., 2007). Conversely, when Ago3 cleaves piRNA precursors at the position between nucleotides complementary to its 10th and 11th guide nucleotides, the fragments generated for Aub loading exhibit the 1U bias again. This 1U and 10A bias, along with the 10-nucleotide overlap between reciprocal piRNA pairs (ping-pong signature), serves as clear evidence that the ping-pong cycle is functioning (Antoniewski, 2014; Brennecke et al., 2007).

In addition to the factors described above, many proteins are involved in the ping-pong cycle in nuage (Table 0.1). These include Tudor domain proteins, RNA

helicases, and factors with diverse functions (Kawaguchi et al., 2025). Many of these factors are thought to contribute to nuage structure maintenance, stabilization of PIWI-piRNA complexes, or enhancement of piRNA biogenesis efficiency, although their detailed molecular mechanisms are still under investigation.

**Table 0.1 piRNA pathway components in *Drosophila* ovary**

| Protein | Expression | Localization | Known Function | Reference |
|---|---|---|---|---|
| **PIWI family proteins** | | | | |
| **Piwi** | Germline, Soma | Nucleus | piRNA binding; transcriptional silencing | (Le Thomas et al., 2013; Saito et al., 2006) |
| **Aub (Aubergine)** | Germline | Nuage, cytoplasm | piRNA binding; slicer activity; ping-pong cycle | |
| **Ago3 (Argonaute 3)** | Germline | Nuage, cytoplasm | piRNA binding; slicer activity; ping-pong cycle | |
| **Tudor domain proteins** | | | | |
| **Krimp (Krimper)** | Germline | Nuage | Scaffold protein; facilitates Aub-Ago3 interaction | (A. K. Lim & Kai, 2007; Sato et al., 2015; Webster et al., 2015) |
| **Tej (Tejas)** | Germline | Nuage | piRNA precursor transport; nuage localization | (Lin et al., 2023; Patil & Kai, 2010) |
| **Tapas** | Germline | Nuage | Nuage component; piRNA biogenesis | (Patil et al., 2014) |
| **Kumo (Qin)** | Germline | Nuage | E3 ubiquitin ligase; ping-pong cycle regulation | (Anand & Kai, 2012; Z. Zhang et al., 2011) |
| **Kotsubu (Kots)** | Germline | Nuage | piRNA production | (L.-X. Lim et al., 2022) |
| **Yb** | Soma | Yb body | RNA binding; piRNA precursor recognition | (Murota et al., 2014; Saito et al., 2010) |
| **SoYb (Sister of Yb)** | Soma | Yb body | RNA helicase; piRNA precursor processing | (Handler et al., 2011) |
| **RNA helicases** | | | | |

| Protein | Expression | Localization | Known Function | Reference |
|---|---|---|---|---|
| **Spn-E (Spindle-E)** | Germline | Nuage | RNA helicase; piRNA precursor transport | (Lin et al., 2023; Malone et al., 2009) |
| **Vas (Vasa)** | Germline | Nuage | RNA helicase; piRNA biogenesis | (Lin et al., 2023; Xiol et al., 2014) |
| **Armi (Armitage)** | Germline, Soma | Mitochondria (germline, soma); Yb body (soma); Nuage (germline) | RNA helicase; piRNA precursor transport to mitochondria | (Ge et al., 2019; Munafò et al., 2019; Saito et al., 2010) |
| **Endonucleases** | | | | |
| **Zuc (Zucchini)** | Germline, Soma | Mitochondrial outer membrane | Endonuclease; phased piRNA production | (Han et al., 2015; Ipsaro et al., 2012; Mohn et al., 2015; Pane et al., 2007) |
| **Mitochondrial localization factors** | | | | |
| **Daed (Daedalus)** | Germline | Mitochondrial outer membrane | Mitochondrial targeting; works with Gasz | (Koga et al., 2024; Munafò et al., 2019) |
| **Gasz** | Germline | Mitochondrial outer membrane | Mitochondrial targeting; piRNA biogenesis | |
| **3' processing enzymes** | | | | |
| **Nib (Nibbler)** | Germline | Cytoplasm | 3'-5' exonuclease; piRNA 3' trimming | (Feltzin et al., 2015; H. Wang et al., 2015) |
| **Hen1** | Germline, Soma | Cytoplasm | 2'-O-methyltransferase; piRNA 3' methylation | (Saito et al., 2007; H. Wang et al., 2015) |
| **Nuclear export factors** | | | | |
| **Nxf2 (Nuclear export factor 2)** | Germline, Soma | Nucleus | piRNA precursor export from nucleus | (Batki et al., 2019; Sienski et al., 2015) |
| **Nxf3 (Nuclear export factor 3)** | Germline | Nucleus | piRNA precursor export; interacts with Ago3 | (ElMaghraby et al., 2019; |

| Protein | Expression | Localization | Known Function | Reference |
|---|---|---|---|---|
| **Boot (Bootlegger)** | Germline | Nucleus | piRNA precursor export; works with Nxf3 | Kneuss et al., 2019) |
| **RDC complex (Rhino-Deadlock-Cutoff)** | | | | |
| **Rhi (Rhino)** | Germline | Nucleus (piRNA clusters) | HP1 paralog; recognizes H3K9me3; promotes noncanonical transcription | (Chen et al., 2021; Mohn et al., 2014) |
| **Del (Deadlock)** | Germline | Nucleus (piRNA clusters) | RDC complex component; piRNA cluster transcription | |
| **Cuff (Cutoff)** | Germline | Nucleus (piRNA clusters) | RDC complex component; piRNA cluster transcription | |
| **Transcriptional silencing factors** | | | | |
| **Panx (Panoramix)** | Germline, Soma | Nucleus | Piwi cofactor; recruits silencing machinery | (Y. Yu et al., 2015) |
| **Egg (Eggless/SetDB1)** | Germline, Soma | Nucleus | H3K9 methyltransferase; heterochromatin formation | (Ninova et al., 2020; Sienski et al., 2015) |
| **Su(var)2-10** | Germline | Nucleus | SUMO E3 ligase; links Piwi to Eggless | (Ninova et al., 2020) |
| **Other factors** | | | | |
| **Vret (Vreteno)** | Soma | Yb body | piRNA precursor processing | (Handler et al., 2011) |
| **Mael (Maelstrom)** | Germline | Nuage, nucleus | Suppresses canonical transcription at piRNA clusters | (Onishi et al., 2020; Sienski et al., 2012) |
| **Transcription factors** | | | | |
| **Ovo** | Germline | Nucleus | Master regulator; activates germline piRNA pathway genes | (Alizada, Hannon, et al., 2025) |
| **Tj (Traffic jam)** | Soma | Nucleus | Maf transcription factor; activates *flamenco* cluster and piRNA pathway genes | (Alizada, Martins, et al., 2025; Rivera et al., 2025) |

# 1. Functional characterization of Kumo as a RING-type E3 ubiquitin ligase essential for transposon silencing

## 1.1 Introduction

### 1.1.1 Known function of Kumo

Kumo (also known as Qin) is a protein possessing an E3 ubiquitin ligase domain (RING domain) and five Tudor domains, reported as a factor involved in the piRNA pathway in germline cells (Anand & Kai, 2012; Z. Zhang et al., 2011). Kumo localizes to nuage, a perinuclear structure in nurse cells, and has been shown to physically interact with other piRNA pathway factors localized in nuage (Anand & Kai, 2012). In *kumo* mutants, marked derepression of transposons is observed, and females become sterile (Anand & Kai, 2012; Z. Zhang et al., 2011). These phenotypes indicate that Kumo plays an important role in transposon suppression.

Previous study has suggested that Kumo promotes interaction between Aub and Ago3 or inhibits interaction between Aub molecules (Z. Zhang et al., 2011). In the ping-pong cycle, heterotypic cycles occur in which Aub and Ago3 reciprocally exchange piRNAs and repress transposons. In wild-type ovaries, piRNAs bound to Aub exhibit a 1U bias at the 5' end, but in *kumo* deficiency, piRNAs with both 1U bias at the 5' end and 10A bias at the 10th position become abundantly bound to Aub (Z. Zhang et al., 2011). Since 10A bias is a characteristic of piRNAs that bind to Ago3, this observation suggests that homotypic ping-pong cycles between Aub-Aub are occurring. Aub-Aub homotypic cycles do not achieve efficient degradation of transposon mRNAs. Therefore, Kumo is thought to maintain normal heterotypic ping-pong cycles (Aub-Ago3) and suppress aberrant homotypic cycles (Aub-Aub), thereby enabling effective transposon suppression.

However, the molecular mechanism by which and how Kumo performs this role remains unknown.

RNF17 (RING finger protein 17) is known as the mammalian homolog of Kumo. Mouse RNF17 is expressed in the testis and has been reported to be involved in germline development and the piRNA pathway (Pan et al., 2005; Wasik et al., 2015). RNF17 forms cytoplasmic granules in culture cells, and its coiled-coil region is required for oligomerization (Pan et al., 2005). Additionally, RNF17 has been reported to interact with specific E2 ubiquitin-conjugating enzymes, although the ubiquitination activity of RNF17 and its physiological substrates had not been clarified (Guo et al., 2017).

### 1.1.2 Ubiquitination

Ubiquitination is a post-translational modification in which a small 76-amino acid protein called ubiquitin is covalently attached to target proteins (Akutsu et al., 2016; Komander & Rape, 2012). Ubiquitination functions as a universal mechanism that regulates diverse cellular processes, including protein degradation, localization, activity control, and protein-protein interactions.

The ubiquitination is achieved through an enzymatic cascade in which three types of enzymes act sequentially (Pickart, 2001). First, E1 enzyme (ubiquitin-activating enzyme) activates ubiquitin by consuming ATP, forming an E1-ubiquitin thioester intermediate. Next, the activated ubiquitin is transferred to E2 enzyme (ubiquitin-conjugating enzyme), forming an E2-ubiquitin intermediate. Finally, E3 enzyme (ubiquitin ligase) recognizes both the E2 enzyme and the substrate protein, bringing them to facilitate ubiquitin transfer to the substrate. The human genome contains one E1, approximately 40 E2s, and over 600 E3s (Metzger et al., 2012). Similarly, *Drosophila*

possesses one E1, approximately 30 E2s, and over 100 E3s (Ketosugbo et al., 2017). This combination of enzymes achieves substrate specificity and diverse regulation.

Ubiquitin is attached to lysine (Lys, K) residues of substrate proteins. Furthermore, ubiquitin itself possesses seven Lys residues (K6, K11, K27, K29, K33, K48, K63) and an N-terminal methionine (M1), enabling multiple ubiquitin molecules to link through these sites and form polyubiquitin chains (Swatek & Komander, 2016). The linkage type of polyubiquitin chains transmits distinct biological signals. K48-linked polyubiquitin chains are the most extensively studied and primarily function as signals for protein degradation by the proteasome. This mechanism plays crucial roles in cell cycle control, signaling pathway termination, and quality control. K63-linked polyubiquitin chains function mainly in signaling pathways and subcellular localization control rather than degradation. K63 chains are involved in DNA damage response, NF-κB signaling, endocytosis, and innate immunity. Other chain types, including K6, K11, K27, K29, K33, and M1 linkages, also mediate specific cellular functions, though their roles are less well characterized. This diversity in chain topology enables ubiquitination to regulate a wide range of cellular processes with remarkable specificity.

E3 ubiquitin ligases are classified into several families based on their structure and mechanism. RING domain-type E3 ligases constitute the largest E3 family and are further categorized into subfamilies such as the TRIM family depending on their additional domains (Deshaies & Joazeiro, 2009). The RING domain possesses a characteristic structure in which cysteine and histidine residues coordinate two zinc ions. RING-type E3s facilitate ubiquitin transfer by bringing the E2 enzyme and substrate into proximity but do not themselves hold ubiquitin. HECT domain-type E3 ligases receive ubiquitin from E2 and form a transient E3-ubiquitin intermediate before transferring

ubiquitin to the substrate (Y. Wang et al., 2020). In addition, E3 ligases such as the RBR family possess characteristics of both RING-type and HECT-type enzymes (Spratt et al., 2014).

In recent years, ubiquitination has emerged as an important regulatory mechanism in the piRNA pathway. For example, the Vasa protein is protected by the deubiquitinating enzyme Fat Facets (Faf), which controls its stability (N. Liu et al., 2003). Additionally, crosstalk between the ubiquitin-like protein SUMO and ubiquitin has been shown to be involved in regulating Piwi function (Andreev et al., 2022; Ninova et al., 2020, 2023). However, no E3 ligase that directly catalyzes ubiquitination in the cytoplasmic piRNA pathway had been identified.

### 1.1.3 Overview of this chapter

In this chapter, I aimed to elucidate the functional role of the RING domain present at the N-terminus of Kumo. The RING domain is a motif conserved in many E3 ubiquitin ligases, and in Kumo it is conserved from insects to mammals. However, how this domain contributes to Kumo's transposon suppression function remained unknown. First, through sequence analysis, I demonstrated that while the cysteine residues essential for RING domain structure are conserved among animals, the mammalian homolog RNF17 does not conserve linchpin residue and is missing the domain following the RING. Next, to examine the function of the RING domain, I created a structure-disrupting mutant in which cysteine residues were mutated (C5 mutant). The C5 mutant lost nuage localization and lost transposon suppression ability. Through *in vitro* ubiquitination assays, I demonstrated that Kumo possesses RING domain-dependent E3 ubiquitin ligase activity. Furthermore, using a strategy employing TUBEs fusion proteins, I found that Kumo undergoes auto-ubiquitination. This study revealed that Kumo's ubiquitin ligase activity

is essential for transposon suppression, demonstrating the importance of ubiquitination control in the piRNA pathway.

## 1.2 Results

### 1.2.1 Kumo possesses a conserved RING domain

Kumo is a multi-domain protein consisting of 1857 amino acids in total. It possesses a RING domain, B-box domain, and coiled-coil domain at the N-terminus and following five Tudor domains at the C-terminus (Figure 1.1 A). While the C-terminal Tudor domains have been reported to possess for protein-protein interactions, the functional roles of the N-terminal RING, B-box, and coiled-coil domains remained unknown. Sequence comparison of the RING domain revealed that cysteine residues essential for maintaining the RING domain structure are conserved from *Drosophila* Kumo to

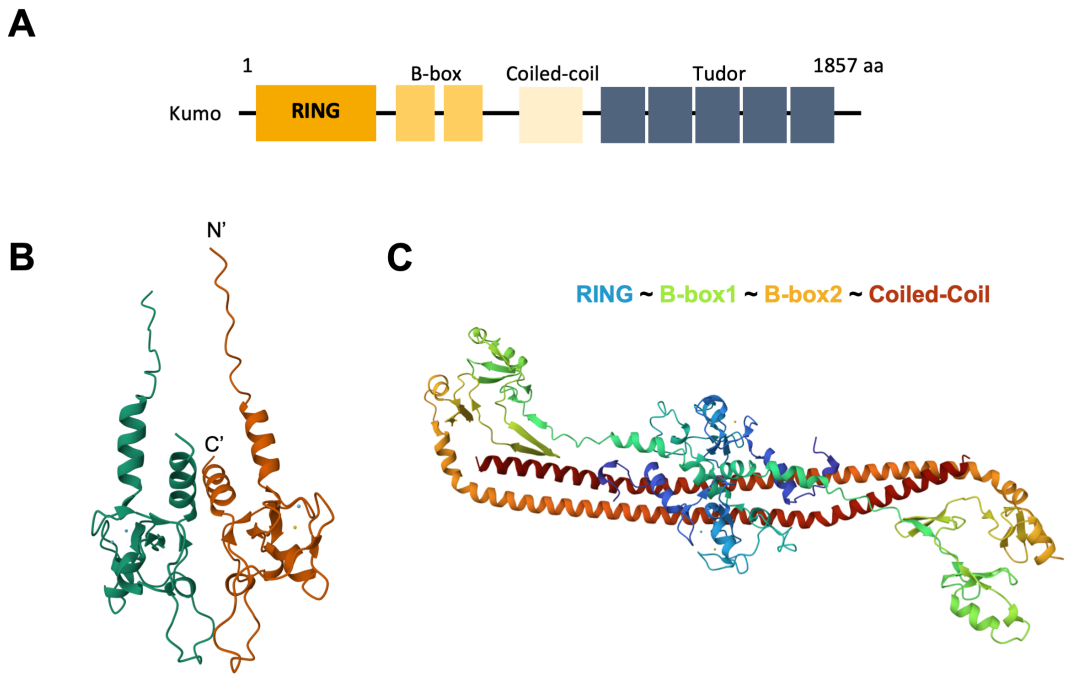



**Figure 1.1 Domain structure and structural prediction of Kumo**

(A) Schematics of domain structure of *Drosophila* Kumo. (B, C) AlphaFold dimer prediction of Kumo 1-115 (B, RING domain, iPTM = 0.37) / 1-350 (C, RING ~ coiled-coil region, iPTM = 0.6) amino acid sequence.

silkworm, mammalian humans and mice, and zebrafish (Figure 1.2). In RING-type E3 ligases, the residue immediately following the last cysteine that interacts with zinc ions is often a basic residue (Arg, Lys, or His), and this residue stabilizes the E2~ubiquitin binding site by interacting with E2~ubiquitin, thereby promoting ubiquitin transfer (Nakasone et al., 2025; Pruneda et al., 2012). This is called the linchpin residue. In *Drosophila melanogaster*, the residue at the corresponding position in Kumo is His, which may function as a linchpin. In contrast, in the mammalian RNF17, a Glu residue (acidic amino acid) is present at this position (Figure 1.2 and 1.3). This difference in the linchpin residue suggests functional divergence between Kumo and RNF17.

Kumo's N-terminal domain organization (RING+B-box+coiled-coil) matches the characteristics of the TRIM family, the largest family of E3 ligases (Meroni & Diez-Roux, 2005). However, sequence comparison of mammalian RNF17 revealed that while the RING domain cysteine residues and coiled-coil are conserved, no clear B-box domain-like sequence is observed (Figure 1.2). Due to this B-box deficiency, RNF17 is not classified in the TRIM family. Considering the linchpin residue difference as well, insect Kumo may have functionally diverged from mammalian RNF17 and obtained distinct functions.

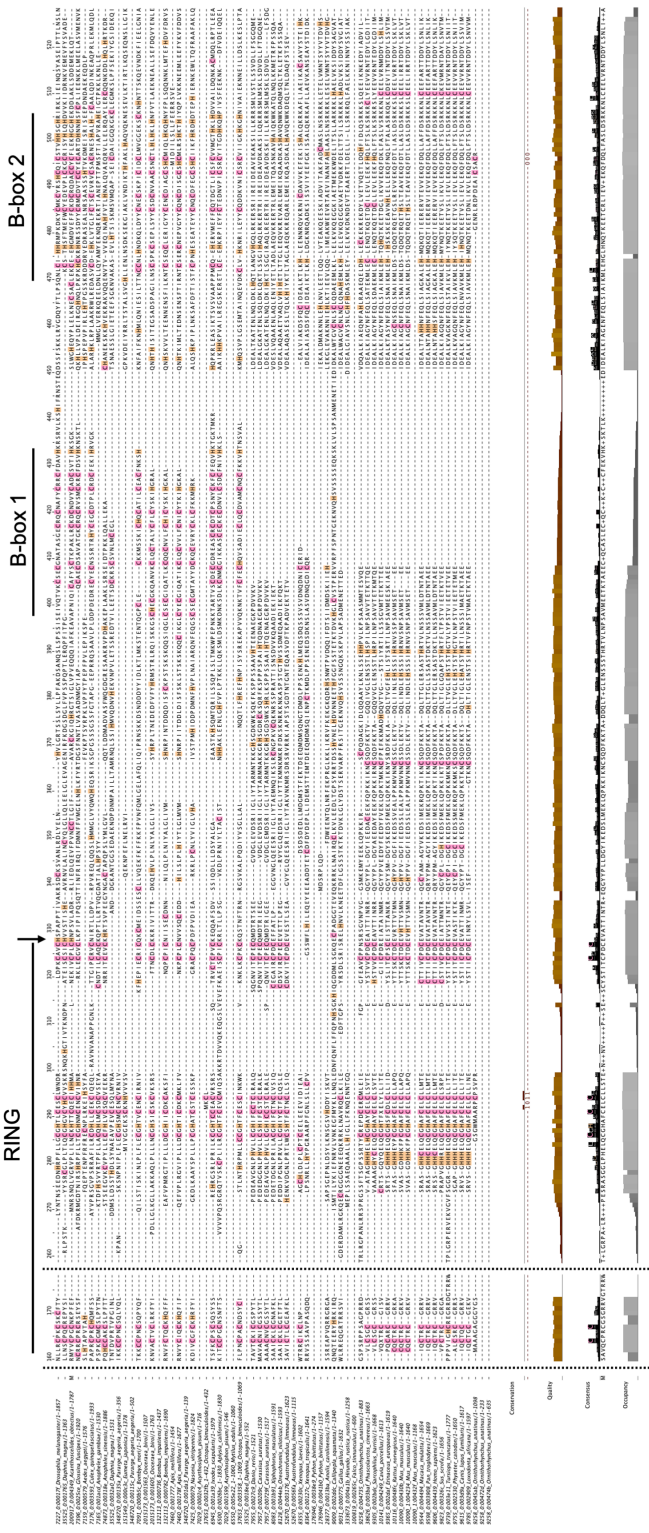



**Figure 1.2 Sequence alignment of N-ter region of Kumo across species**

Sequence alignment of Kumo (RNF17) homologues in representative species. Consensus of RING: CXXC-$X_{(9,39)}$-C-$X_{(1-3)}$-H-$X_{(2-3)}$-CXXC-$X_{(4-48)}$-CXX(C/D), B-box1: CXX(C/D)-$X_{(7-12)}$-CXXC-$X_{(4)}$-CXX(C/H)-$X_{(3-4)}$-H-$X_{(4-9)}$-H, B-box2: CXXH-$X_{(7-9)}$-CXX(C/D/E/H)-$X_{(4)}$-CXXC-$X_{(3-6)}$-H-$X_{(2-4)}$-(H/C) and linchpin position (arrow) are indicated. Dotted line indicates skip.

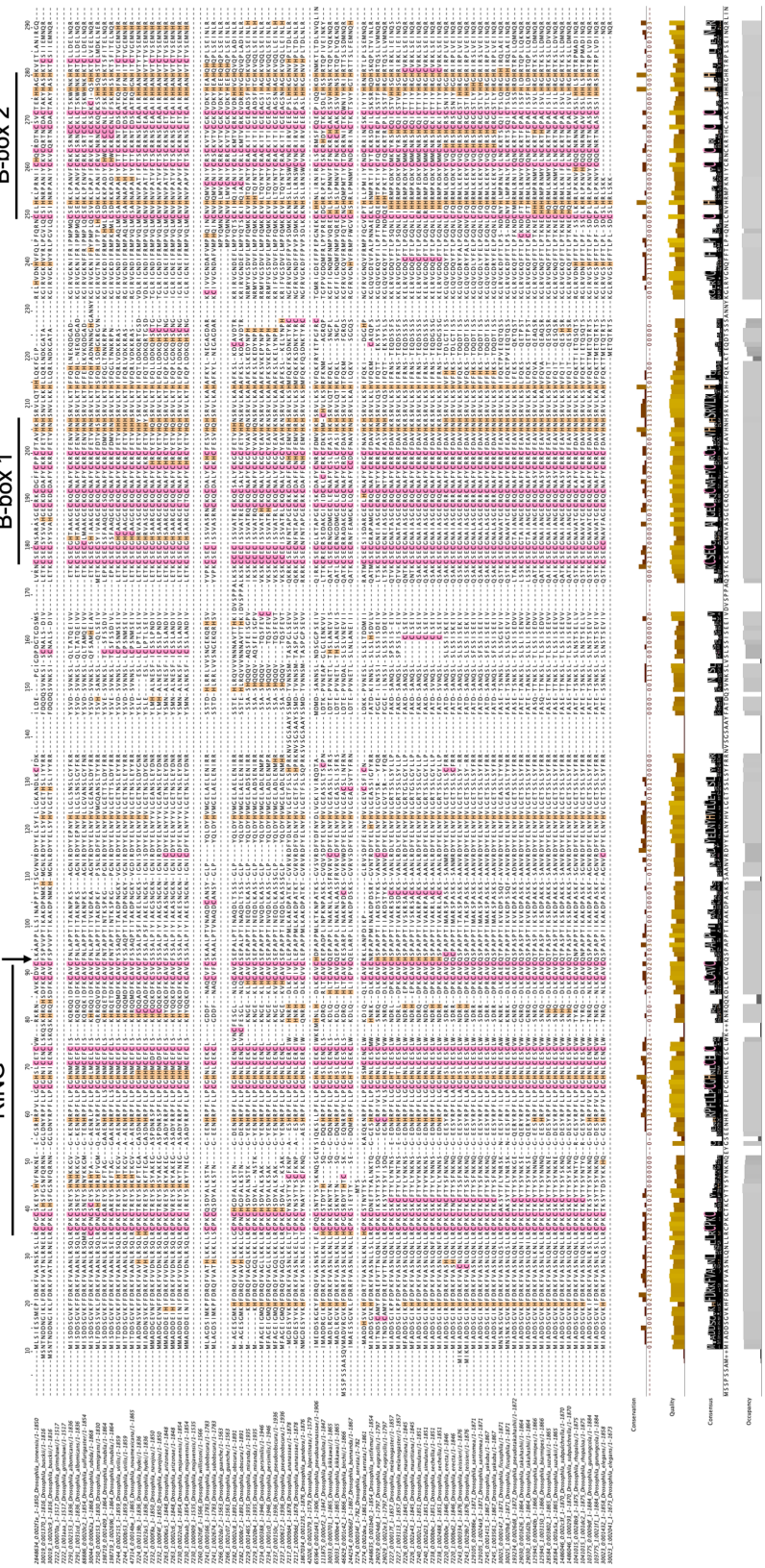



**Figure 1.3 Sequence alignment of N-ter region of Kumo in *Drosophila* species**

RING, B-box1, B-box2 and linchpin are indicated as Figure 1.2.

Structural prediction of the RING domain revealed α-helical structures flanking the core region (Figure 1.1 B). In TRIM family proteins, these α-helices have been reported to interact with another RING domain to form dimers. Similar dimer formation was predicted for Kumo, although the prediction score was low (iPTM = 0.37). In addition, AlphaFold-based structural prediction of Kumo's N-terminal region (including RING, B-box, and coiled-coil) indicated strong binding through the coiled-coil region to form dimers (Figure 1.1 C, iPTM = 0.6). These results suggest that Kumo may function as a dimer.

### 1.2.2 The intact RING domain is essential for nuage localization of Kumo

To examine whether Kumo's RING domain possesses a functional role, I generated a mutant in which the RING domain structure was disrupted (Figure 1.4 A). The RING domain maintains its three-dimensional structure through cysteine residues interacting with zinc ions. Therefore, I created a mutant in which multiple cysteine residues within Kumo's RING domain were substituted with alanine, naming it the C5 mutant ($Kumo^{C5}$). To compare the localization pattern of the C5 mutant with wild-type Kumo, I performed immunostaining of ovaries expressing these transgenes (Figure 1.4 B). Myc-tagged wild-type Kumo (Myc-$Kumo^{WT}$) localized clearly to perinuclear nuage. In contrast, in ovaries expressing Myc-$Kumo^{C5}$, they did not localize to nuage but was broadly dispersed throughout the cytoplasm. This change in localization pattern indicates that the structural integrity of the RING domain is essential for Kumo's proper subcellular localization.

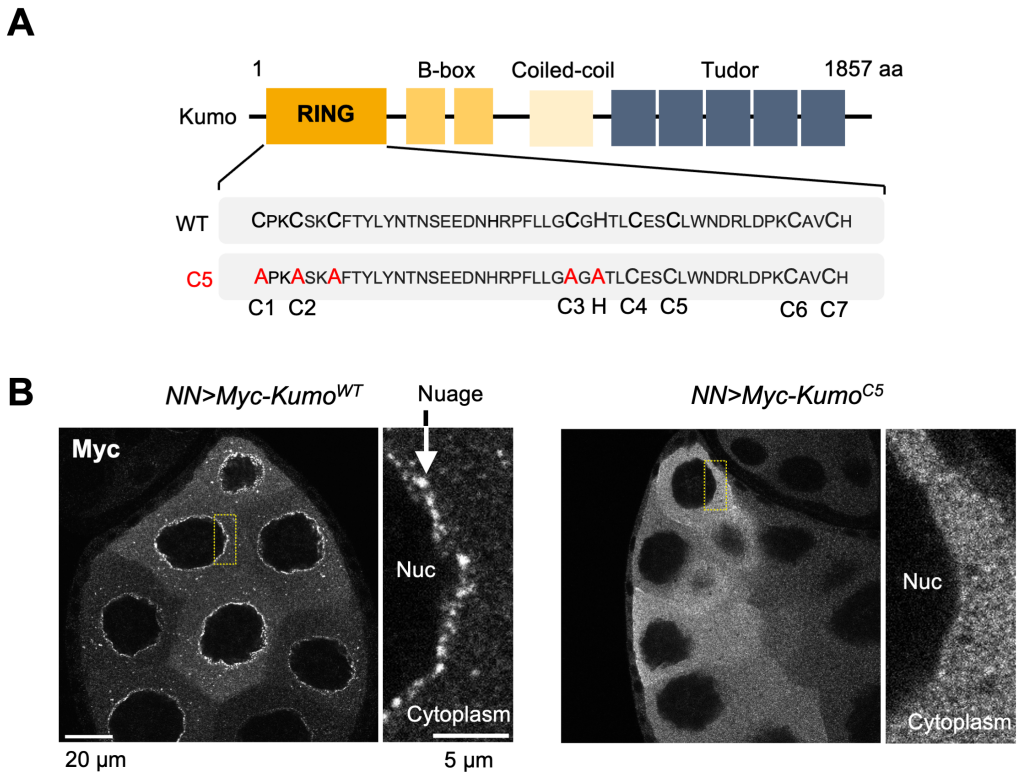



**Figure 1.4 RING domain mutant Kumo dispersed in cytoplasm**

(A) A schematic of Kumo C5 mutant. Four Cys and one His predicted to bind to zinc ion are substituted to Ala in C5 mutant. Although the third Cys is not the core residue according to sequence alignment, I substituted it because it can be served as core referring RING definition. (B) Immunostaining image of ovary expressing Myc-tagged Kumo$^{WT}$ (left) or Kumo$^{C5}$ (right) transgene driven by NN (*nos-Gal4; NGT40*) driver under UASp promoter.

### 1.2.3 The RING domain of Kumo is essential for transposon suppression

Next, to examine whether the RING domain is also important for Kumo's transposon suppression function, I performed rescue experiments. In *kumo* mutants (*Df/kumo*), *HeT-A,* one of transposons, is derepressed, and the translated Gag protein is known to accumulate in oocytes. Therefore, I expressed Myc-Kumo$^{WT}$ or Myc-Kumo$^{C5}$ in *kumo* mutants and evaluated the accumulation level of *HeT-A* gag protein by immunostaining (Figure 1.5). When Myc-Kumo$^{WT}$ was expressed, *HeT-A* gag protein accumulation was markedly suppressed, confirming that transposon suppression function was restored. In contrast, when the Myc-Kumo$^{C5}$ transgene was expressed, *HeT-A* gag protein

accumulated at high levels in oocytes like the mutant. These results indicate that the RING domain structure, or the resulting nuage localization, is essential for Kumo-mediated transposon suppression.

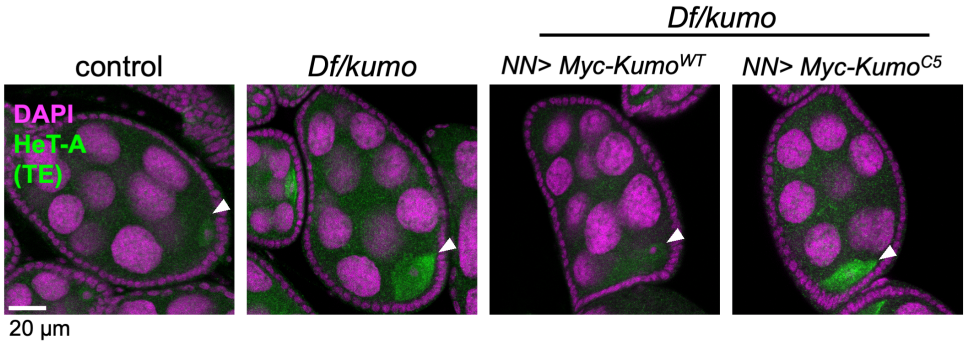



**Figure 1.5 *HeT-A* transposon repression was not recovered in Kumo$^{C5}$ rescue ovary**
Immunostaining image of ovary. *HeT-A* gag protein is accumulated at oocyte (arrowhead) in *kumo* deficiency and Kumo$^{C5}$ rescue condition.

### 1.2.4 Kumo possesses E3 ubiquitin ligase activity *in vitro*

To examine whether the RING domain possesses E3 ubiquitin ligase activity, I established an *in vitro* ubiquitination assay system. RING domain-type E3 ligases interact with E2 enzymes and facilitate ubiquitin transfer to substrates and/or elongation of ubiquitin chains, thereby forming polyubiquitin chains. The E2 enzyme that interacts with Kumo *in vivo* has not been identified, but I used Effete (the *Drosophila* homolog of human UbE2D1/2/3/4), an E2 that has been reported to interact with diverse RING domain-type E3 ligases (Asaoka et al., 2016; Cipressa & Cenci, 2013). In the assay, I incubated E1 enzyme, E2 enzyme (Effete), ubiquitin, ATP, and GFP-tagged Kumo protein, and evaluated ubiquitin chain formation (Figure 1.6 A). *In vitro* assay results confirmed that polyubiquitin chains were formed under conditions where both wild-type Kumo and ATP were present. In contrast, when the C5 mutant was used, ubiquitin chain formation was not observed under the same conditions. Furthermore, in control conditions without E3

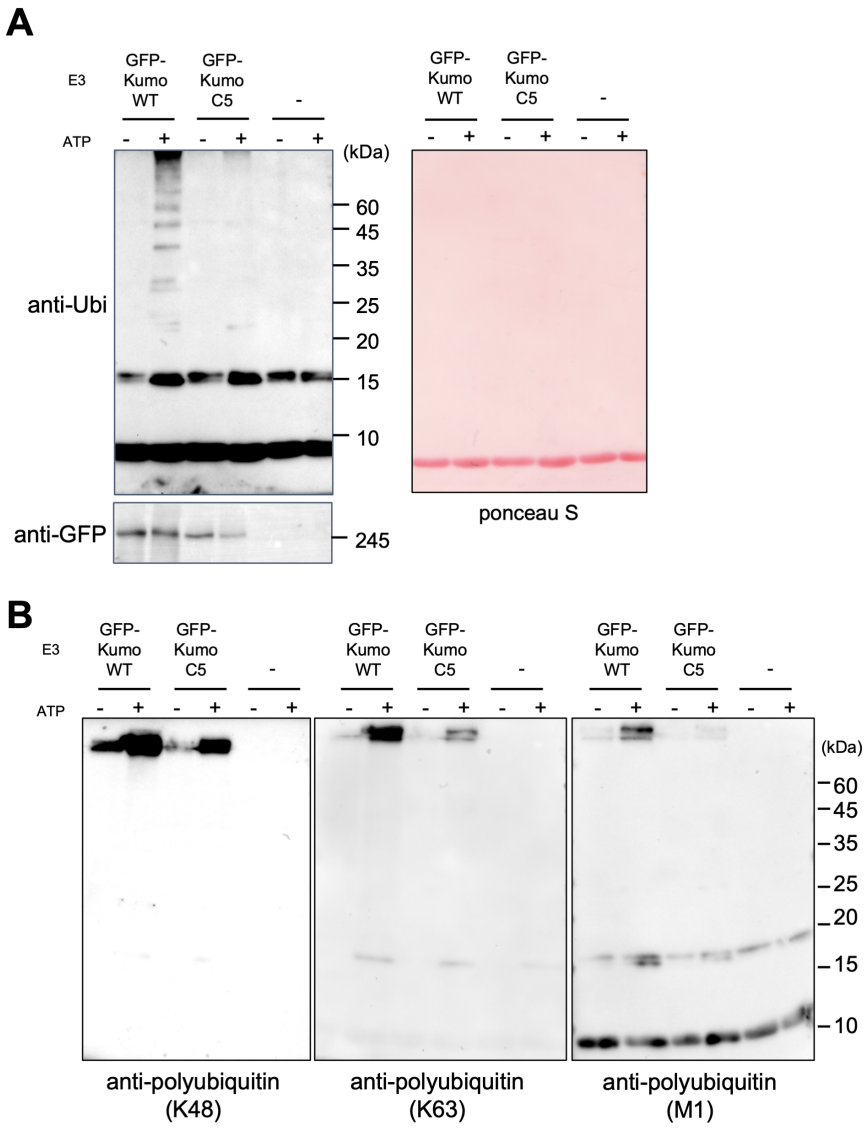



**Figure 1.6 *In vitro* ubiquitination assay reveals ubiquitination activity of Kumo**
Western blot results of *in vitro* ubiquitination assay. Ubiquitin (A, upper left), GFP (A, bottom left), K48-chain (B, left), K63-chain (B, middle) and M1-chain (B, right) blot and ponceau S staining result (A, right) are shown.

ligase, no ubiquitin chain formation was observed. These results indicate that Kumo possesses E3 ubiquitin ligase activity and that this activity depends on the structure of the RING domain.

To examine the type of ubiquitin chains formed by Kumo, I performed blotting using antibodies specific for each chain type (K48, K63, M1). Strong signals were

observed for all chain types, particularly with wild-type Kumo (Figure 1.6 B). This suggests that Kumo may form not a single ubiquitin chain type but various chain types.

### 1.2.5 Kumo undergoes auto-ubiquitination *in vivo*

To identify substrates that Kumo ubiquitinates *in vivo*, I employed a strategy utilizing TUBEs (Tandem Ubiquitin Binding Entities) (Hjerpe et al., 2009; Watanabe et al., 2020; Yoshida et al., 2015). TUBEs are artificial proteins in which multiple ubiquitin-binding domains are arranged in tandem and bind to polyubiquitin chains with high affinity. Proteins carrying K48-type polyubiquitin chains are rapidly degraded by the proteasome *in vivo*, but when TUBEs bind to ubiquitin chains, they protect proteins from degradation, enabling purification and detection of ubiquitinated proteins. To employ this strategy, I created constructs in which HA tag and TUBEs were fused to either the N-terminus or C-terminus of Kumo and expressed them in ovaries. First, I evaluated whether these fusion proteins function as endogenous one by immunostaining (Figure 1.7). I confirmed that TUBEs fused to either the N-terminus or C-terminus localized to nuage, like wild-type Kumo. Additionally, when TUBEs were fused to the C5 mutant, the protein was dispersed throughout the cytoplasm. These findings indicate that TUBE fusion does not affect Kumo localization and that tagged Kumo is functional.

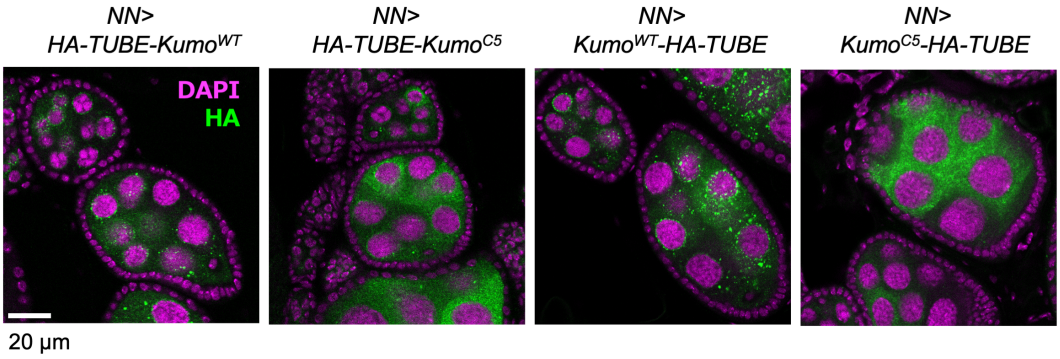



**Figure 1.7 Localization of TUBE-fusion Kumo proteins in ovary**

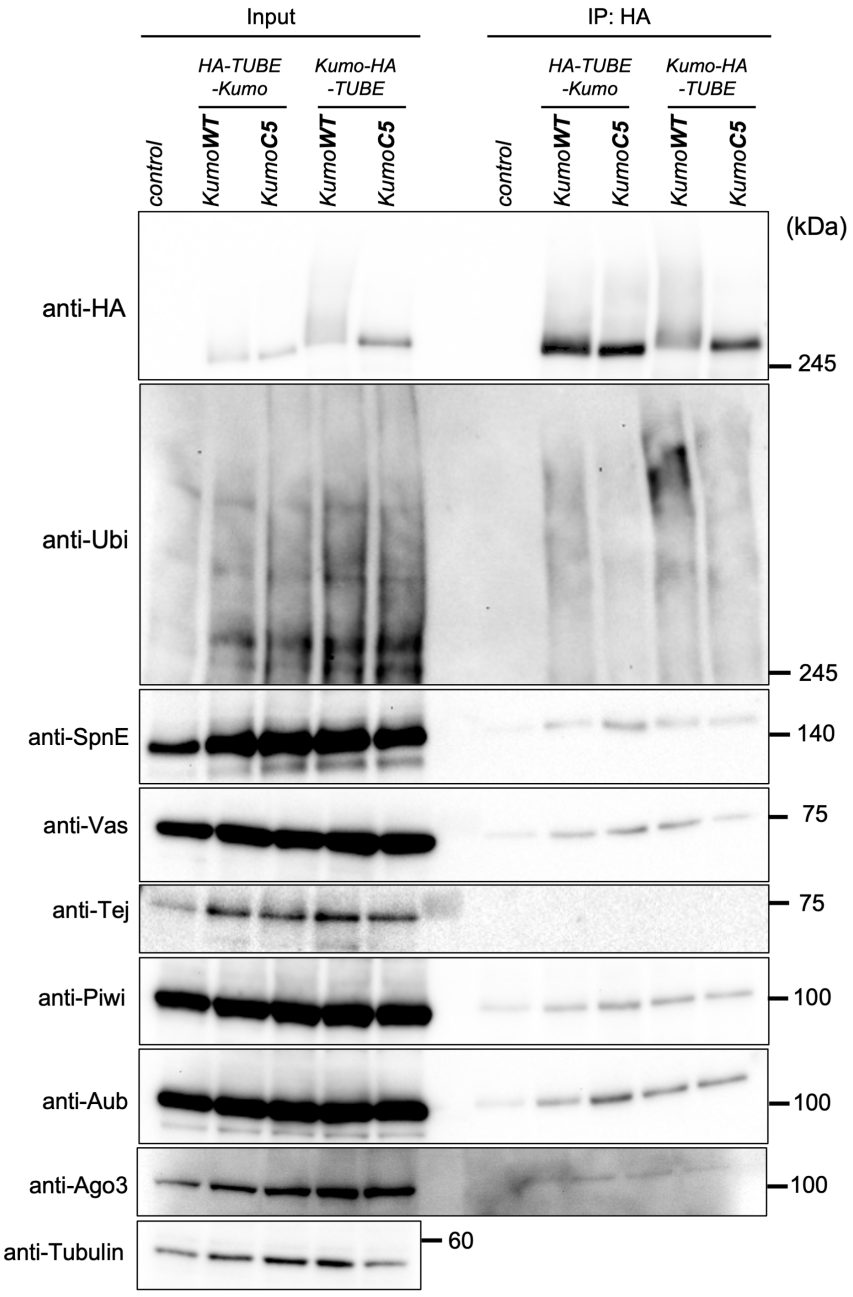



**Figure 1.8 TUBE-fusion Kumo shows auto-ubiquitination *in vivo***

Western blot results of anti-HA-Immunoprecipitation from ovaries indicated at top.

Next, I performed immunoprecipitation using the HA tag from ovaries expressing these TUBE-fused Kumo proteins and conducted Western blot analysis (Figure 1.8). With wild-type Kumo fused with TUBEs at the C-terminus, the anti-HA antibody signal was

detected as a smear toward the high-molecular-weight region. This smear pattern suggests that the Kumo protein was modified with multiple ubiquitin molecules, and it was protected by TUBE. Furthermore, the anti-ubiquitin antibody showed a strong signal at positions corresponding to the wild-type Kumo smear. In contrast, such smear patterns or strong signals with the anti-ubiquitin antibody were not detected with the C5 mutant. Other nuage-localized proteins analyzed by Western blot did not show such smear patterns. These results suggest that Kumo undergoes RING domain-dependent auto-ubiquitination.

## 1.3 Discussion

### 1.3.1 Auto-ubiquitination and RING domain-dependent functions of Kumo

This study revealed that Kumo undergoes RING domain-dependent auto-ubiquitination. In experiments using TUBE fusion proteins, auto-ubiquitination was detected particularly efficiently with Kumo fused with TUBEs at the C-terminus. This observation suggests several possibilities regarding the position of ubiquitination sites and protein tertiary structure. First, the ubiquitination sites may be in close proximity to the C-terminal TUBE in the tertiary structure. In this case, the TUBE could function through two possible mechanisms: in cis, by protecting Kumo's own ubiquitination sites, or in trans, by protecting the ubiquitination sites of the partner Kumo molecule in the predicted dimer. Second, N-terminal TUBE fusion may sterically interfere with the interaction between the RING domain and E2 enzyme, resulting in particularly efficient ubiquitination and protection in the C-terminal fusion construct. Verification of these possibilities will require examination of the tertiary structure of the entire construct including TUBEs and direct identification of ubiquitination sites by mass spectrometry.

I demonstrated that ubiquitination activity of Kumo is essential for its function. The C5 mutant, in which the RING domain structure was disrupted, completely lost *in vitro* ubiquitin ligase activity and lost nuage localization in ovaries. More importantly, the C5 mutant transgene failed to rescue the transposon suppression defect in kumo mutants. These results indicate that the structural integrity of the RING domain and the ubiquitination activity dependent on it are indispensable for Kumo's biological function. Previous studies reported that neither the N-terminal region alone (RING+B-box+coiled-coil) nor the C-terminal region alone (five Tudors) of Kumo localized to nuage when expressed (Anand & Kai, 2012). Together with these results, both the RING domain-dependent function (likely ubiquitination) at the N-terminus and protein-protein interactions via Tudor domains at the C-terminus likely work cooperatively to recruit Kumo to nuage and stably anchor it there. A plausible model is that Tudor domains first interact with piRNA pathway proteins to guide Kumo to the nuage vicinity, after which RING domain-dependent ubiquitination occurs, enabling Kumo or its interaction partners to be stably anchored.

In *Drosophila* species, Kumo retains a His residue (basic amino acid) at the linchpin position of the RING domain and possesses B-box and coiled-coil domains, whereas mammalian RNF17 has the linchpin position substituted with a Glu residue (acidic amino acid) and lacks obvious B-box domains. The basic residue at the linchpin position is known to play an important role when the RING domain interacts with E2 enzyme (Nakasone et al., 2025; Pruneda et al., 2012), and the basic His residue retained by Kumo is thought to support efficient E2 interaction and ubiquitin transfer. In contrast, the acidic Glu residue possessed by RNF17 is predicted to be unfavorable for this interaction, suggesting relatively low E3 ligase activity. Additionally, the B-box domain

is known to contribute to higher-order structure formation in TRIM proteins; for example, in TRIM5α, the B-box 2 domain forms trimeric vertices important for constructing hexagonal lattice structures (Wagner et al., 2016). The B-box domain retained by Kumo may be necessary for its function in the specialized subcellular structure called nuage. However, experimental verification is required to determine what functional differences these structural differences cause.

Intriguingly, despite these structural differences, mammalian RNF17 shares functional commonalities with *Drosophila* Kumo. RNF17 is expressed in germline cells and localizes to cytoplasmic granules (Pan et al., 2005), and *rnf17* deficiency causes spermatogenesis defects and affects the piRNA population (Wasik et al., 2015). This raises important questions about whether RNF17 retains E3 ligase activity or has evolved alternative mechanisms for granule localization and piRNA pathway function. If RNF17 lacks E3 activity yet maintains localization, this would suggest that ubiquitination activity is not universally essential for granule localization, and $Kumo^{C5}$ phenotype may reflect *Drosophila* specific piRNA processing. Conversely, if RNF17 retains E3 activity, the ubiquitination function itself would be evolutionarily conserved despite structural divergence. Distinguishing these possibilities through direct biochemical characterization of RNF17 remains an important direction for future research.

### 1.3.2 Protein modifications and Kumo's role in the piRNA pathway

Recent studies have revealed that post-translational modifications of proteins play important roles in regulating the piRNA pathway. Ubiquitination and SUMOylation have been reported to be involved in the functional regulation of piRNA pathway proteins. Comprehensive analysis by Ninova et al. revealed that heterochromatin and piRNA pathway proteins, including PIWI family proteins, are extensively SUMOylated.

Su(var)2-10 and the SUMO pathway have been shown to link piRNA-mediated target recognition with chromatin silencing, suggesting that SUMOylation plays important roles in downstream effector mechanisms of the piRNA pathway. Such protein modifications may regulate piRNA complex formation, nuclear localization, or interactions with chromatin modifying factors. Regarding Vasa, another important factor involved in the piRNA pathway, regulation by ubiquitination has also been reported. Liu et al. showed that the deubiquitinating enzyme Faf interacts with Vasa and protects Vasa from ubiquitin-dependent degradation. Since Faf deficiency reduces Vasa protein levels and causes defects in germline cell formation, the balance between ubiquitination and deubiquitination is suggested to be important for maintaining Vasa stability and function. These findings indicate that the piRNA pathway is subject to multilayered regulation by protein modifications. This study identified Kumo as an E3 ubiquitin ligase with RING domain-type activity, representing the direct identification of an E3 ligase that catalyzes ubiquitination in the piRNA pathway. Kumo-mediated ubiquitination may provide a new regulatory layer to the piRNA pathway.

Ubiquitination has diverse functions, including regulating substrate protein degradation, localization, activity, or protein-protein interactions (Komander & Rape, 2012; Pickart, 2001; Swatek & Komander, 2016). In the case of Kumo, in addition to auto-ubiquitination, it may ubiquitinate piRNA pathway proteins such as Aub and Ago3, or nuage components, thereby controlling the efficiency of the ping-pong cycle and the dynamics of piRNA complexes. Although this study detected Kumo's auto-ubiquitination using TUBE-fused Kumo, Western blot analysis of other nuage-localized proteins did not reveal smear patterns indicative of ubiquitination. This suggests that Kumo-mediated substrate ubiquitination may be a transient modification occurring at low frequency, or

that ubiquitinated substrates are rapidly degraded and difficult to detect at steady state. Comprehensive substrate identification using mass spectrometry and other approaches will be necessary in the future.

This study opens a new door to understanding ubiquitination control in the piRNA pathway. Kumo's discovery revealed that the piRNA pathway is subject to precise regulation by ubiquitination. Through substrate identification, and determination of ubiquitination sites and chain types deeper understanding of the molecular basis of genome defense mechanisms in germline cells is expected. Such integrated understanding will reveal the complete picture of multilayered regulatory mechanisms in the piRNA pathway and highlight the importance of post-translational modifications in germline development and genome stability maintenance.

# 2. Proximity proteomics reveals Set1 as a key regulator of piRNA-directed TE silencing

## 2.1 Introduction

### 2.1.1 Challenges in identifying piRNA pathway components

piRNA-directed TE silencing is achieved through interactions between PIWI proteins and other components. These include nuclear factors involved in Piwi-piRNA-directed target heterochromatinization (e.g., Panx, Nxf2, SetDB1/Eggless) (Batki et al., 2019; Fabry et al., 2019; Murano et al., 2019; Sienski et al., 2015; Y. Yu et al., 2015; Zhao et al., 2019). In cytoplasm, Tudor domain proteins (Krimper, Tejas, Tapas, Qin/Kumo, Kots) and RNA helicases (Spn-E, Vas) are enriched in nuage and support the ping-pong cycles mediated by Aub and Ago3 (Anand & Kai, 2012; Handler et al., 2011; Kawaguchi et al., 2025; Lim and Kai, 2007; Lin et al., 2023; Wang et al., 2023; Webster et al., 2015; Z. Zhang et al., 2011). Nonetheless, characterizing the interactions between PIWI members and other factors are often challenging because of their dynamics in piRNA biogenesis and TE silencing. Hence, the repertoire of piRNA pathway components is heretofore unelucidated, and our understanding of piRNA-directed TE silencing remains incomplete.

### 2.1.2 Proximity-dependent biotin labelling as a tool for studying protein interactions

Proximity-dependent biotin labelling (BioID/TurboID) is a powerful tool for characterizing the physical interactions and proximity relationships of proteins *in vivo* (Branon et al., 2018; Choi‐Rhee et al., 2004; Roux et al., 2012). These techniques rely on the promiscuous biotin ligase activity exhibited by BirA derived from Escherichia coli. The engineered BirA variants lack substrate specificity and catalyze biotinylation of lysine residues on proteins within approximately 10 nm radius (Branon et al., 2018;

Choi‐Rhee et al., 2004; Roux et al., 2012). By fusing BirA variants to a protein of interest, researchers can label and subsequently purify proteins in its physical proximity, followed by mass spectrometry identification. TurboID utilizes an efficient and compact BirA variant called mini(m)Turbo established through directed evolution (Branon et al., 2018). Compared to the original BioID, TurboID exhibits enhanced enzymatic activity, allowing shorter labeling time and reduced expression levels, which minimizes potential toxicity and perturbation to cellular processes.

Unlike conventional approaches, proximity labeling offers several advantages for studying piRNA pathway. First, it captures transient or weak interactions that may be lost during cell lysis and immunoprecipitation. Second, it can identify proteins that are spatially proximal but do not necessarily form stable complexes. Third, biotinylation occurs in living cells, preserving the native subcellular context. These features make proximity labeling particularly suitable for dissecting the dynamic molecular networks underlying piRNA biogenesis and TE silencing.

### 2.1.3 Set1 and COMPASS complex: conserved regulators of transcription

Set1 is a highly conserved histone methyltransferase responsible for catalyzing the methylation of histone 3 at lysine 4 (H3K4), a modification associated with transcriptionally active chromatin. Set1 was originally identified in *Saccharomyces cerevisiae* as a member of the COMPASS (Complex of Proteins Associated with Set1) complex (Briggs et al., 2001; Miller et al., 2001). The COMPASS complex contains multiple subunits that regulate Set1's catalytic activity and substrate specificity, enabling the precise deposition of H3K4 methylation at gene promoters and enhancers (Ardehali et al., 2011; Briggs et al., 2001; Jaiswal et al., 2017). H3K4 can be mono-, di-, or tri-methylated (H3K4me1, H3K4me2, H3K4me3), and these different methylation states are

associated with distinct chromatin contexts and regulatory functions (Barski et al., 2007; Shilatifard, 2012; H. Yu & Lesch, 2024). H3K4me3 is predominantly found at active gene promoters and correlates with high transcriptional activity. H3K4me1 is enriched at enhancers and other distal regulatory elements, while H3K4me2 shows broader distribution and may mark both active promoters and poised regulatory regions. In *Drosophila*, Set1 specifically catalyzes H3K4me2 and H3K4me3, but not H3K4me1, which is deposited by other methyltransferases such as Trithorax (Trx) (Ardehali et al., 2011; Miller et al., 2001; Mohan et al., 2011). In contrast, mammalian COMPASS complexes can generate all three methylation states in a processive manner, with their catalytic activity being modulated by associated subunits (Shilatifard, 2012). In mammals, Set1 has two orthologues, SETD1A and SETD1B, which form COMPASS-like complexes. Additionally, mammals possess the MLL (Mixed Lineage Leukemia) family proteins (MLL1-4), which share the SET domain with Set1 and catalyze H3K4 methylation (Sugeedha et al., 2021). These mammalian COMPASS and MLL complexes play critical roles in development, cell differentiation, and disease, highlighting the conserved importance of H3K4 methylation in gene regulation (Crump & Milne, 2019).

In *Drosophila*, Set1 is encoded by a single gene and functions as part of the COMPASS complex analogous to that in yeast and mammals (Ardehali et al., 2011; Mohan et al., 2011). *Drosophila* COMPASS subunits include Rbbp5, Wdr82, Wds and Ash2, which are conserved across species (Mohan et al., 2011). Previous studies have demonstrated that *Drosophila* Set1 is essential for proper development and cell differentiation. Loss of Set1 function results in developmental defects and lethality, consistent with its role as a global transcriptional regulator (Ardehali et al., 2011; Hallson et al., 2012). In the male germline, Set1 has been shown to be required for

spermatogenesis, with Set1 mutants exhibiting defects in testis development and sperm production (Vidaurre et al., 2024). However, the function of Set1 in the female germline and its potential involvement in piRNA-directed TE silencing have not been previously investigated.

Recent studies in yeast have revealed that Set1 possesses functions independent of its catalytic activity. Set1 can repress gene expression and regulate chromatin organization in subtelomeric regions through H3K4 methylation-independent mechanisms (Jezek et al., 2023; Lorenz et al., 2012). These findings suggest that Set1 may function not only as an enzyme but also as a structural or scaffolding protein that recruits other regulatory factors to chromatin. Whether *Drosophila* Set1 also exhibits catalytic activity-independent functions remains an open question.

### 2.1.4 Diversity of piRNA cluster transcription mechanisms

piRNA precursors are mainly transcribed from genomic loci called piRNA clusters, which are composed of fragmented and truncated TE sequences accumulated over evolutionary time. Intriguingly, not all piRNA clusters are regulated by the same molecular mechanisms. Recent studies have revealed remarkable diversity in the transcriptional control of different piRNA clusters, with distinct clusters requiring different sets of chromatin modifiers and transcription factors.

The Rhino-Deadlock-Cutoff (RDC) complex represents a well-characterized pathway for piRNA precursor transcription in *Drosophila* germline cells (Chen et al., 2021; Mohn et al., 2014). Rhi, a HP1 paralogue, recognizes H3K9me3 marks at dual-strand piRNA clusters and recruits Del and Cuff to promote noncanonical transcription. The RDC pathway is responsible for transcribing many major germline piRNA clusters,

and loss of RDC components leads to severe reduction of piRNAs and widespread TE derepression (Mohn et al., 2014).

Beyond RDC, recent studies highlight other chromatin modifiers and transcription factors contribute to cluster-specific transcription. For example, Kipferl, a DNA-binding protein, is required for piRNA precursor transcription from specific cluster loci but not others (Baumgartner et al., 2022). Similarly, E(z) (Enhancer of zeste), the *Drosophila* orthologue of mammalian EZH2 and the catalytic subunit responsible for H3K27me3 deposition, has been implicated in the regulation of certain piRNA clusters (Akkouche et al., 2025). These findings highlight that piRNA cluster transcription is not governed by a single universal mechanism but rather employs a diverse array of regulatory strategies tailored to individual clusters.

### 2.1.5 Overview of this chapter

In order to deepen the understanding of piRNA-directed TE silencing, this study explored the proximity factors of individual PIWI proteins expressed in germline cells. Using TurboID-based proximity labeling followed by mass spectrometry, I characterized the proteomes in the physical proximity of Piwi, Aub, and Ago3. The obtained proximity proteome not only confirmed reported interactions but also revealed unrecognized links between PIWI proteins and other factors. Moreover, PIWI proximity proteome contained a list of factors which have not been characterized in piRNA pathway thus far.

To identify functionally relevant factors among the proximity proteome, I conducted a germline knockdown (GLKD) screening, examining the effects of individual factor depletion on nuage integrity and TE silencing. This screening identified Set1 as a proximity factor of Piwi that is crucial for TE silencing. Given Set1's known role as a

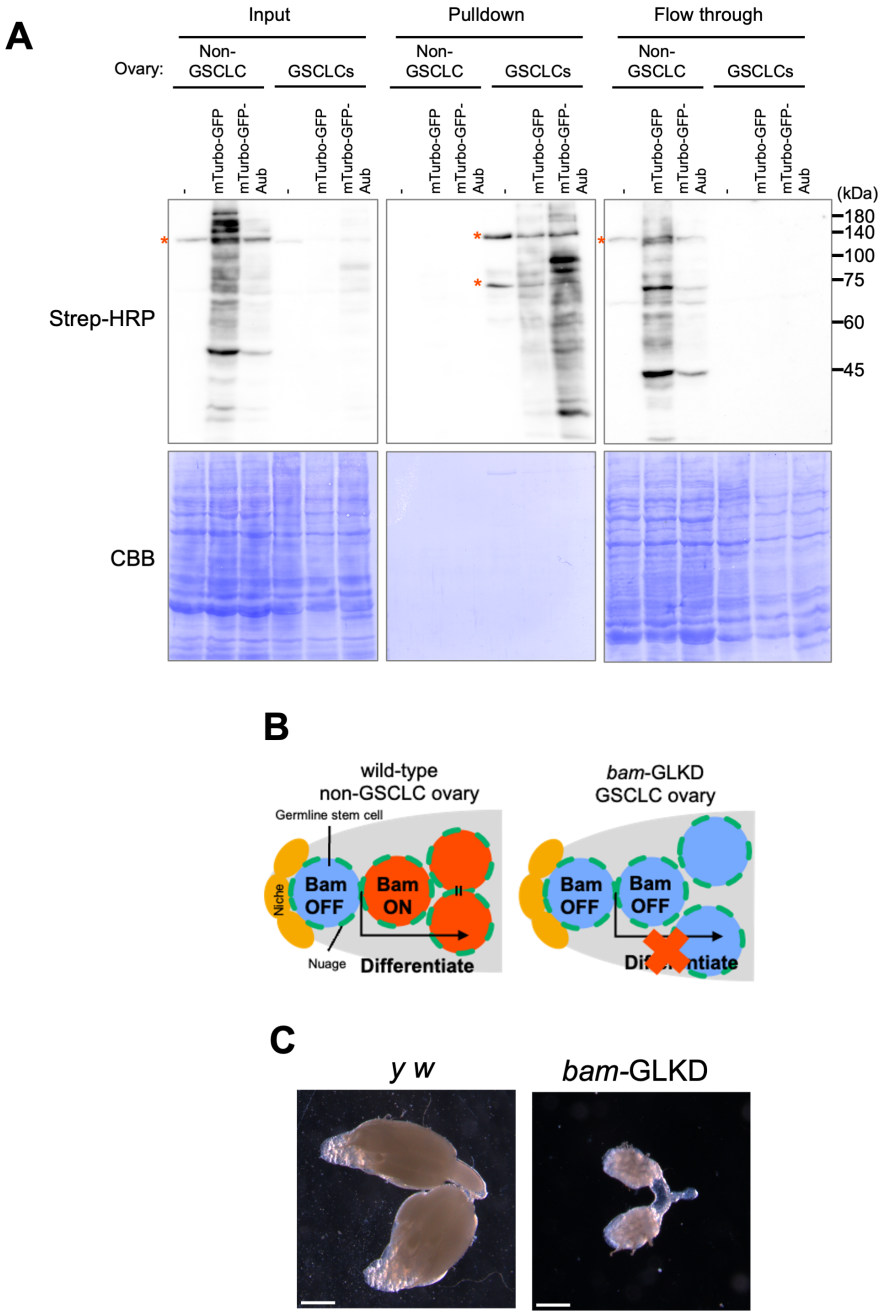
transcriptional activator through H3K4 methylation, I hypothesized that Set1 might be involved in piRNA precursor transcription from specific cluster loci.

This chapter father describes the characterization of Set1's function in piRNA-directed TE silencing. I demonstrate that Set1 is especially important for silencing telomeric *HTT* families and that this function is associated with piRNA precursor transcription from subtelomeric clusters. Through transcriptome profiling, piRNA sequencing, and chromatin profiling, I reveal that Set1 functions in both catalytic activity-dependent and -independent manners to maintain the unique chromatin landscape at subtelomeric piRNA clusters. Furthermore, I show that Set1 physically interacts with Piwi and cooperates in establishing heterochromatin at piRNA cluster loci. These findings highlight the hitherto unappreciated importance of Set1 in PIWI/piRNA-directed silencing and illuminate the diverse regulatory strategies employed for piRNA precursor transcription from different genomic contexts.

## 2.2 Results

### 2.2.1 Labelling of PIWI proximity factors and purification from germline cells

To characterize the proximity proteome of PIWI proteins using TurboID, I generated a series of transgenes encoding mTurbo-GFP-fused Piwi, Aub, or Ago3. These transgenes were expressed in ovarian germline cells under the control of *nos* promoter activity (UASp/Gal4 binary system using *NGT40*; *nos-Gal4* (NN) driver) (Grieder et al., 2000; Rørth, 1998). The biotinylation activities of individual fusion proteins were confirmed in the proteins extracted from ovaries (Figure 2.1 A). However, pulldown using streptavidin was inefficient and biotinylated proteins largely remained in the flow through fraction, possibly due to interfering factors accumulated during oocyte differentiation. To circumvent this technical challenge, I shifted to using germline stem cell-like cells




(GSCLCs) ovaries, in which differentiation was arrested by depletion of a differentiation factor bag of marbles (bam) via germline knockdown (GLKD) (Figure 2.1 B, C) (McKearin & Spradling, 1990). Although TurboID in GSCLC showed weaker biotinylation signals in the input, the pulldown efficiency was dramatically improved (Figure 2.1 A).

**Figure 2.1 Optimization of germline PIWI proximity labelling and purification**
(A) Efficiency of protein biotinylation and purification was compared between non-GSCLC and GSCLC ovaries. Upper panels; signals from streptavidin-HRP. Lower panels; Coomassie brilliant blue (CBB) staining serving as protein loading control. Ovaries expressing mTurbo-GFP or mTurbo-GFP-Aub were analyzed with negative control (without mTurbo fusion protein). Asterisks indicate non-specific signals. (B) Schematic illustration for germline differentiation and the function of Bam. Left; the germarium in wild-type ovaries. A germline stem cell (GSC, blue) divides to produce a daughter cell (red) that is sufficiently distant from the niche to express Bam, initiating differentiation. For simplicity, the drawing of 2–3 GSCs maintained in a germarium was omitted. Right: bam-GLKD ovaries, where daughter cells fail to differentiate and accumulate as GSCLCs. (C) A pair of wild-type ovaries (*y w*, left) and that of *bam*-GLKD ovaries (right) were observed under light microscopy. *bam*-GLKD ovaries do not produce eggs and are smaller than wild-type ovaries. Scale bar: 1 mm.

In GSCLCs, mTurbo-GFP alone showed a broad distribution pattern in nucleus and cytoplasm (Figure 2.2 A, B). In contrast, mTurbo-GFP-PIWI proteins exhibited subcellular localizations that resemble those of endogenous proteins; Piwi accumulated in nucleus, while Aub and Ago3 were enriched in the perinuclear nuage. The consistency suggests that N-terminal mTurbo-GFP fusions did not impair the functions of individual PIWI members. Notably, steady-state levels of fusion proteins varied between PIWI members. mTurbo-GFP-Ago3 protein was barely detectable in the input (Figure 2.2 C, anti-GFP), accounting for the weak biotinylation signals in Ago3-TurboID (Figure 2.2 C, Strep-HRP). Nevertheless, the streptavidin pulldown fractions displayed unique biotinylation signals, suggesting the enrichment of distinct factors in individual PIWI-TurboID conditions.

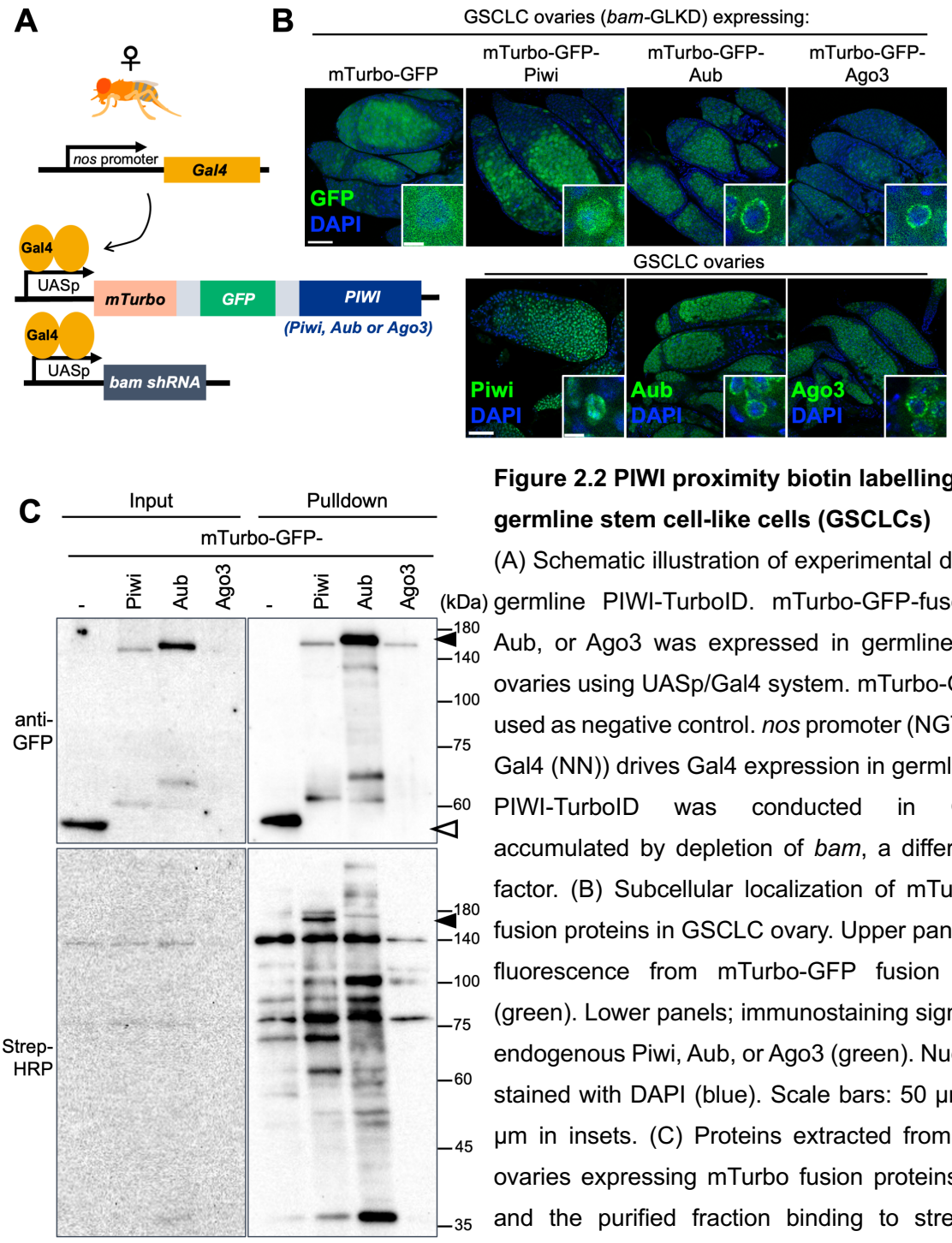



**Figure 2.2 PIWI proximity biotin labelling in germline stem cell-like cells (GSCLCs)**

(A) Schematic illustration of experimental design for germline PIWI-TurboID. mTurbo-GFP-fused Piwi, Aub, or Ago3 was expressed in germline cells of ovaries using UASp/Gal4 system. mTurbo-GFP was used as negative control. *nos* promoter (NGT40;*nos*-Gal4 (NN)) drives Gal4 expression in germline cells. PIWI-TurboID was conducted in GSCLCs accumulated by depletion of *bam*, a differentiation factor. (B) Subcellular localization of mTurbo-GFP fusion proteins in GSCLC ovary. Upper panels; GFP fluorescence from mTurbo-GFP fusion proteins (green). Lower panels; immunostaining signals from endogenous Piwi, Aub, or Ago3 (green). Nuclei were stained with DAPI (blue). Scale bars: 50 μm, and 5 μm in insets. (C) Proteins extracted from GSCLC ovaries expressing mTurbo fusion proteins (Input), and the purified fraction binding to streptavidin-conjugated magnet beads (Pulldown). Upper panels; immunoblotting using anti-GFP. Lower panels; signals from Streptavidin-HRP. White and black arrowheads indicate mTurbo-GFP and mTurbo-GFP-PIWI proteins, respectively.

### 2.2.2 Characterization of germline PIWI proximity proteomes

Mass spectrometry analysis and the label-free quantification (LFQ) of streptavidin pulldown samples identified the proximity factors of individual PIWI proteins (average abundance ratios >1 compared to the control GFP-TurboID conditions in biological duplicates). These included 37, 33, and 49 factors for Piwi, Aub, and Ago3, respectively (Figure 2.3 A, B). Notably, the identified proximity factors contained known piRNA pathway components (Figure 2.3 A, highlighted; Table 2.1), and the significant enrichment was confirmed by Gene Ontology (GO) analysis (Figure 2.3 C). These results suggest that the proteome reflects the physical and functional interactions between PIWI members and other factors in germline cells.

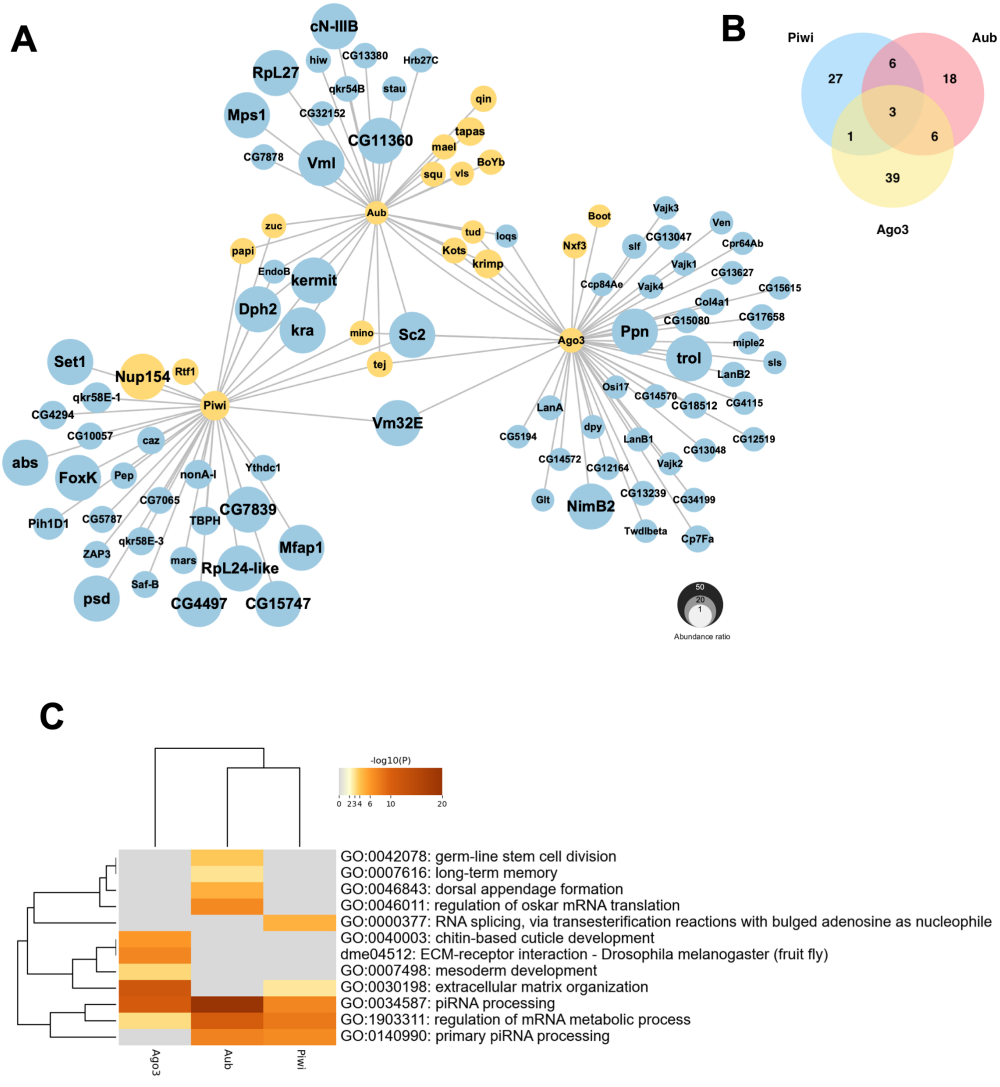


**Figure 2.3 Proximity proteome of PIWI proteins in germline cells**

(A) Network diagram summarizes the proximity factors of individual PIWI members (Piwi, Aub, and Ago3) identified by nanoLC-MS/MS measurement and label-free quantification. Yellow nodes indicate the factors involved in piRNA pathway. Circle size reflects the mean of abundance ratio (mTurbo-GFP-PIWI/mTurbo-GFP) of biological duplicates samples. TurboID was conducted twice from independent crosses. (B) Venn diagram shows the number of proximity proteins uniquely identified by one of PIWI members and that shared by multiple PIWI members. (C) GO enrichment analysis of proximity factors. Hierarchical clustering and heatmap show significantly enriched GO terms given by the identified PIWI proximity factors. Color intensity represents the significance of enrichment (-log10 p-value).

**Table 2.1 Known piRNA pathway components identified in PIWI proximity proteomes**

| **Proximity category** | ***gene*** | **Known interaction with PIWI** | **Localization** | **References** |
|---|---|---|---|---|
| Piwi+Aub+Ago3 | *mino* | | mitochondria | (Vagin et al., 2013) |
| Piwi+Aub+Ago3 | *tej* | Piwi, Aub, Ago3 | nuage | (Lin et al., 2023; Patil & Kai, 2010) |
| Piwi+Aub | *papi* | Piwi, Ago3 | mitochondria | (Hayashi et al., 2016; L. Liu et al., 2011; Y. Zhang et al., 2018) |
| Piwi+Aub | *zuc* | Piwi, Aub, Ago3 | mitochondria | (Haase et al., 2010; H. Huang et al., 2014; Pane et al., 2007) |
| Aub+Ago3 | *kots* | Aub, Ago3 | nuage | (L.-X. Lim et al., 2022) |
| Aub+Ago3 | *krimp* | Aub, Ago3 | nuage | (X. Huang et al., 2021; Sato et al., 2015; Webster et al., 2015) |
| Aub+Ago3 | *tud* | Aub, Ago3 | nuage, pole granule | (Kirino et al., 2010; Nishida et al., 2009) |
| Piwi | *rtf1* | | nucleus | (Clark et al., 2017) |

| Proximity category | *gene* | Known interaction with PIWI | Localization | References |
|---|---|---|---|---|
| Piwi | *nup154* | | nucleus | (Muerdter et al., 2013) |
| Aub | *boYb* | | nuage | (Handler et al., 2011) |
| Aub | *mael* | Piwi | nucleus, nuage | (Findley et al., 2003; Onishi et al., 2020; Sienski et al., 2012) |
| Aub | *qin* | Aub | nuage | (Anand & Kai, 2012; Z. Zhang et al., 2011) |
| Aub | *squ* | Aub, Piwi | nuage | (Haase et al., 2010; Pane et al., 2007) |
| Aub | *vls* | Aub | nuage | (X. Huang et al., 2021) |
| Aub | *tapas* | Aub, Ago3 | nuage | (Patil et al., 2014) |
| Ago3 | *boot* | | nucleus, nuage | (ElMaghraby et al., 2019; Kneuss et al., 2019) |
| Ago3 | *nxf3* | | nucleus, nuage | (ElMaghraby et al., 2019; Kneuss et al., 2019) |

### 2.2.3 Screening of PIWI proximity factors involved in piRNA production and TE silencing

Most factors identified in the proximity of PIWI members have not been functionally characterized in piRNA pathway or TE silencing. Hence, I investigated the possible involvement of 54 factors, for which short hairpin-based RNAi lines were available, by germline knockdown (GLKD) screening. Given that impaired piRNA biogenesis can be associated with nuage collapse and mislocalization of its components, I examined the localization of Krimp, a key scaffold of nuage (A. K. Lim & Kai, 2007; Sato et al., 2015;

Webster et al., 2015). In parallel, I observed the accumulation of Gag protein encoded by a nonLTR retroelement *HeT-A*, as a readout of TE derepression (Shpiz et al., 2011). I confirmed that GLKD of *aub* leads to the mislocalization of Krimp and the accumulation of *HeT-A* Gag in the oocytes of developing egg chambers (Figure 2.4 A).

GLKD screening identified several factors including Hrb27C and Set1, the proximity factor of Aub and Piwi, respectively (Figure 2.3 A). Both factors are conserved across eukaryotes, and their molecular and physiological functions have been characterized. Hrb27C (also known as Hrp48) is an hnRNP family member, regulating the translation and localization of interacting mRNAs, required for germline stem cell maintenance and differentiation (Goodrich et al., 2004; Lomoschitz et al., 2025; Yano et al., 2004). Set1 is a SET domain-containing enzyme responsible for di- and tri-methylation of histone H3 at lysine 4 (H3K4me2/3) at gene promoters and functioning as transcriptional activator (Ardehali et al., 2011; Hallson et al., 2012; Vidaurre et al., 2024). *hrb27C*-GLKD and *set1*-GLKD showed distinct phenotypes. In *hrb27C*-GLKD, Krimp failed to localize in nuage, forming small foci in the cytoplasm, while *HeT-A* Gag accumulation was under detectable level (Figure 2.4 A). Conversely, in *set1*-GLKD, the accumulation of *HeT-A* Gag was clearly observed, while Krimp was merely affected and remained in perinuclear nuage. RT-qPCR confirmed the downregulation of *aub*, *hrb27C* and *set1* in their GLKD conditions (Figure 2.4 C). Of note, their proximity partners, Aub and Piwi did not show discernible changes in localization in *hrb27c*- and *set1*-GLKD, respectively (Figure 2.4 B).

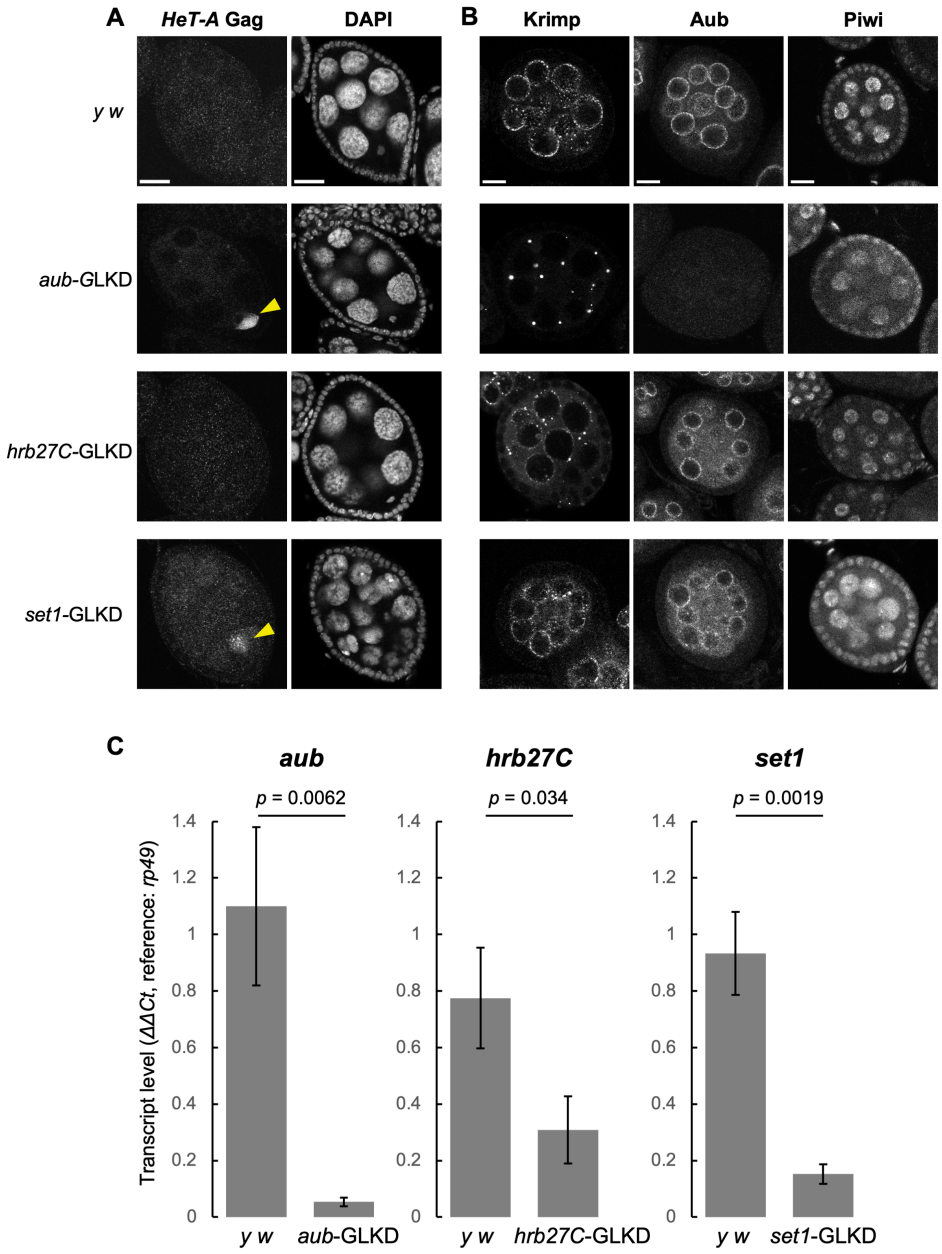



**Figure 2.4 Germline knockdown (GLKD) screening of PIWI proximity factors**

(A) Immunofluorescence signals from *HeT-A* Gag protein (left panels) in egg chambers of control (*y w*) or GLKD of indicated genes. Nuclei stained with DAPI (right panels). Arrowheads highlight the accumulation of HeT-A Gag in oocyte. Scale bars; 20 μm.(B) Immunofluorescence signals show the localization of Krimp (nuage), Aub (nuage), and Piwi (nucleus) in an egg chamber of control (*y w*) or GLKD of indicated genes. Scale bars; 10 μm. Transcript levels of *aub*, *hrb27C* and *set1* upon individual GLKD were measured by *ΔΔ*Ct method using *rp49* as reference. Error bars are standard deviation (SD) from three biological replicates. *p* values of unpaired Student's t-test are indicated.

### 2.2.4 Set1 and Hrb27C control distinct TE families in germline cells

To investigate the global effect of *hrb27C*- and *set1*-GLKDs on the expression of TEs, I compared their transcriptomes with that in control *gfp*-GLKD (Figure 2.5 A, B). Transcriptome was analyzed using RNAs extracted from whole ovaries. The analysis also included a condition of ovaries accumulating germline stem cell-like cells (GSCLCs) where PIWI proximity proteome was characterized. To understand the baseline differences between non-GSCLC vs. GSCLC ovaries, I compared the transcriptomes of control *gfp*-GLKD ovaries and found that many TE families are more abundant in GSCLC ovaries (Figure 2.5 C). This feature would account for the milder derepression of TEs upon *aub*-GLKD in GSCLC ovaries (Figure 2.5 A, B).

Unlike *aub*-GLKD, *hrb27C*-GLKD did not show clear derepression of TEs in the non-GSCLC ovaries (Figure 2.5 A). Contrastively, TE derepression was recognized in GSCLC condition, albeit at weaker levels compared to *aub*-GLKD (Figure 2.5 B). Nonetheless, the derepression patterns showed positive correlation between *hrb27C*- and *aub*-GLKDs (r = 0.57, Figure 2.5 D), supporting the notion that Hrb27C has a function associated with Aub in GSCLCs.

Transcriptome analysis revealed that *set1*-GLKD caused remarkable derepression of selected TEs in non-GSCLC ovaries (Figure 2.5 A). These included *HeT-A*, consistent with its Gag protein accumulation (Figure 2.4 A), together with *TAHRE* and *TART*, the other two *HTT* family (Villasante et al., 2007). Beside *HTT*, LTR retrotransposons including *gypsy12* and *HMS-Beagle* represented the derepressed TEs in *set1*-GLKD ovaries (Figure 2.5 A). However, the derepression pattern was not correlated with that in *aub*-GLKD (r = -0.02, Figure 2.5 E, left). Similarly, no clear correlation was seen between *set1*- and *aub*-GLKD in GSCLC setting (r = 0.13, Figure 2.5 E, right). Of note, *HTT* derepression was much milder in GSCLC of *set1*-GLKD (Figure 2.5 B).

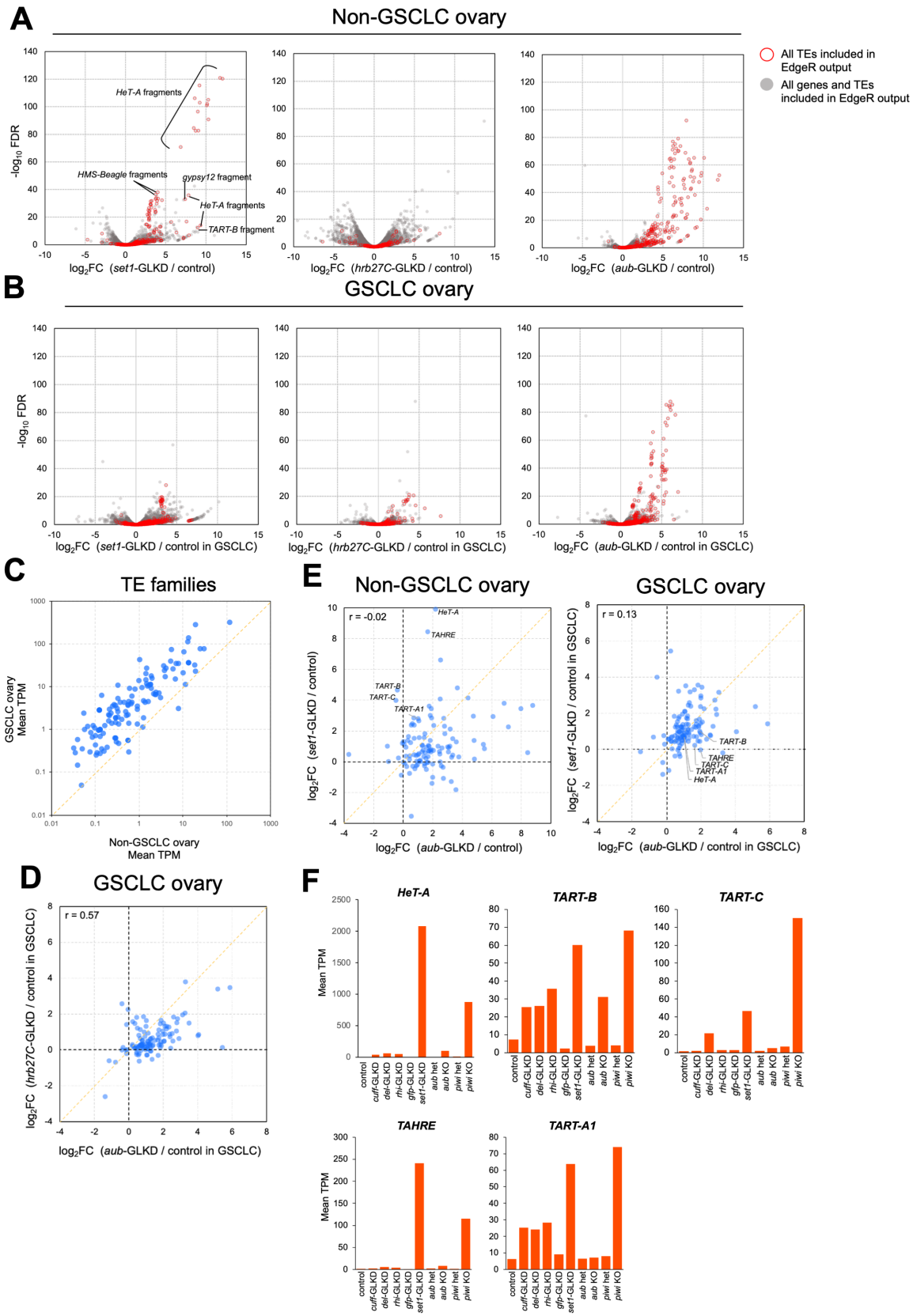

A
Non-GSCLC ovary
All TEs included in EdgeR output
All genes and TEs included in EdgeR output
HeT-A fragments
HMS-Beagle fragments
gypsy12 fragment
HeT-A fragments
TART-B fragment
-log10 FDR
log2FC (set1-GLKD / control)
log2FC (hrb27C-GLKD / control)
log2FC (aub-GLKD / control)
B
GSCLC ovary
log2FC (set1-GLKD / control in GSCLC)
log2FC (hrb27C-GLKD / control in GSCLC)
log2FC (aub-GLKD / control in GSCLC)
C
TE families
GSCLC ovary Mean TPM
Non-GSCLC ovary Mean TPM
D
GSCLC ovary
r = 0.57
log2FC (hrb27C-GLKD / control in GSCLC)
log2FC (aub-GLKD / control in GSCLC)
E
Non-GSCLC ovary
GSCLC ovary
r = -0.02
r = 0.13
HeT-A
TAHRE
TART-B
TART-C
TART-A1
log2FC (set1-GLKD / control)
log2FC (set1-GLKD / control in GSCLC)
log2FC (aub-GLKD / control)
log2FC (aub-GLKD / control in GSCLC)
F
HeT-A
TART-B
TART-C
TAHRE
TART-A1
Mean TPM
control
cuff-GLKD
del-GLKD
rhi-GLKD
gfp-GLKD
set1-GLKD
aub het
aub KO
piwi het
piwi KO

**Figure 2.5 Effect of GLKD on TE transcript levels in non-GSCLC and GSCLC ovaries**
(A) Non-GSCLC ovary transcriptome comparison. Dots in the volcano plots show individual genes (gray dots) and TEs (gray dots with red circle) included in the differential expression analysis (EdgeR). Expression (TPM) in *set1*-GLKD (left), *hrb27C*-GLKD (middle), or *aub*-GLKD (right) was compared to those in the control (*gfp*-GLKD). (B) GSCLC ovary transcriptome comparison. Differential expression analysis outputs were displayed as in the non-GSCLC ovaries. (C) Scatter plot compares the expression levels (TPMs) of individual TE families between non-GSCLC and GSCLC ovaries in control *gfp*-GLKD condition. (D) Scatter plot compares the fold changes (*hrb27C*-GLKD/*gfp*-GLKD and *aub*-GLKD/*gfp*-GLKD) of transcript levels (TPMs) for individual TE families in GSCLC ovaries. r; Pearson correlation coefficient. (E) Scatter plot compares fold changes (*set1*-GLKD/*gfp*-GLKD and *aub*-GLKD/*gfp*-GLKD) of transcript levels (TPMs) for individual TE families in non-GSCLC ovaries (left) or GSCLC ovaries (right). r; Pearson correlation coefficient. (F) Bar graph shows transcript levels (TPM) of telomeric TE families (*HeT-A*, *TAHRE*, *TART-A1*, *TART-B*, and *TART-C*) in different transcriptome dataset. Control; mean of SRR1187952 and SRR1187953, *cuff*-GLKD; SRR1187955, *del*-GLKD; SRR1187956, *rhi*-GLKD; SRR1187954 (GSE55824) (Mohn et al., 2014). *gfp*-GLKD and *set1*-GLKD; mean of biological duplicate of in-house library data. *aub* het; mean of SRR6012944 and SRR6012946, *aub* KO; mean of SRR6012947 and SRR6012949, *piwi* het; mean of SRR6012950 and SRR6012952, *piwi* KO; mean of SRR6012953 and SRR6012954 (GSE103582) (Teixeira et al., 2017).

To obtain insight into the robust *HTT* derepression observed in *set1*-GLKD, I re-analyzed the publicly available datasets of piwi-lacking ovaries (Teixeira et al., 2017) and found that the *HTT* derepression profiles were comparable to those observed in *set1*-GLKD (Figure 2.5 F). In contrast, *HTT* derepression was much milder in ovaries lacking *aub*, consistent with *aub*-GLKD condition in this study. I also found that *HTT* derepression was not robust in ovaries depleting *rhi*, *del*, and *cuff*, whose products are crucial in piRNA precursor transcription (Mohn et al., 2014). Taken together, these results imply the functions of Set1 to repress TEs represented by *HTT* is associated with the mechanisms mediated by Piwi, rather than those mediated by Aub or RDC.

### 2.2.5 Set1 localizes to germline nuclei and physically interacts with Piwi

To further investigate the functional relationship between Set1 and Piwi, I examined the subcellular localization of Set1 and tested whether Set1 physically interacts with Piwi. For this purpose, I utilized transgenes encoding GFP-tagged wild-type Set1 (GFP-

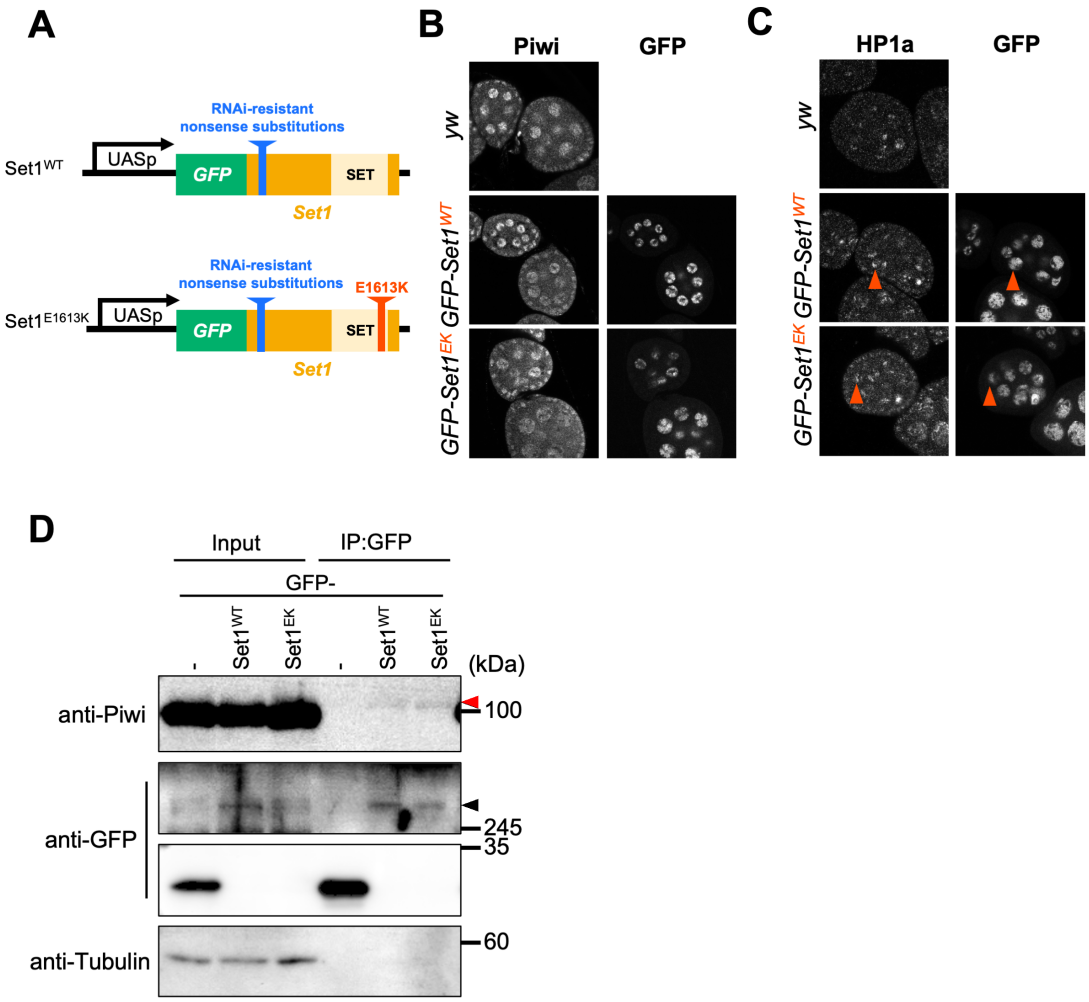



**Figure 2.6 Set1 colocalizes and physically interacts with Piwi.**

(A) Schematic representation of GFP-Set1 transgenes. Wild-type Set1 (Set1$^{WT}$) and catalytically inactive mutant (Set1$^{E1613K}$) were expressed under the control of UASp promoter (modified from Vidaurre et al., 2024). (B, C) Immunofluorescence images of ovaries expressing GFP-Set1$^{WT}$ or GFP-Set1$^{E1613K}$ driven by *osk-Gal4* driver, co-stained with anti-Piwi (B) or anti-HP1 (C) antibodies. Red arrowheads indicate co-localizing signals. (D) Crosslink-CoIP analysis from ovarian lysates expressing GFP, GFP-Set1$^{WT}$ or GFP-Set1$^{E1613K}$ driven by NN. Piwi (red arrowhead) was co-immunoprecipitated with both GFP-Set1$^{WT}$ and GFP-Set1$^{E1613K}$ (black arrowheads).

Set1$^{WT}$) or a catalytically inactive mutant (GFP-Set1$^{E1613K}$) that are resistant to RNAi targeting endogenous *set1* (Vidaurre et al., 2024) (Figure 2.6 A). These transgenes were expressed in germline cells using the Gal4 driver, allowing visualization of Set1 localization and biochemical analysis of its interactions.

Immunostaining analysis of ovaries expressing GFP-Set1$^{WT}$ revealed that Set1 predominantly localizes to germline nuclei (Figure 2.6 B, C). To determine whether Set1 co-localizes with Piwi, I performed double immunostaining using anti-GFP and anti-Piwi antibodies. The results showed clear co-localization of GFP-Set1 and Piwi in germline nuclei (Figure 2.6 B). Additionally, I examined the localization of Set1 relative to HP1, a heterochromatin-associated protein known to localize at telomeric regions(Fanti et al., 1998). GFP-Set1 also showed co-localization with HP1 (Figure2.6 C), suggesting that Set1 may be enriched at telomeric regions where *HTT* elements reside. Notably, the catalytically inactive mutant GFP-Set1$^{E1613K}$ exhibited similar localization patterns from those of wild-type Set1, indicating that nuclear localization and enrichment at specific chromatin regions do not require Set1's methyltransferase activity (Figure 2.6 B, C).

To test whether Set1 and Piwi form a physical complex, I performed co-immunoprecipitation (co-IP) experiments using ovaries expressing GFP-Set1 transgenes. I found that Piwi co-immunoprecipitated with GFP-Set1$^{WT}$ (Figure 2.6 D), confirming the physical interaction between these two proteins. Notably, Piwi also co-immunoprecipitated with the catalytically inactive mutant GFP-Set1$^{E1613K}$ at comparable levels (Figure 2.6 D), demonstrating that the Set1-Piwi interaction does not depend on Set1's methyltransferase activity. These biochemical data corroborate the proximity relationship identified by TurboID and suggest that Set1 and Piwi function in a common molecular pathway for piRNA-directed TE silencing.

Taken together, these results establish that Set1 localizes to germline nuclei where it co-localizes with both Piwi and telomeric heterochromatin markers. The physical interaction between Set1 and Piwi occurs independently of Set1's catalytic activity, suggesting that Set1 may serve structural or scaffolding roles in addition to its enzymatic function in chromatin modification.

### 2.2.6 Catalytic activity-dependent and -independent functions of Set1 repress TEs

I next examined whether the catalytic activity is crucial for the TE silencing function of Set1. For this purpose, RNAi-resistant transgene encoding GFP-tagged Set1$^{WT}$ or Set1$^{E1613K}$ was expressed in *set1*-GLKD of non-GSCLC ovaries (Figure 2.6 A). Transcriptome profiling showed that *HTT* and other TE families were re-repressed by GFP-Set1$^{WT}$ expression, with the transcript levels comparable to those in the control *gfp*-GLKD condition (Figure 2.7 A). The perfect recovery ruled out the possible off-target

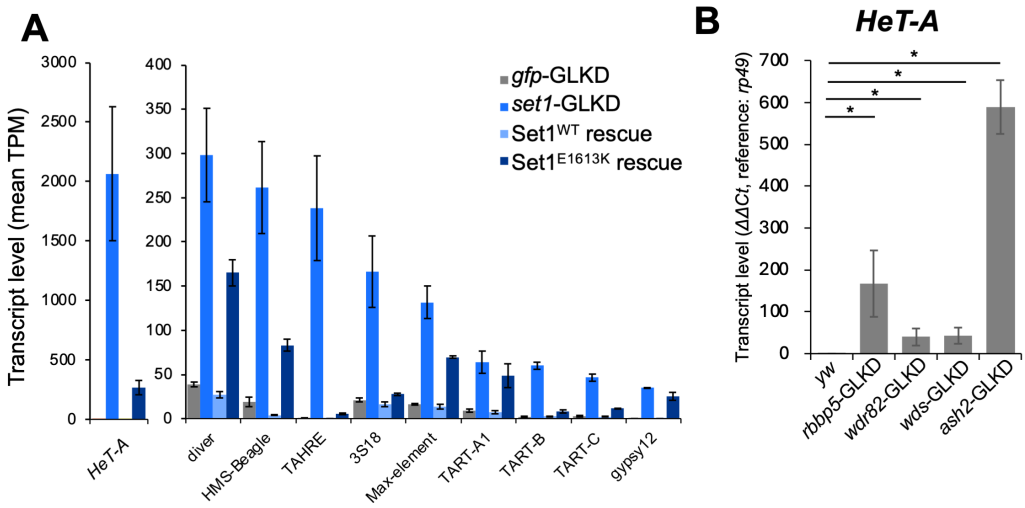



**Figure 2.7 Effects of Set1 and COMPASS components on TE repression**

(A) Transcript levels (TPMs) of TE families in *gfp*-GLKD (control), *set1*-GLKD and the rescue conditions (expressing siRNA-resistant GFP-Set1$^{WT}$ or GFP-Set1$^{E1613K}$ transgene in *set1*-GLKD condition). Error bars show SD of biological duplicates. (B) Transcript levels of *HeT-A* upon individual GLKD were measured by *ΔΔCt* method using *rp49* as reference. Error bars are standard deviation (SD) from three biological replicates. Significance was determined using unpaired Student's t-test. Asterisks indicate $p < 0.05$.

effects of GLKD and indicates the depletion of *set1* was causal for TE derepression. I further confirmed that GLKD of individual COMPASS subunits derepressed *HeT-A* by RT-qPCR, suggesting Set1 is functional as COMPASS complex for TE silencing (Figure 2.7 B). On the other hand, the expression of GFP-Set1$^{E1613K}$ in *set1*-GLKD partially re-repressed many TE families. The degree of re-repression was variable; *TART-A1* was least affected while *TART-B* and *TART-C* showed strong recovery between *HTT* members (Figure 2.7 A). These results suggest that both catalytic activity-dependent and -independent functions of Set1 are involved in TE silencing.

### 2.2.7 Set1 is crucial in producing piRNAs targeting *HTT* families

Set1 might be important in TE silencing, simply because its general transcriptional activator function promotes the expression of piRNA pathway components independently of the proximity to Piwi. However, this is unlikely given the reduction of transcript levels of piRNA pathway components was marginal in non-GSCLC ovaries upon *set1*-GLKD (Figure 2.8 A). Moreover, although Aub and Ago3 protein levels were clearly decreased in *set1*-GLKD (Figure 2.8 B), nuage remained in perinuclear region (Figure 2.4 B), and the TE derepression pattern differed from that observed in *aub*-GLKD (Figure 2.5 E). Furthermore, Piwi protein level and its localization in germline nuclei were unaffected in *set1*-GLKD (Figure 2.4 B). These observations suggest that *set1*-GLKD partially impairs but does not completely disrupt piRNA pathway.

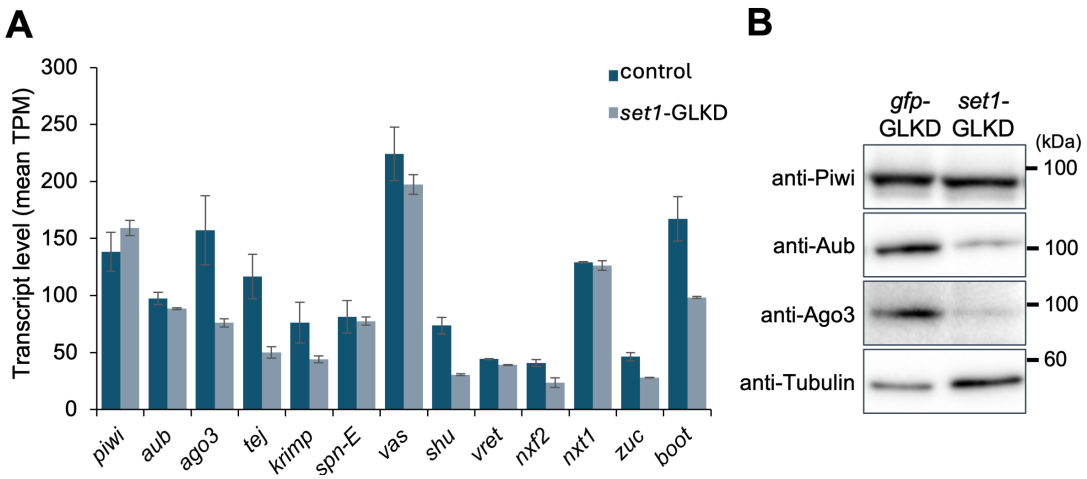



**Figure 2.8 Effect of *set1*-GLKD on piRNA pathway components**

(A) Bar graph shows the transcript levels (TPMs) of genes encoding piRNA pathway components in control (gfp-GLKD) and set1-GLKD conditions. Error bars are SD of biological duplicates. (B) Immunoblotting shows the protein levels of PIWI family members in ovarian lysates of gfp-GLKD and set1-GLKD conditions. Tubulin serves as protein loading control.

I next analyzed piRNAs accumulating in non-GSCLC ovaries and examined the effect of *set1*-GLKD by deep sequencing. In line with the maintenance of the piRNA pathway in *set1*-GLKD, the overall abundance of piRNAs (23~29-nt fragments and those containing TE sequences) remained largely unchanged (Figure 2.9 A). However, analysis of piRNAs mapping to individual TEs revealed a striking and specific loss of piRNAs targeting *HTT* members in *set1*-GLKD (Figure 2.9 B). Notably, antisense piRNAs, which directly target cognate TE transcripts, were more severely affected than sense piRNAs (Figure 2.9 C). On the other hand, piRNAs mapping to somatic TEs (*gypsy*, *gypsy5*, *gypsy10*, *ZAM*, *tabor*, *gtwin*) were largely unaffected in *set1*-GLKD, consistent with the germline-restricted nature of the knockdown (Figure 2.9 B). The ping-pong signature (10-nt overlap frequencies) was maintained in both total piRNAs and *HTT* mappers, further supporting the maintenance of piRNA biogenesis in nuage in *set1*-GLKD (Figure 2.9 D). Taken together, these results highlight the specialized role of Set1 in producing piRNAs targeting telomeric *HTT*.

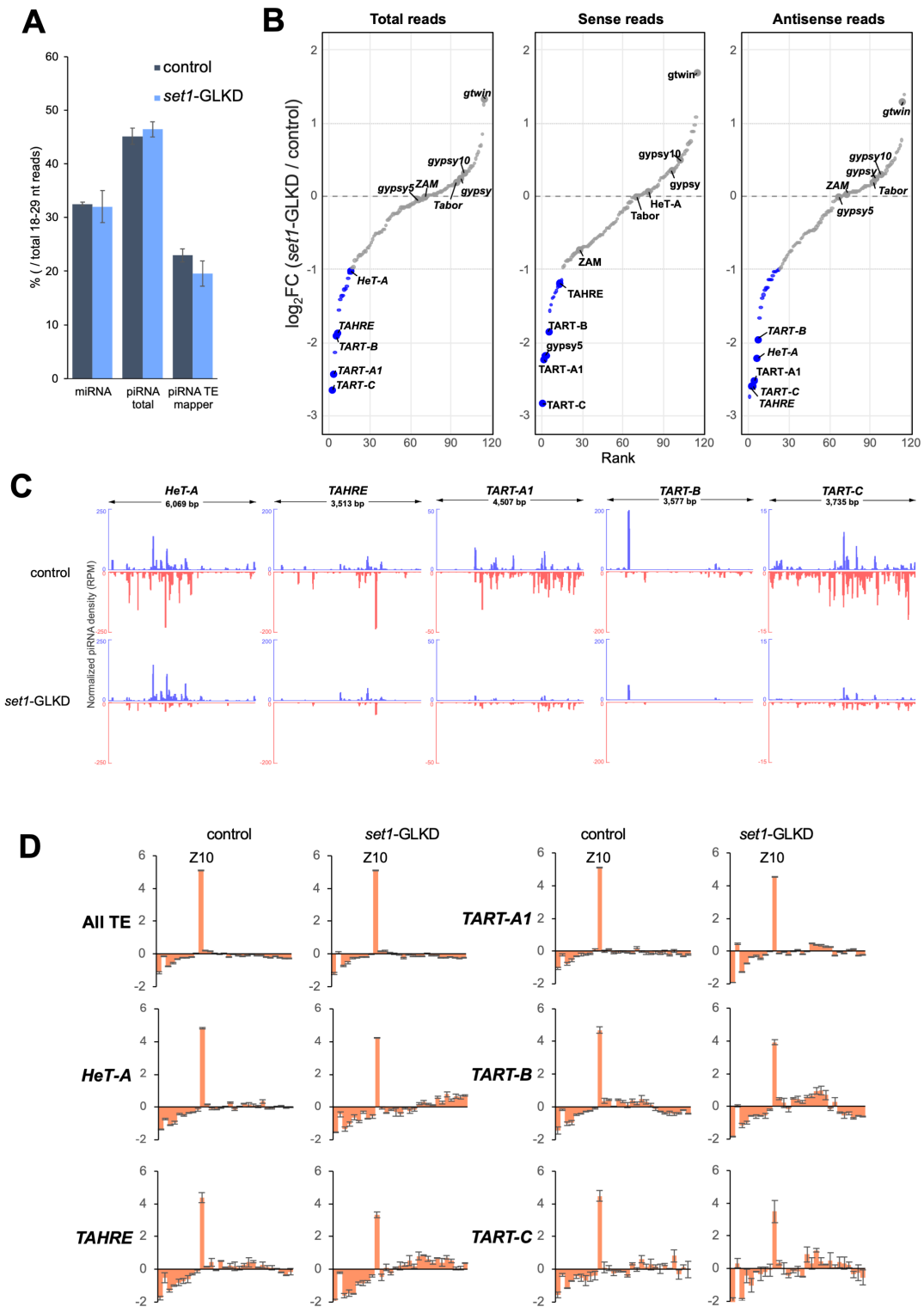

A
control
set1-GLKD
% ( / total 18-29 nt reads)
miRNA
piRNA total
piRNA TE mapper
B
Total reads
Sense reads
Antisense reads
log2FC (set1-GLKD / control)
Rank
gtwin
gypsy10
gypsy
ZAM
Tabor
gypsy5
HeT-A
TAHRE
TART-B
TART-A1
TART-C
C
HeT-A
6,069 bp
TAHRE
3,513 bp
TART-A1
4,507 bp
TART-B
3,577 bp
TART-C
3,735 bp
control
set1-GLKD
Normalized piRNA density (RPM)
D
control
set1-GLKD
Z10
All TE
TART-A1
HeT-A
TART-B
TAHRE
TART-C

**Figure 2.9 Deep sequencing analysis of *set1*-GLKD ovary**

(A) The proportion of small RNAs (miRNA or piRNA) in control or *set1*-GLKD ovaries. Control values; mean of *gfp*-GLKD and GFP-Set1$^{WT}$-rescue conditions. *set1*-GLKD; mean of biological duplicate of *set1*-GLKD (one replicate is from the sibling control of GFP-Set1$^{WT}$-rescue progenies). miRNA: 18~29-nt reads mapping to miRNA precursors, piRNA; 23~29-nt reads, and the mappers on consensus sequences of TE families. Error bars show SD of biological duplicates.(B) Dot plots show the fold changes of the levels (RPMs) of piRNAs mapped on individual TE families (those RPM >5 is indicated). Left; sum of sense and antisense piRNAs, middle; sense piRNAs, right; antisense piRNAs. Blue dots highlight TE families with log2FC < -1.(C) Track view for piRNAs mapping to the consensus sequences of telomeric TE families. Blue; sense piRNAs, red; antisense piRNAs. (D) piRNA overlap feature analysis. Z10; 10-nt overlap frequencies and ping-pong signature. Error bars are SD of biological duplicates.

### 2.2.8 Set1 maintains chromatin status at subtelomeric piRNA cluster loci

Given its role in producing piRNAs targeting *HTT* (Figure 2.9), I hypothesized that Set1 might contribute to their precursor transcription from piRNA cluster loci. Near the ends of chromosome 4 and X, cluster 3 and 22 have been characterized with enrichment of *HTT* fragments (Iyer et al., 2023). To support my hypothesis, CUT&Tag-based chromatin profiling in GSCLC ovaries (not in non-GSCLC ovaries; see below the reason) revealed the accumulation of H3K4me2 and H3K4me3 signals in both cluster 3 and 22 (Figure 2.10 A, *gfp*-GLKD). However, I found these clusters were also enriched with H3K9me3, a repressive histone mark. The overlap of active (H3K4me2/3) and repressive (H3K9me3) marks on *HTT*-enriched loci was not seen in other cluster loci where H3K9me3 dominated (Figure 2.10 A *gfp*-GLKD) (Mohn et al., 2014). These characteristics suggest distinct mechanisms underlying piRNA precursor transcription from cluster 3 and 22.

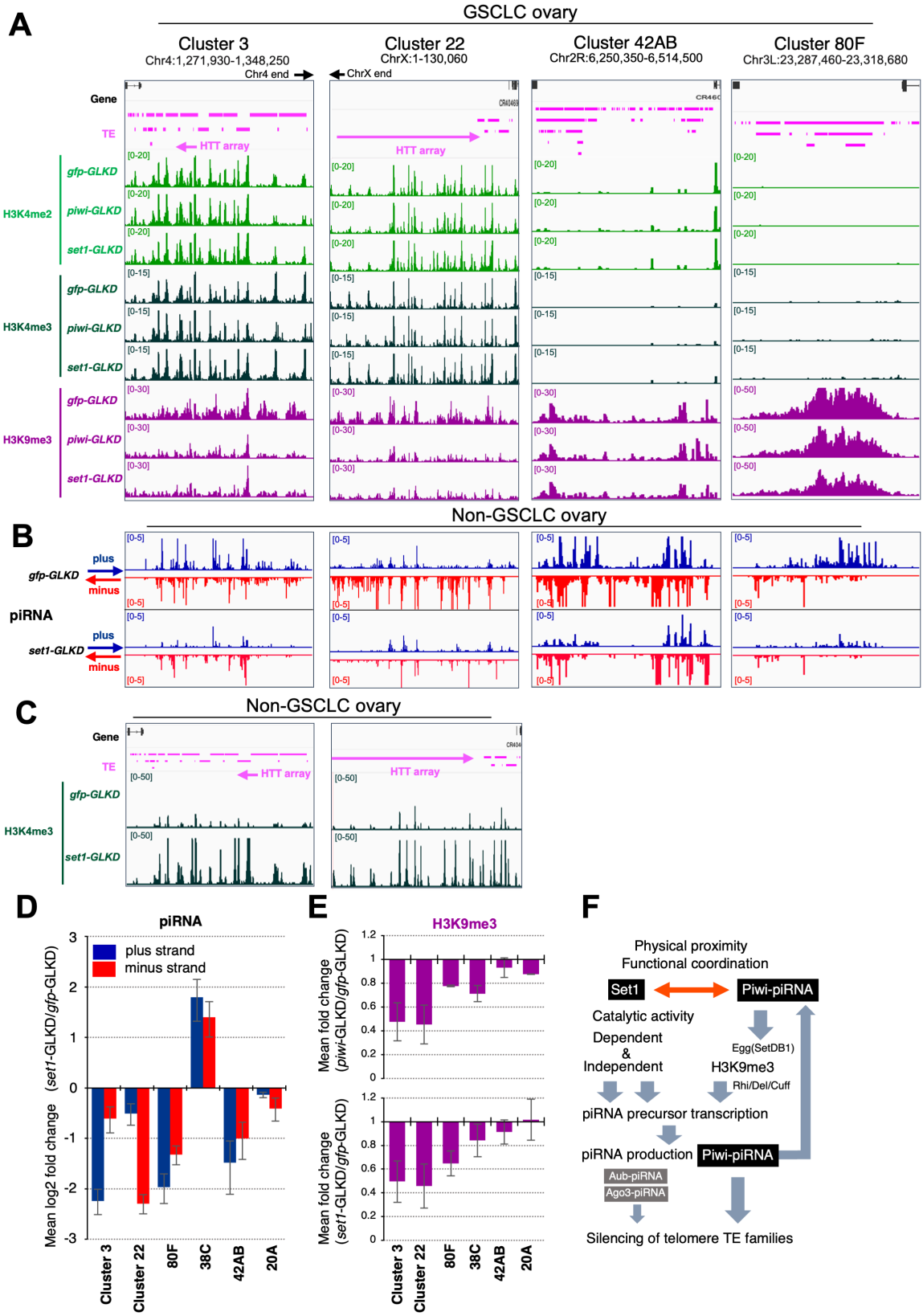

A
GSCLC ovary
Cluster 3
Chr4:1,271,930-1,348,250
Chr4 end
Cluster 22
ChrX:1-130,060
ChrX end
Cluster 42AB
Chr2R:6,250,350-6,514,500
Cluster 80F
Chr3L:23,287,460-23,318,680
Gene
TE
HTT array
H3K4me2
H3K4me3
H3K9me3
gfp-GLKD
piwi-GLKD
set1-GLKD
B
Non-GSCLC ovary
plus
minus
piRNA
C
Non-GSCLC ovary
D
piRNA
plus strand
minus strand
Mean log2 fold change (set1-GLKD/gfp-GLKD)
Cluster 3
Cluster 22
80F
38C
42AB
20A
E
H3K9me3
Mean fold change (piwi-GLKD/gfp-GLKD)
Mean fold change (set1-GLKD/gfp-GLKD)
F
Physical proximity
Functional coordination
Set1
Piwi-piRNA
Catalytic activity
Dependent
&
Independent
Egg(SetDB1)
H3K9me3
Rhi/Del/Cuff
piRNA precursor transcription
piRNA production
Piwi-piRNA
Aub-piRNA
Ago3-piRNA
Silencing of telomere TE families

**Figure 2.10 Effect of *set1*- and *piwi*-GLKD on chromatin status in piRNA cluster loci**
(A) Track view for H3K9me3 (purple), H3K4me2 (light green), H3K4me3 (dark green) signals on indicated cluster loci, in *gfp*-GLKD, *piwi*-GLKD, and *set1*-GLKD conditions in GSCLC ovaries. Gene and TE tracks are shown on the top. (B) piRNAs in *gfp*-GLKD and *set1*-GLKD in non-GSCLC ovaries on indicated cluster loci in (A). Blue; genomic plus strand, red; genomic minus strand. (C) Track view for H3K4me3 (dark green) signals on indicated cluster loci (A), in *gfp*-GLKD and *set1*-GLKD conditions in non-GSCLC ovaries. (D) Fold change (set1-GLKD/gfp-GLKD) of the abundance of piRNA (RPM) mapping to indicated cluster loci. Error bars show SD of biological duplicates. (E) Fold change (*piwi*-GLKD/*gfp*-GLKD, *set1*-GLKD/*gfp*-GLKD,) of H3K9me3 signals in indicated piRNA clusters. Error bars show SD of biological duplicates. (F) The working model for the mode of actions of Set1 in piRNA-directed TE silencing.

Genome-wide piRNA profiling revealed a remarkable loss of piRNAs mapping to cluster 3, 22, 80F, and 42AB in *set1*-GLKD (Figure 2.10 D). Of those, cluster 3 and 22 lost their mapping piRNAs in genomic strand-biased manners (Figure 2.10 B, D). The strand more sensitive to *set1*-GLKD (plus strand in cluster 3, minus strand in cluster 22) was opposite to the unidirectional head-to-tail arrays of *HTT* (Pardue & DeBaryshe, 2011). This observation suggests that Set1 activates transcription toward chromosomal ends to provide precursors of antisense piRNAs targeting *HTT*. If this model is correct, H3K4me2/3 signals would decrease upon *set1*-GLKD. However, H3K4me2/3 levels on cluster 3 and 22 remained largely unchanged (Figure 2.10 A; *set1*-GLKD). I interpret this as an equilibrium between loss (due to Set1 depletion) and gain (due to *HTT* activation) of H3K4me2/3 marks in *set1*-GLKD conditions. Supporting this interpretation, H3K4me3 signals showed dramatic accumulation in non-GSCLC ovaries upon *set1*-GLKD (Figure 2.10 C), which serves as the reason why CUT&Tag was conducted in GSCLC condition where derepression of *HTT* was much milder (Figure 2.5). Alternatively, these results might emphasize the catalytic activity-independent role of Set1 (Figure 2.7).

In contrast to H3K4me2/3 signals, H3K9me3 signals showed a severe reduction in cluster 3 and 22 upon *set1*-GLKD (Figure 2.10 A, E). Similarly, a milder reduction was observed in other cluster loci including 80F and 42AB (Figure 2.10 A, E). The pattern of H3K9me3 reduction resembled that observed in *piwi*-GLKD, which directly impairs the recruitment of Eggless/SetDB1, the H3K9me3 writer, to target loci including piRNA clusters (Figure 2.10 A, E; *piwi*-GLKD) (Akkouche et al., 2017; Sienski et al., 2015). These results indicate that Set1 is essential for establishing heterochromatin at selected cluster loci, a function relevant to its proximity with Piwi (Figure 2.10 F).

## 2.3 Discussion

### 2.3.1 Hrb27C emerged as a functionally relevant partner of Aub

Hrb27C emerged as a functionally relevant partner of Aub (Figure 2.4, 2.5). As a member of hnRNP family, Hrb27C has been shown to regulate the transport, localization, and translation of interacting mRNAs during *Drosophila* oogenesis (Goodrich et al., 2004; Lomoschitz et al., 2025; Yano et al., 2004). Consistent with my observation of Aub-Hrb27C interaction, both proteins have been reported as essential for GSC maintenance (Finger et al., 2023; Ma et al., 2017). In this study, I provided evidence supporting the involvement of Hrb27C in Aub-directed TE silencing in GSCLCs (Figure 2.5). The cooperation between Hrb27C and Aub in GSCs should be further dissected in future studies.

### 2.3.2 Set1 is crucial for piRNA-directed silencing of telomeric TEs

Set1 was identified and characterized as a key factor in piRNA-directed TE silencing (Figure 2.5-2.10). My results suggest that Set1 is especially important in transcribing the precursors of piRNAs targeting telomeric *HTT* families. Set1-dependency of piRNA precursor transcription has been overlooked in *Drosophila* germline cells, where major

piRNA clusters are largely heterochromatinized (H3K4me2/3 is nearly absent) and noncanonically transcribed (Chen et al., 2021; Mohn et al., 2014). Different from these major piRNA clusters, I found the subtelomeric clusters are characteristic by accumulating H3K4me2/3, together with H3K9me3, which is in line with the Set1-dependency of piRNA precursor transcription.

Recent studies also revealed cluster-selective molecular underpinnings for piRNA precursor transcription. These include DNA-binding protein, Kipferl, and enhancer of zeste, E(z), the writer of H3K27me3, each required at distinct cluster loci (Akkouche et al., 2025; Baumgartner et al., 2022). Additionally, the NSL (nonspecific lethal) complex, a multi-subunit chromatin modifier known for its role in transcriptional activation, has been shown to contribute to piRNA precursor transcription from telomeric clusters. Germline-specific depletion of NSL complex subunits results in dramatic reduction of piRNAs mapping to telomeric clusters 3 and 22, accompanied by decreased levels of H3K9me3, HP1a, and Rhi at these loci (Iyer et al., 2023). Remarkably, NSL2 directly binds to the 3'-promoters of *HTT* transposons, distinguishing it from typical NSL complex targets where binding occurs at 5'-promoters. This telomere-specific binding suggests that the NSL complex promotes canonical transcription of *HTT*-derived piRNA precursors. The functional parallels between Set1 and the NSL complex—both being associated with transcriptional activation and H3K4 methylation—raise the possibility that these factors may cooperatively establish the unique bivalent chromatin state at subtelomeric piRNA clusters. Hence, piRNA precursor transcription involves multiple chromatin modifiers and transcriptional regulators. Similar to *Drosophila*, mouse protects the genome from TEs using piRNAs during spermatogenesis. When entering to meiotic prophase I, spermatocytes express pachytene-piRNA having distinct roles in

spermiogenesis. The transition from pre-pachytene-piRNA to pachytene-piRNA is achieved by a transcription factor A-MYB that recognizes the promoters of pachytene stage-specific clusters and accumulate H3K4me3 through transcriptional activation (X. Z. Li et al., 2013). In *Drosophila* germline cells, there is no proof for fly MYB orthologue involvement in piRNA pathway, however, convergent evolution developed Ovo, derived from different transcription family, as master activator of germline piRNA pathway (Alizada, Hannon, et al., 2025). In gonadal soma, Traffic jam (Tj), a fly orthologue of large Maf transcription factors, activates soma-restricted cluster, *flamenco* (Alizada, Martins, et al., 2025; Rivera et al., 2025). Which transcription factor(s) can cooperate with Set1 in germline piRNA precursor transcription is to be elucidated. Overall, piRNA precursor transcription shows variation in the underlying mechanisms, depending on cluster loci, cell lineages, and developmental stages. The variation would be beneficial by enabling the spaciotemporal control of piRNA repertoire to perform the multitasks.

### 2.3.3 Developmental timing of Set1 function and the specification of subtelomeric piRNA clusters

The functional link between Set1 and Piwi raises an important question regarding the developmental timing of their cooperation. piRNA cluster loci are specified during embryogenesis, where Piwi-mediated deposition of H3K9me3 marks establishes the heterochromatic identity of these genomic regions (Akkouche et al., 2017). This developmental specification persists into adulthood, where the pre-established clusters serve as the major sources of piRNA precursors in germline cells. My identification of Set1 as a Piwi proximity factor in adult ovaries suggests that their functional interaction may also be rooted in embryonic development.

I propose a two-phase model for Set1 function in piRNA cluster regulation (Figure 2.10 F). In the first phase during embryogenesis, Set1 cooperates with Piwi to

establish the chromatin landscape at subtelomeric piRNA clusters. This collaboration results in the unique bivalent state characterized by the co-occurrence of active (H3K4me2/3) and repressive (H3K9me3) histone marks. Unlike canonical piRNA clusters that are dominated by H3K9me3 alone, this bivalent chromatin state at subtelomeric loci may enable RDC-independent transcription mechanisms. In the second phase during adulthood, the bivalent chromatin established in embryos is maintained, allowing sustained production of *HTT*-targeting piRNAs without requiring continuous RDC activity. This model is supported by the distinct TE derepression patterns observed upon depletion of different factors. Knockdown of Rhi, a core component of the RDC complex, leads to global reduction of piRNA levels including those targeting *HTT* (Mohn et al., 2014). However, the derepression of *HTT* elements themselves remains relatively mild compared to other TEs. In striking contrast, Set1 depletion causes dramatic and selective derepression of *HTT* families despite maintaining overall piRNA pathway integrity (Figure 2.5-2.10). This phenotypic divergence suggests that subtelomeric clusters employ a transcription mechanism distinct from the RDC-dependent pathway utilized by most germline piRNA clusters.

The biological significance of this distinct regulatory mechanism may lie in the dual nature of *HTT* elements. Unlike typical TEs that are purely deleterious, *HTT* families serve an essential cellular function by maintaining telomeres in *Drosophila*, which lacks telomerase (Casacuberta, 2017). Therefore, complete silencing of *HTT* would be negative to genome stability. The bivalent chromatin state established by Set1 and Piwi may provide a fine-tuned regulatory balance: sufficient piRNA production to prevent excessive *HTT* mobilization, while permitting controlled *HTT* activity for telomere maintenance. This interpretation is consistent with the observation that Set1 depletion

severely reduces antisense piRNAs targeting *HTT* (Figure 2.9), which would directly impact the surveillance capacity against *HTT* mobilization.

However, several aspects of this model require further investigation. First, whether Set1 and Piwi physically interact during embryogenesis remains to be demonstrated. My proximity proteome was characterized in adult GSCLCs, and how this condition recapitulates protein interactions during embryogenesis is uncertain. Second, the precise chromatin changes occurring at subtelomeric clusters during embryonic development need to be characterized by stage-specific profiling. Third, the identity of transcription factor(s) cooperating with Set1 to initiate precursor transcription from subtelomeric clusters awaits discovery. Unlike Ovo in germline cells or Traffic jam in somatic cells, which activate canonical piRNA clusters (Alizada, Hannon, et al., 2025; Alizada, Martins, et al., 2025; Rivera et al., 2025), the specific activator(s) for subtelomeric clusters remain unknown.

Nonetheless, the functional specialization of Set1 for *HTT* regulation highlights an important principle in piRNA biology: the piRNA pathway employs diverse molecular strategies tailored to distinct TE families and genomic contexts. This flexibility may have evolved to address the unique challenges posed by different classes of TEs, particularly those like *HTT* that occupy the boundary between parasitic elements and host-beneficial sequences.

### 2.3.4 Catalytic activity-dependent and -independent functions of Set1 in TE silencing

Another layer of complexity arises from my finding that Set1 can support TE silencing independent of its methyltransferase activity (Figure 2.6-2.7). Expression of catalytically inactive Set1 mutant ($Set1^{E1613K}$) in *set1*-depleted germline cells partially rescued the silencing of multiple TE families, although the degree of rescue varied among different

*HTT* members (Figure 2.7). This finding is reminiscent of yeast Set1 repressing genes, TEs, and chromatin in subtelomeric regions in H3K4 methylation-independent manners (Jezek et al., 2023). Though yeast does not express piRNAs, repressor non-coding RNAs have been also characterized in Set1-dependent transposon silencing (Berretta et al., 2008). These previous findings on yeast Set1 will help understand the mode of actions of fly Set1 in piRNA-directed TE silencing in future studies.

The catalytic activity-independent function of Set1 might involve scaffolding roles in recruiting other factors to piRNA cluster loci, or in stabilizing the COMPASS complex at these genomic regions. Alternatively, Set1 protein itself might serve as a platform for assembly of transcription machinery, independent of its enzymatic output. Dissecting these possibilities will require detailed biochemical characterization of Set1 interactions at different developmental stages and in different catalytic states.

### 2.3.5 Conclusions and future perspectives

In summary, this study has expanded our understanding of the molecular network underlying piRNA-directed TE silencing in *Drosophila* germline cells. Through proximity proteomics, I identified previously unrecognized factors in the vicinity of PIWI proteins and functionally characterized Set1 as a critical regulator of *HTT* silencing. My findings reveal that: (1) Subtelomeric piRNA clusters possess unique chromatin features and regulatory requirements distinct from canonical clusters (2) Set1 cooperates with Piwi to establish and/or maintain the specialized chromatin state at these loci (3) The Set1-Piwi axis functions through both catalytic activity-dependent and -independent mechanisms. This regulatory framework likely reflects the dual nature of *HTT* elements as both TEs and telomere maintenance factors. Future studies addressing the developmental dynamics of Set1-Piwi cooperation, the identity of collaborating

transcription factors, and the molecular basis of catalytic activity-independent functions will further illuminate the sophisticated regulatory strategies employed by germline cells to balance TE silencing with essential cellular functions.

# 3. Materials and Methods

## 3.1 Fly husbandry

All stocks and crosses were raised at 25˚C on a molasses/yeast medium [5% (w/v) dry yeast, 5% (w/v) corn flower, 2% (w/v) rice bran, 10% (w/v) glucose, 0.7% (w/v) agar, 0.2% (v/v) propionic acid, and 0.05% (v/v) p-hydroxy butyl benzoic acid]. Fly stocks used in this study are listed in Table 3.1.

**Table 3.1 Fly lines used in this study**

| Name | Genotype | Reference |
|---|---|---|
| yw | *y w* | |
| NN | *NGT40-Gal4; nos-Gal4 VP16* | Grieder et al., 2000 |
| *osk*-Gal4 | *$w^{1118}$;P{w[+mC]=osk-GAL4::VP16}F/TM3, Sb* | BL (Bloomington Drosophila Stock Center) #44242 |
| Myc-Kumo$^{WT}$ | *w {UASp-6xMyc-Kumo$^{WT}$}attP40/CyO* | Lim and Kai, unpublished |
| Myc-Kumo$^{C5}$ | *w {UASp-6xMyc-Kumo$^{C5}$}attP40/CyO* | Lim and Kai, unpublished |
| TUBE-Kumo$^{WT}$ | *w {UASp-3xHA-TUBE-Kumo$^{WT}$}attP40/CyO* | This thesis |
| TUBE-Kumo$^{C5}$ | *w {UASp-3xHA-TUBE-Kumo$^{C5}$}attP40/CyO* | This thesis |
| Kumo$^{WT}$-TUBE | *w {UASp -Kumo$^{WT}$-3xHA-TUBE}attP40/CyO* | This thesis |
| Kumo$^{C5}$-TUBE | *w {UASp -Kumo$^{C5}$-3xHA-TUBE}attP40/CyO* | This thesis |
| *bam* shRNA | *y[1] v[1]; P{y[+t7.7] v[+t1.8]=TRiP.HMJ22155}attP40* | BL #58178 |
| *bam* shRNA | *y[1] v[1]; P{y[+t7.7] v[+t1.8]=TRiP.HMS00029}attP2* | BL # 33631 |
| attP-3B | *y[1] M{RFP[3xP3.PB] GFP[E.3xP3]=vas-int.Dm}ZH-2A w[*] v[1] P{y[+t7.7]=nanos-phiC31¥int.NLS}X; PBac{y[+]-attP-3B}VK00033* | BL #32543 |
| attP-40 | *y[1] v[1] P{y[+t7.7]=nanos-phiC31¥int.NLS}X; P{y[+t7.7]=CaryP}Msp300[attP40]* | BL #25709 |
| attP-2 | *P{y[+t7.7]=nanos-phiC31¥int.NLS}X, y[1] sc[1] v[1] sev[21]; P{y[+t7.7]=CaryP}attP2* | BL #25710 |

| Name | Genotype | Reference |
|---|---|---|
| *mTurbo-GFP* | *w; {UASp-miniTurbo-GFP}attP40/CyO* | This study |
| *mTurbo-GFP-Piwi* | *w; {UASp-miniTurbo-GFP-Piwi}attP2/TM3 Sb* | This study |
| *mTurbo-GFP-Aub* | *w; {UASp-miniTurbo-GFP-Aub}attP3B/TM3 Sb* | This study |
| *mTurbo-GFP-Ago3* | *w; {UASp-miniTurbo-GFP-Ago3}attP40/CyO* | This study |
| *hrb27C* shRNA | *y[1] sc[*] v[1] sev[21]; P{y[+t7.7] v[+t1.8]=TRiP.HMS00597}attP2* | BL #33716 |
| *set1* shRNA | *y[1] sc[*] v[1] sev[21]; P{y[+t7.7] v[+t1.8]=TRiP.HMS00581}attP2* | BL #33704 |
| *aub* shRNA | *y[1] sc[*] v[1] sev[21]; P{y[+t7.7] v[+t1.8]=TRiP.HMS00611}attP2* | BL #33728 |
| *gfp* shRNA | *y[1] sc[*] v[1] sev[21]; P{y[+t7.7] v[+t1.8]=VALIUM20-EGFP.RNAi.1}attP40* | BL #41555 |
| *gfp* shRNA | *y[1] sc[*] v[1] sev[21]; P{y[+t7.7] v[+t1.8]=VALIUM20-EGFP.RNAi.1}attP2* | BL #41556 |
| Set1 WT rescue | *UASp-FRT-EGFP-set1 (WT rescue)-PolyA-FRT/CyO; P{y[+t7.7] v[+t1.8]=TRiP.HMS00581}attP2/ TM3 Sb* | Vidaurre et al., 2024 |
| Set1 E1613K rescue | *UASp-FRT-EGFP-set1 (Mutant rescue)-PolyA-FRT ; P{y[+t7.7] v[+t1.8]=TRiP.HMS00581}attP2/ TM3 Sb* | Vidaurre et al., 2024 |
| *ash2* shRNA | *y[1] sc[*] v[1] sev[21]; P{y[+t7.7] v[+t1.8]=TRiP.GL00307}attP2/TM3, Sb[1]* | BL #35388 |
| *rbbp5* shRNA | *y[1] v[1]; P{y[+t7.7] v[+t1.8]=TRiP.HMJ02113}attP40* | BL #42819 |
| *wds* shRNA | *y[1] sc[*] v[1] sev[21]; P{y[+t7.7] v[+t1.8]=TRiP.HMS00746}attP2* | BL #32952 |
| *wdr82* shRNA | *y[1] sc[*] v[1] sev[21]; P{y[+t7.7] v[+t1.8]=TRiP.HMS00718}attP2* | BL #32926 |
| *piwi* shRNA | *y[1] sc[*] v[1] sev[21]; P{y[+t7.7] v[+t1.8]=TRiP.GL00626}attP40* | BL #37483 |

## 3.2 Generation of plasmids and fly stocks

All the primers used for plasmid construction are listed in Table 3.2.

### 3.2.1 TUBE-tagged Kumo transgene generation

TUBE sequence was amplified using pRSET-6xTR-TUBE (addgene #110313) as template and TUBE-Fw and TUBE-Rv as primers. Vector fragment was amplified by PCR using Vec-HA-Link-Fw/Vec-HA-Link-Rv as primer and UASp-K10-attB vector (Koch et al., 2009) as template. TUBE fragment was cloned into the vector fragment to obtain HA-tagged TUBE using In-Fusion HD Cloning (Takara). Kumo and HA-TUBE fragment was amplified using Linker-Kumo-Fw/Kumo-Vec-Rv and Vec-HA-Fw/TUBE-linker-Rv for N-terminal tag and Vec-Kumo-Fw/Kumo-Linker-Rv and Linker-HA-Fw/TUBE-Vec-Rv for C-terminal tag. Resulted fragments were cloned into the XbaI site in the UASp-K10-attB vector (Koch et al., 2009) using In-Fusion HD Cloning (Takara). Plasmids were injected into attP-40 flies.

### 3.2.2 miniTurbo fly generation

To generate UASp-mTurbo-GFP, UASp-mTurbo-GFP-Piwi, UASp-mTurbo-GFP-Aub and UASp-mTurbo-GFP-Ago3, mTurbo fragment was amplified by PCR using attB_miniTurbo_Fw_general and miniTurbo_linker_Rv_general as primers and 3xHA-miniTurboNLS_pCDNA3 (addgene #107172) as template. GFP fragment was amplified by PCR using 2-1vLinker>GFP5_F and Ti876-GFP-G5-R as primers. Piwi, Aub or Ago3 fragment was amplified by PCR using primer pairs of Linker_to_Piwi and Piwi_to_Vector, Ti893-G5-Aub-CDS-F and Ti894-Aub-UASp-R1, or Linker_to_Ago3 and Ago3_to_Vector, respectively, with cDNA from *yw* ovaries as template. PCR fragments were introduced into the XbaI site in pUASp-K10-attB vector (Koch et al., 2009) using In-Fusion HD Cloning (Takara). UASp-mTurbo-GFP and UASp-mTurbo-

GFP-Ago3 were integrated to attP40, while UASp-mTurbo-GFP-Piwi and UASp-mTurbo-GFP-Aub were integrated to attP2, and attP-3B sites, respectively.

**Table 3.2 Primer list for plasmid construction**

| Name | Sequence (5' to 3') |
|---|---|
| TUBE-Fw | GGTGGAGGCGGTGGCGGTATGGCTAGCATGACTGGT |
| TUBE-Rv | CGAGGTCGACTCTAGTTAGGATCCCCCACCGC |
| Vec-HA-Link-Fw | ATCTGGATCCTCTAGCAAAATGTACCCATACGATGTTCCTGACTATGCG GGCTATCCCTATGACGTCCCGGACTATGCAGGATCCTATCCATATGACG TTCCAGATTACGCTGGTGGAGGCGGTGGC |
| Vec-HA-Link-Rv | GCCACCGCCTCCACCAGCGTAATCTGGAACGTCATATGGATAGGATCC TGCATAGTCCGGGACGTCATAGGGATAGCCCGCATAGTCAGGAACATC GTATGGGTACATTTTGCTAGAGGATCCAGAT |
| Vec-HA-Fw | ATCTGGATCCTCTAGCAAAATGTAC |
| TUBE-linker-Rv | ACCGCCACCTCCGCCGGATCCCCCACCGCCACT |
| Linker-Kumo-Fw | GGCGGAGGTGGCGGTATTGCCGACGACAGTGGAATAAAG |
| Kumo-Vec-Rv | CGAGGTCGACTCTAGTTATGATTTTTTCAGGAACATCCAA |
| Vec-Kumo-Fw | ATCTGGATCCTCTAGCAAAATGATTGCCGACGACAGTGGAA |
| Kumo-Linker-Rv | ACCGCCACCTCCGCCTGATTTTTTCAGGAACATCCAATTT |
| Linker-HA-Fw | GGCGGAGGTGGCGGTTACCCATACGATGTTCCTGACTATG |
| TUBE-Vec-Rv | CGAGGTCGACTCTAGTTAGGATCC |
| attB_miniTurbo_Fw_general | ATCTGGATCCTCTAGCAAAATGATCCCGCTGCTGAACGCTA |
| miniTurbo_linker_Rv_general | GCCGCCGCCTCCGCCGTCGGCCCTGCTGAATTCCT |

| Name | Sequence (5' to 3') |
|---|---|
| 2-1vLinker> GFP5_F | GGCGGAGGCGGCGGCATGGTGAGCAAGGGC |
| Ti876-GFP-G5-R | GCCACCGCCTCCACCCTTGTACAGCTCGTCCATGCCG |
| Ti893-G5-Aub-CDS-F | GGTGGAGGCGGTGGCAATTTACCACCAAACCCTGTAAT |
| Ti894-Aub-UASp-R1 | CGAGGTCGACTCTAGTTACAAAAAGTACAATTGATTC |
| Linker to Piwi | GGTGGAGGCGGTGGCGCTGATGATCAGGGACGTGGAC |
| Piwi to Vector | CGAGGTCGACTCTAGTTATAGATAATAAAACTTCTTTT |
| Linker to Ago3 | GGTGGAGGCGGTGGCTCTGGAAGAGGAAATTTGTTGA |
| Ago3 to Vector | CGAGGTCGACTCTAGTTAAAGATAAAATAGTTTTTCAG |

### 3.3 Structure prediction using AlphaFold

Protein structure predictions were performed using the AlphaFold Server (https://alphafoldserver.com). Input sequences used for prediction are listed in Table 3.3. Predicted structures and associated confidence metrics were downloaded directly from the AlphaFold Server. Structures were visualized using the server's built-in visualization tools, and structure images were exported for figure preparation.

**Table 3.3 Amino acid sequence for AlphaFold prediction**

| Name | Sequence |
|---|---|
| Kumo1_115 | FDPKFVASNLQNLLRCPKCSKCFTYLYNTNSEEDNHRPFLLGCGHTLCE SCLWNDRLDPKCAVCHSPAPPTIVAKRSDCKSVANLRDLYELNYHVLGR TSSLSYL |

| | |
|---|---|
| Kumo1_350 | MIADDSGIKPFDPKFVASNLQNLLRCPKCSKCFTYLYNTNSEEDNHRPF<br>LLGCGHTLCESCLWNDRLDPKCAVCHSPAPPTIVAKRSDCKSVANLRDL<br>YELNYHVLGRTSSLSYLLPFAKDSANQSLSPSSISEIVQTVKCSECGNAT<br>ASGECRQCNAFYCRRCFDAVHKRSRVLKSHIFRNSTEQDSSFSKKLRV<br>GDQYFTLPSQNLCIHHRMPKDKYCMKCYRSHCQICSTVHHSGHRIRKLI<br>EINQSYASEIPTTLNSLNMAHIHVLNGKQVVQRAKQKLNDYATETLASISK<br>RFSHLHGLLQVAELQVIEKLRESSLPPQLKLNEAMGQLSGYETVIERLTK<br>SLNS |

### 3.4 Sequence alignment

Multiple sequence alignments of Kumo/RNF17 orthologs were performed using MUSCLE (Multiple Sequence Comparison by Log-Expectation) algorithm with default parameters. Amino acid sequences were obtained from OrthoDB v12.2 (https://www.orthodb.org/) by searching for the RNF17 ortholog group. For cross-species comparison, sequences from representative organisms were retrieved from the OrthoDB database. For analysis within the *Drosophila* genus, all available sequences from *Drosophila* species annotated as RNF17 orthologs in OrthoDB were retrieved. Sequence alignments were visualized in Jalview, with coloring cysteine and histidine residues.

### 3.5 Immunostaining and image acquisition

Ovaries were dissected from adult females in 1x PBS buffer supplemented with 0.4% (w/v) bovine serum albumin (BSA; Wako) and fixed in 5.3% (v/v) paraformaldehyde (Nacalai) in 0.67x PBS buffer for 10 min. To observe DNA, ovaries were incubated with 1 μM 40,6-diamidino-2-phenylindole (DAPI) in PBX buffer [1x PBS containing 0.2% (v/v) Triton X-100]. For *HeT-A* immunostaining, fixed ovaries were washed with PBX and incubated with Image-iT™ FX Signal Enhancer (Invitrogen) for 30 min. Fixed samples were blocked with PBX containing 2% (w/v) BSA for 30 min. The primary antibody incubation was performed overnight at 4˚C, and ovaries were washed with PBX

at RT for 1 hour. The secondary antibody incubation was then performed at RT for 2 hours, and then ovaries were washed with PBX at RT for 1 hour. The antibodies used for immunostaining were rat anti-HA (1:1000, 3F10, Roche), mouse anti-Myc (1:1000, 9E10, Wako), rabbit anti-HeT-A Gag (1:2000) (Lin et al., 2023), guinea pig anti-Krimp (1:2000)(A. K. Lim & Kai, 2007), mouse anti-Piwi (1:50, Santa Cruz, sc-390946), guinea pig anti-Aub (1:500) (L.-X. Lim et al., 2022), mouse anti-GFP (1:50, Invitrogen, A11120). Secondary antibodies were as follows: Alexa Fluor 488- and 555-conjugated goat antibodies at 1:500 (Molecular Probes) and CF®633 goat antibodies at 1:500 (Biotium). Antibodies were diluted in 0.4% (w/v) BSA containing PBX as the working solution. Images were taken by ZEISS LSM 900 using C-Apochromat 40x/1.20 W Korr objective lens and processed with ZEISS ZEN 3.0 and Fiji.

### 3.6 *In vitro* ubiquitination assay

#### 3.6.1 Protein purification

For recombinant $Kumo^{WT}$/$Kumo^{C5}$ protein expression in insect cells, the ExpiSf™ Expression System (Thermo Fisher Scientific) was used following the manufacturer's protocol. Bacmid DNA was transfected into ExpiSf9™ cells using ExpiFectamine™ Sf Transfection Reagent to generate P0 baculovirus stock. ExpiSf9™ cells were seeded in ExpiSf™ CD Medium in 125-mL PETG sterile, non-baffled, vented shake flasks and transfected with bacmid DNA-lipid complexes. Transfection cultures were incubated at 27°C in a non-humidified, non-$CO_2$ atmosphere incubator on an orbital shaker platform at 120 rpm. P0 baculovirus stock was collected 120 hours post-transfection by centrifugation at 300 ×g for 5 minutes, and the clarified supernatant was stored at 4°C protected from light. For protein expression, ExpiSf9™ cells were seeded in ExpiSf™ CD Medium supplemented with ExpiSf™ Enhancer. Cells were infected with P0

baculovirus stock, 24 hours after Enhancer addition. Infected cultures were incubated at 27°C on an orbital shaker platform at 120 rpm. Cells were harvested 96 hours post-infection by centrifugation. Cell pellets were resuspended in lysis buffer [100 mM Tris-HCl (pH8.0), 150 mM NaCl, 1% (v/v) Triton X-100, 1 mM 1,4-dithiothreitol (DTT)] supplemented with cOmplete Protease Inhibitor Cocktail (Roche) (PIC) and 1 mM PMSF. Cells were sonicated and cleared by centrifugation at 15,000 ×g for 1h at 4°C. The clarified lysate was applied to Strep-Tactin Sepharose (iba, 2-1201-010). The column was washed with wash buffer [100 mM Tris-HCl (pH8.0), 500 mM NaCl, 1 mM DTT, 1× PIC, 1 mM PMSF], and bound proteins were eluted with elution buffer [100 mM Tris-HCl (pH8.0), 150 mM NaCl, 1 mM DTT, 5 mM desthiobiotin, 1×PIC]. Eluted proteins were flash-frozen in liquid nitrogen, and stored at −80°C.

### 3.6.2 *In vitro* reaction

Recombinant E1 ubiquitin-activating enzyme (Ube1) and E2 ubiquitin-conjugating enzyme (Effete) were gifts from prof. Ikeda. Purified GFP-tagged KumoWT or KumoC5 proteins were used as E3 ubiquitin ligases. Reaction mixtures were prepared containing 100 nM E1, 1 μM E2, and 0.1 μM E3 proteins in a buffer containing 50 mM HEPES, 150 mM NaCl, 0.5 mM $MgSO_4$, pH 8.0. Reactions were initiated by addition of 100 μM ubiquitin (Sigma Aldrich, U6253) and 2 mM ATP, then incubated at 25°C for 18h. Reactions were terminated by addition of SDS sample buffer [final: 25 mM Tris–HCl, 2% (w/v) SDS and 0.2 M DTT] and boiling at 95°C for 1 minute. Proteins were resolved by SDS-PAGE and analyzed by immunoblotting.

## 3.7 Co-Immunoprecipitation

Ovaries from 50 females from *yw* control and TUBE-tagged Kumo transgenic line were dissected and homogenized with a pestle in homemade buffer [25 mM Tris–HCl (pH7.5),

150 mM NaCl, 0.5% (v/v) Triton-X, 5 mM EDTA, 0.5 mM DTT and 10% glycerol] supplemented with cOmplete Protease Inhibitor Cocktail (Roche). 20 µL Pierce™ Anti-HA Magnetic Beads (Thermo Scientific, 88836) were added to ovarian lysate and incubated overnight at 4°C. Proteins were rinsed with homemade buffer and eluted from beads in SDS sample buffer at 95°C.

### 3.8 Western blotting and biotinylated protein detection

Samples were denatured at 95°C for 5 min in 2× protein loading buffer [4% (w/v) SDS, 200 mM DTT, 0.1% (v/v) bromophenol blue (BPB), and 20% (v/v) glycerol] saturated with biotin, resolved by SDS–polyacrylamide gel electrophoresis (SDS-PAGE) and transferred to 0.45-µm polyvinylidene difluoride membrane (Millipore) using the semi-dry system (Trans-blot Turbo, Bio-Rad). The membrane was blocked in 3% (w/v) skim milk (Nacalai) in 1× phosphate-buffered saline (PBS) supplemented with 0.1% (v/v) Tween 20 and further incubated with the following antibodies: rabbit anti-GFP (1:1000, Clonetech), mouse anti-ubiquitin (1:1000, P4D1, Cell Signaling Technology (CST)), rabbit anti-K48 specific polyubiquitin (1:1000, CST), rabbit anti-K63 specific polyubiquitin (1:1000, CST), mouse anti-M1 specific polyubiquitin (1:1000, LUB9, Sigma Aldrich), rat anti-HA (1:1000, 3F10, Roche), rat anti-Spn-E (1:2000) (Patil & Kai, 2010), guinea pig anti-Vasa (1:5,000) (Patil & Kai, 2010), rat anti-Tejas (1:200) (Lin et al., 2023), mouse anti-Piwi (1:100) (Saito et al., 2006), guinea pig anti-Aub (1:1000) (L.-X. Lim et al., 2022), rat anti-Ago3 (1:200) (L.-X. Lim et al., 2022), mouse anti-Tubulin (1:3000, Santa Cruz), anti-guinea pig immunoglobulins-HRP (1:1000, Dako), anti-rabbit immunoglobulin G (IgG)–HRP (1:3000, Bio-Rad), anti-mouse IgG-HRP (1:3000, Bio-Rad), anti-rat IgG (1:1000, DAKO). HRP-conjugated Streptavidin (Clonetech) was used for detecting biotinylated Proteins. The chemiluminescent signals generated with Chemi-

Lumi One (Nacalai) were detected by Chemidoc MP Imaging system (Bio-Rad). The images were processed with Fiji.

### 3.9 TurboID proximity labeling and streptavidin pulldown

After eclosion, females expressing mini(m)Turbo-GFP-PIWI proteins were reared at 25˚C for 2-3 (non-GSCLC ovaries) or 5-7 days (GSCLC ovaries) in the modified molasses/yeast medium supplemented with 100 μM biotin (Nacalai). To obtain GSCLC ovaries expressing mTurbo-GFP-PIWI proteins, *bam* shRNA and *mTurbo-GFP-PIWI* transgenes were combined (*bam* shRNA; *mTurbo-GFP-Piwi*, *bam* shRNA; *mTurbo-GFP-Aub*, *mTurbo-GFP-Ago3*; *bam* shRNA, *bam* shRNA; *mTurbo-GFP*) and crossed with NN. From 300 ovaries, biotinylated proteins were purified as described previously with some modification.(Iki et al., 2023; Roux et al., 2012) After exchanging the buffer with 150 μL of PI-lysis buffer [50 mM Tris-HCl (pH 7.5), 500 mM NaCl, 2 mM EDTA, 2 mM dithiothreitol (DTT), 0.4% (w/v) SDS, and cOmplete Protease Inhibitor Cocktail Tablet (Roche)] ovaries were homogenized using Bioruptor (Diagenode) for 30s (power H) for six times with 30s intervals. Triton X-100 was added to sample mixtures at a final concentration of 2% (v/v), and homogenization was further performed for 30s for three times with 30s intervals. After centrifugation (20,000*g*, 10 min, 4˚C), the supernatant was diluted by mixing with equal amount of 50 mM Tris-HCl (pH 7.5) solution and incubated with pre-equilibrated 15-μL slurry volume of Dynabeads MyOne Streptavidin C1 (Thermo Fisher Scientific) overnight at 4˚C with gentle rotation. Next day, beads were washed twice with W1 buffer [50 mM Tris-HCl (pH 7.5), 250 mM NaCl, 0.2% (w/v) SDS, 1 mM EDTA, and 1 mM DTT], twice with W2 buffer [50 mM HEPES-KOH (pH 7.4), 500 mM NaCl, 0.1% (w/v) deoxycholate (Nacalai), 1% (v/v) Triton X-100, and 1 mM EDTA], twice with W3 buffer [10 mM Tris-HCl (pH 8.0), 250 mM LiCl, 0.5% (w/v)

deoxycholate, 0.5% (v/v) NP-40 (Nacalai), and 1 mM EDTA], and four times with W4 buffer [50 mM Tris-HCl (pH 7.5) and 50 mM NaCl]. The purified biotinylated proteins bound to magnet beads were stored at -80˚C until shipment for mass spectrometry analysis.

### 3.10 Mass spectrometry and proteomics analysis

After purification, biotinylated protein-bound streptavidin beads were analyzed by mass spectrometry followed by label free quantification (LFQ) analysis by Dr. Hata and Dr. Oyama at the University of Tokyo. Mass spectrometry and analysis were performed in duplicate; after LFQ analysis, the proximity factor was selected as the one that increased more than GFP both times (Abundance ratio >1) and was significantly different ($p < 0.05$) in either of the two analyses. GO analysis was conducted using MetaScape (Zhou et al., 2019).

### 3.11 Reverse transcription and qPCR analysis

Total RNA was extracted from ovaries using TRIzol™ LS (Invitrogen) following the manufacturer's instructions. Using DNase I (NEB)–treated RNA, cDNA was synthesized with 2.5 μM oligo(dT) adaptor using SuperScript III reverse transcriptase (Thermo Fisher Scientific). Quantitative reverse transcription PCR (qPCR) reaction was performed using SYBR™ Green qPCR Master Mix (Thermo Fisher Scientific) and gene-specific primers (Table 3.4) in QuantStudio 5 Real-Time PCR system (ABI).

**Table 3.4 Primer list for qPCR**

| Name | Sequence (5' to 3') |
|---|---|
| rp49 Fw | CCGCTTCAAGGGACAGTATCTG |
| rp49 Rv | ATCTCGCCGCAGTAAACGC |
| HeT-A Fw | TCATTGACGATACCAGCGCATC |
| HeT-A Rv | TCCGGGTGCGTTTAGGTGAG |

| Name | Sequence (5' to 3') |
|---|---|
| aub_PP35447_Fw | TTACGCCTGATGTGGAGGCTA |
| aub_PP35447_Rv | GGGGCTATCTTGAACAGCTTTG |
| hrb27C_PD70445_Fw | ACATGCCACCTAACTCTGCC |
| hrb27C_PD70445_Rv | TTGAGCACGCGAGTACATGT |
| set1 Fw | CAAAAGGCATTGATGCCGAAG |
| set1 Rv | GGTCAGTTGTGCAGTGATCCACC |

### 3.12 Transcriptome analysis

Total RNA was extracted from 100 ovaries (non-GSCLC ovaries or GSCLC ovaries) using TRIzol™ LS (Invitrogen). To obtain GSCLC ovaries expressing shRNA for *aub*, *hrb27C*, *set1* or *gfp*, shRNA lines were combined (*bam* shRNA; *aub* shRNA, *bam* shRNA; *hrb27C* shRNA, *bam* shRNA; *set1* shRNA, *bam* shRNA; *gfp* shRNA) and crossed with NN. DNase I-treated RNA was sent to Rhelixa (Japan) for library construction and deep-sequencing. Polyadenylated RNA selection was performed with NEBNext Poly(A) mRNA Magnetic Isolation Module (NEB). Libraries were constructed with the NEBNext Ultra II Directional RNA Library Prep Kit (NEB) and sequenced by using NovaSeq 6000 (Illumina). Trimming was performed by Cutadapt (v1.18, -j 12 -a AGATCGGAAGAGCACACGTCTGAACTCCAGTCA -A AGATCGGAAGAGCGTCGTGTAGGGAAAGAGTGT, -m 20). Trimmed paired-end reads were mapped to the dm6 genome using STAR (v2.7.10b, --outFilterMultimapNmax 100 --outSAMmultNmax 1 --outMultimapperOrder Random). Read counting was performed with featureCounts (v2.0.6, -p -t exon -g gene_id) using Drosophila_melanogaster.BDGP6.46.112.gtf (ensembl.org). Using the sum of RPK (read per kilobase) for individual genes and TEs, TPM (transcript per million) was calculated.

Trimmed paired-end reads were also mapped to consensus sequences of individual TE families (http://ftp.flybase.net/flybase/transposons/) with STAR using the same options. Mappers on individual TE families were counted using pileup.sh (BBMap). Using the sum of RPK given by featureCounts output, TPM values for individual TE families were calculated.

### 3.13 Crosslink Co-Immunoprecipitation

Ovaries from one hundred females from yw control and TUBE-tagged Kumo transgenic line were dissected, crosslinked in 0.1% PFA at room temperature for 10 min. Samples were homogenized with a pestle in IP buffer (20 mM Tris–HCl [pH7.5], 135 mM NaCl, 1.5 mM $MgCl_2$, 0.2% (v/v) Triton-X, and 10% glycerol) supplemented with cOmplete Protease Inhibitor Cocktail (Roche). 10 µL Anti-GFP mAb-Magnetic Beads (MBL, D153-11) were added to ovarian lysate and incubated overnight at 4°C. Proteins were rinsed with homemade buffer and eluted from beads in SDS sample buffer at 95°C.

### 3.14 Small RNA deep sequencing and analysis

Biological duplicate dataset for Set1-present condition was provided by *gfp-GLKD* ovaries (control RNAi condition), and *set1*-GLKD ovaries expressing GFP-$Set1^{WT}$ (rescue condition). Dataset for Set1-depleted condition was provided by *set1*-GLKD ovaries, and the siblings of rescue conditions (CyO). Total RNA was extracted using TRIzol™ LS (Invitrogen) from 60 to 100 ovaries of ~3 days old adult females. After the addition of chloroform and centrifugation (12,000 ×g 15 min, 4˚C), short (< ~200 nt) RNA in the aqueous phase was purified using RNA Clean & Concentrator 5 (R1015 Zymo). To deplete 2S ribosomal RNA (rRNA), 2 pmol of complementary oligo DNA (5'-AGTCTTACAACCCTCAACCATATGTAGTCCAAGCAGCACT-3') was added per 1 µg of RNA. The mixture was heated (95˚C, 2 min), gradually cooled down to form

DNA/RNA hybrid, and then treated with RNase H (NEB) at 37˚C for 30min. RNase H was inactivated by heating at 65˚C for 20 min. The 2S rRNA-depleted RNA mixture was loaded onto 8 M urea-polyacrylamide gel (12%) and size-separated in parallel with visible RNA ladder (Dynamarker DM253, BioDynamics Laboratory Inc.) in 0.5x Tris-borate EDTA buffer. Gel within the range from 20 to 30 nt was excised and passed through a small hole opened by needle (23Gx1, TERUMO) at the bottom of 0.5 mL DNA LoBind tubes (Eppendorf) by centrifugation (15,000 ×g). The fine particles were recovered in 2.0 mL DNA LoBind tubes, and RNAs were eluted overnight at 4˚C with gentle rotation in the presence of 300 mM NaOAc (pH 5.2). After removing the particles using cellulose 0.22 μm membrane filter Spin-X (Costar, 8160), RNA was precipitated in the presence of 80% (v/v) ethanol and glycogen (40 μg/mL) (Nacalai) for overnight at -20˚C. After centrifugation (20,000 ×g, 20 min, 4˚C), RNA pellet rinsed twice with 80% (v/v) ethanol was resuspended in RNase-free water. Small RNA libraries were prepared using NEBNext® Multiplex Small RNA Library Prep Set for Illumina (NEB, E7300S) following manufacture's procedure. After 15 cycles of PCR amplification, the libraries were purified using MagMAX™ Pure Bind Beads (Applied Biosystems), size-separated in 3% (w/v) low melting agarose (HydraGene) in the presence of SYBR gold (Thermo Fisher). ~150-bp library fragments containing 20~30-bp inserts were purified using QIAquick gel extraction kit (Qiagen). Libraries were sequenced by RIMD NGS core facility (The University of Osaka) using the NovaSeqX Plus platform (Illumina). Adaptor sequences (AGATCGGAAGAGC) were removed by Trim Galore (v0.6.2, --length 15) with quality filter cut off (Phred ≥20). Adaptor-trimmed reads were mapped to rRNA, tRNA, snoRNA, and snRNA sequences using bowtie (v1.3.1), and the unmappers were collected (samtools view -f 4). From the unmappers, 18~29-nt reads were selected as

small RNAs using seqkit (v2.4.0) and mapped to miRNA precursors using bowtie (-v 0) to collect “miRNA” populations. The size-selected (23~29-nt) unmappers were considered as “piRNA”. These piRNA fragments were mapped to TE consensus sequences using bowtie (-v 3 -M 1 --best --strata). Fw and Rv mappers were counted for individual TEs using pileup.sh. Read counts were normalized using the sum of 18~29-nt reads and reads per million (RPM) was calculated. For visualization, Fw and Rv mappers were separated using splitsam.sh. Bedgraph was generated using bedtools (v2.26.0, genomecov -bga -split), values normalized using scale factors given by the sum of 18~29-nt reads. Mean values of biological replicates were obtained using bedtools unionbedg. Track view was generated in IGV (v2.16.0). piRNA overlap scores (z) were measured using signature.py (Antoniewski, 2014).

### 3.15 CUT&Tag

Anderson et al. was referred for performing whole ovary (non-GSCLC ovaries or GSCLC ovaries) CUT&Tag. To obtain GSCLC ovaries expressing shRNA for *piwi*, *set1* or *gfp*, shRNA lines were combined (*piwi* shRNA; *bam* shRNA, *bam* shRNA; *set1* shRNA, *bam* shRNA; *gfp* shRNA) and crossed with NN. Around twenty ovaries from 10 adult females at 3~5 days old were dissected in PBS buffer supplemented with cOmplete Protease Inhibitor (Roche). Ovaries were permeabilized in PBX buffer (PBX containing 0.2%(v/v) Triton-X100) for 30 min at RT in 1.5 mL tubes. After removing PBX, ovaries were washed once with Wash+ buffer (20mM HEPES [pH 7.4], 150 mM NaCl, 0.5 mM spermidine [Nacalai], 2 mM EDTA, 1%[w/v] BSA, cOmplete Protease Inhibitor) and incubated overnight at 4˚C with primary antibodies diluted by 1:50 with Wash+ buffer. Anti-H3K4me2 (#9725, C64G9, rabbit, Cell Signaling), anti-H3K4me3 (#61979, mouse, Active Motif), anti-H3K9me3 (rep1: #39065, rabbit, Active Motif, rep2: #61013, mouse,

Active Motif) were used. After removing the secondary antibody solution, ovaries were washed three times with 300Wash+ buffer (20 mM HEPES [pH 7.4], 300 mM NaCl, 0.5 mM spermidine, cOmplete Protease Inhibitor) and incubated for 1h at RT with loaded pAG-Tn5 (79561S, Cell Signalling) diluted by 1:25 in 300Wash+ buffer. After removing the Tn5 solution, ovaries were washed three times with 300Wash+ buffer. Tagmentation was performed by incubating ovaries in 300Wash+ buffer supplemented with 10 mM $MgCl_2$ for 1h at 37˚C. After removing the supernatant, ovaries were treated with collagenase (2 mg/mL, Sigma C9407) in HEPESCA buffer (50 mM HEPES [pH 7.4], 360 μM $CaCl_2$) for 1h at 37˚C. Then, the reaction mixture was added with SDS, EDTA, and proteinase K (Nacalai) (final concentration 0.2%[w/v], 16 mM, and 0.3 mg/mL, respectively), and further incubated for 1h at 58˚C. After the reaction, DNA was purified by using Quick-DNA Microprep kit (ZYMO, D3020). Using the purified DNA as template, libraries were synthesized by PCR (72˚C 5min, 98˚C 30s, 14 cycles of [98˚C 10s, 63˚C 15s], 65˚C 5min) using Ultra II Q5 Master Mix (NEB) and dual-indexed primers (Table S5). Generated libraries were purified using x1.3 volume of AmpureXP (beckman). The concentration of libraries was measured using Qubit dsDNA HS assay kit (Thermo). Libraries were sequenced with NovaSeqX (Illumina) and 150+150bp paired-end reads were obtained (RIMD, The University of Osaka). Trimming was performed by Cutadapt (-a CTGTCTCTTATACACATCTCCGAGCCCACGAGAC -A CTGTCTCTTATACACATCTGACGCTGCCGACGA, -m 20). Trimmed r2 reads were used for mapping to *D. melanogaster* genome (dm6) not allowing mismatch using Bowtie (-v 0 -M 1 --best --strata). Read counts were normalized using deeptools (bamCoverage --normalizeUsing CPM -of bigwig --binSize=10).

# 4. References


Akkouche, A., Kneuss, E., Bornelöv, S., Renaud, Y., Eastwood, E. L., van Lopik, J., Gueguen, N., Jiang, M., Creixell, P., Maupetit-Mehouas, S., Sobieszek, A., Gui, Y., Czech Nicholson, B., Brasset, E., & Hannon, G. J. (2025). Binding of heterochromatin protein Rhino to a subset of piRNA clusters depends on a combination of two histone marks. *Nature Structural & Molecular Biology*, *32*(8), 1517–1527. https://doi.org/10.1038/s41594-025-01584-8

Akkouche, A., Mugat, B., Barckmann, B., Varela-Chavez, C., Li, B., Raffel, R., Pélisson, A., & Chambeyron, S. (2017). Piwi Is Required during Drosophila Embryogenesis to License Dual-Strand piRNA Clusters for Transposon Repression in Adult Ovaries. *Molecular Cell*, *66*(3), 411-419.e4. https://doi.org/10.1016/j.molcel.2017.03.017

Akutsu, M., Dikic, I., & Bremm, A. (2016). Ubiquitin chain diversity at a glance. *Journal of Cell Science*, *129*(5), 875–880. https://doi.org/10.1242/jcs.183954

Alizada, A., Hannon, G. J., & Nicholson, B. C. (2025). Transcriptional regulation of the piRNA pathway by Ovo in animal ovarian germ cells. *Genes & Development*, *39*(3–4), 221–241. https://doi.org/10.1101/gad.352120.124

Alizada, A., Martins, A., Mouniée, N., Rodriguez Suarez, J. V., Bertin, B., Gueguen, N., Mirouse, V., Papameletiou, A.-M., Rivera, A. J., Lau, N. C., Akkouche, A., Maupetit-Méhouas, S., Hannon, G. J., Czech Nicholson, B., & Brasset, E. (2025). The transcription factor Traffic jam orchestrates the somatic piRNA pathway in Drosophila ovaries. *Cell Reports*, *44*(4), 115453. https://doi.org/10.1016/j.celrep.2025.115453

Anand, A., & Kai, T. (2012). The tudor domain protein Kumo is required to assemble the nuage and to generate germline piRNAs in *Drosophila*. *The EMBO Journal*, *31*(4), 870–882. https://doi.org/10.1038/emboj.2011.449

Anderson, J. T., Henikoff, S., & Ahmad, K. (2023). Chromosome-specific maturation of the epigenome in the Drosophila male germline. *ELife*, *12*. https://doi.org/10.7554/ELIFE.89373.3

Andreev, V. I., Yu, C., Wang, J., Schnabl, J., Tirian, L., Gehre, M., Handler, D., Duchek, P., Novatchkova, M., Baumgartner, L., Meixner, K., Sienski, G., Patel, D. J., & Brennecke, J. (2022). Panoramix SUMOylation on chromatin connects the piRNA pathway to the cellular heterochromatin machinery. *Nature Structural & Molecular Biology*, *29*(2), 130–142. https://doi.org/10.1038/s41594-022-00721-x

Antoniewski, C. (2014). Computing siRNA and piRNA Overlap Signatures. In *Methods in Molecular Biology* (Vol. 1173, pp. 135–146). Humana Press Inc. https://doi.org/10.1007/978-1-4939-0931-5_12

Ardehali, M. B., Mei, A., Zobeck, K. L., Caron, M., Lis, J. T., & Kusch, T. (2011). *Drosophila* Set1 is the major histone H3 lysine 4 trimethyltransferase with role in transcription. *The EMBO Journal*, *30*(14), 2817–2828. https://doi.org/10.1038/emboj.2011.194

Asaoka, T., Almagro, J., Ehrhardt, C., Tsai, I., Schleiffer, A., Deszcz, L., Junttila, S., Ringrose, L., Mechtler, K., Kavirayani, A., Gyenesei, A., Hofmann, K., Duchek, P., Rittinger, K., & Ikeda, F. (2016). Linear ubiquitination by LUBEL has a role in *Drosophila* heat stress response. *EMBO Reports*, *17*(11), 1624–1640. https://doi.org/10.15252/embr.201642378

Barski, A., Cuddapah, S., Cui, K., Roh, T. Y., Schones, D. E., Wang, Z., Wei, G., Chepelev, I., & Zhao, K. (2007). High-Resolution Profiling of Histone Methylations in the Human Genome. *Cell*, *129*(4), 823–837. https://doi.org/10.1016/j.cell.2007.05.009

Bastock, R., & St Johnston, D. (2008). Drosophila oogenesis. *Current Biology*, *18*(23), R1082–R1087. https://doi.org/10.1016/j.cub.2008.09.011

Batki, J., Schnabl, J., Wang, J., Handler, D., Andreev, V. I., Stieger, C. E., Novatchkova, M., Lampersberger, L., Kauneckaite, K., Xie, W., Mechtler, K., Patel, D. J., & Brennecke, J. (2019). The nascent RNA binding complex SFiNX licenses piRNA-guided heterochromatin formation. *Nature Structural & Molecular Biology*, *26*(8), 720–731. https://doi.org/10.1038/s41594-019-0270-6

Baumgartner, L., Handler, D., Platzer, S. W., Yu, C., Duchek, P., & Brennecke, J. (2022). The Drosophila ZAD zinc finger protein Kipferl guides Rhino to piRNA clusters. *ELife*, *11*. https://doi.org/10.7554/eLife.80067

Berretta, J., Pinskaya, M., & Morillon, A. (2008). A cryptic unstable transcript mediates transcriptional *trans* -silencing of the Ty1 retrotransposon in *S. cerevisiae*. *Genes & Development*, *22*(5), 615–626. https://doi.org/10.1101/gad.458008

Branon, T. C., Bosch, J. A., Sanchez, A. D., Udeshi, N. D., Svinkina, T., Carr, S. A., Feldman, J. L., Perrimon, N., & Ting, A. Y. (2018). Efficient proximity labeling in living cells and organisms with TurboID. *Nature Biotechnology*, *36*(9), 880–887. https://doi.org/10.1038/nbt.4201

Brennecke, J., Aravin, A. A., Stark, A., Dus, M., Kellis, M., Sachidanandam, R., & Hannon, G. J. (2007). Discrete Small RNA-Generating Loci as Master Regulators

of Transposon Activity in Drosophila. *Cell*, *128*(6), 1089–1103. https://doi.org/10.1016/j.cell.2007.01.043

Briggs, S. D., Bryk, M., Strahl, B. D., Cheung, W. L., Davie, J. K., Dent, S. Y. R., Winston, F., & Allis, C. D. (2001). Histone H3 lysine 4 methylation is mediated by Set1 and required for cell growth and rDNA silencing in *Saccharomyces cerevisiae*. *Genes & Development*, *15*(24), 3286–3295. https://doi.org/10.1101/gad.940201

Casacuberta, E. (2017). Drosophila: Retrotransposons Making up Telomeres. *Viruses*, *9*(7), 192. https://doi.org/10.3390/v9070192

Cavaliere, V., Bernardi, F., Romani, P., Duchi, S., & Gargiulo, G. (2008). Building up the *Drosophila* eggshell: First of all the eggshell genes must be transcribed. *Developmental Dynamics*, *237*(8), 2061–2072. https://doi.org/10.1002/dvdy.21625

Chen, P., Luo, Y., & Aravin, A. A. (2021). RDC complex executes a dynamic piRNA program during Drosophila spermatogenesis to safeguard male fertility. *PLOS Genetics*, *17*(9), e1009591. https://doi.org/10.1371/journal.pgen.1009591

Choi-Rhee, E., Schulman, H., & Cronan, J. E. (2004). Promiscuous protein biotinylation by *Escherichia coli* biotin protein ligase. *Protein Science*, *13*(11), 3043–3050. https://doi.org/10.1110/ps.04911804

Cipressa, F., & Cenci, G. (2013). Effete, an E2 ubiquitin-conjugating enzyme with multiple roles in *Drosophila* development and chromatin organization. *Fly*, *7*(4), 256–262. https://doi.org/10.4161/fly.26567

Clark, J. P., Rahman, R., Yang, N., Yang, L. H., & Lau, N. C. (2017). Drosophila PAF1 Modulates PIWI/piRNA Silencing Capacity. *Current Biology*, *27*(17), 2718-2726.e4. https://doi.org/10.1016/j.cub.2017.07.052

Crump, N. T., & Milne, T. A. (2019). Why are so many MLL lysine methyltransferases required for normal mammalian development? *Cellular and Molecular Life Sciences*, *76*(15), 2885–2898. https://doi.org/10.1007/s00018-019-03143-z

Cui, M., Bai, Y., Li, K., & Rong, Y. S. (2021). Taming active transposons at Drosophila telomeres: The interconnection between HipHop's roles in capping and transcriptional silencing. *PLOS Genetics*, *17*(11), e1009925. https://doi.org/10.1371/journal.pgen.1009925

Darricarrère, N., Liu, N., Watanabe, T., & Lin, H. (2013). Function of Piwi, a nuclear Piwi/Argonaute protein, is independent of its slicer activity. *Proceedings of the National Academy of Sciences*, *110*(4), 1297–1302. https://doi.org/10.1073/pnas.1213283110

Dej, K. J., & Spradling, A. C. (1999). The endocycle controls nurse cell polytene chromosome structure during *Drosophila* oogenesis. *Development*, *126*(2), 293–303. https://doi.org/10.1242/dev.126.2.293

del Valle Rodríguez, A., Didiano, D., & Desplan, C. (2012). Power tools for gene expression and clonal analysis in Drosophila. *Nature Methods*, *9*(1), 47–55. https://doi.org/10.1038/nmeth.1800

Deniz, Ö., Frost, J. M., & Branco, M. R. (2019). Regulation of transposable elements by DNA modifications. *Nature Reviews Genetics*, *20*(7), 417–431. https://doi.org/10.1038/s41576-019-0106-6

Deshaies, R. J., & Joazeiro, C. A. P. (2009). RING Domain E3 Ubiquitin Ligases. *Annual Review of Biochemistry*, *78*(1), 399–434. https://doi.org/10.1146/annurev.biochem.78.101807.093809

Dönertas, D., Sienski, G., & Brennecke, J. (2013). *Drosophila* Gtsf1 is an essential component of the Piwi-mediated transcriptional silencing complex. *Genes & Development*, *27*(15), 1693–1705. https://doi.org/10.1101/gad.221150.113

Eddy, E. M. M. (1976). Germ Plasm and the Differentiation of the Germ Cell Line. In *international review of cytology* (Vol. 43, Number C, pp. 229–280). Academic Press. https://doi.org/10.1016/S0074-7696(08)60070-4

ElMaghraby, M. F., Andersen, P. R., Pühringer, F., Hohmann, U., Meixner, K., Lendl, T., Tirian, L., & Brennecke, J. (2019). A Heterochromatin-Specific RNA Export Pathway Facilitates piRNA Production. *Cell*, *178*(4), 964-979.e20. https://doi.org/10.1016/j.cell.2019.07.007

Fabry, M. H., Ciabrelli, F., Munafò, M., Eastwood, E. L., Kneuss, E., Falciatori, I., Falconio, F. A., Hannon, G. J., & Czech, B. (2019). piRNA-guided co-transcriptional silencing coopts nuclear export factors. *ELife*, *8*. https://doi.org/10.7554/eLife.47999

Fanti, L., Giovinazzo, G., Berloco, M., & Pimpinelli, S. (1998). The heterochromatin protein 1 prevents telomere fusions in Drosophila. *Molecular Cell*, *2*(5), 527–538. https://doi.org/10.1016/s1097-2765(00)80152-5

Feltzin, V. L., Khaladkar, M., Abe, M., Parisi, M., Hendriks, G., Kim, J., & Bonini, N. M. (2015). The exonuclease Nibbler regulates age-associated traits and modulates piRNA length in *Drosophila* . *Aging Cell*, *14*(3), 443–452. https://doi.org/10.1111/acel.12323

Findley, S. D., Tamanaha, M., Clegg, N. J., & Ruohola-Baker, H. (2003). *Maelstrom* , a *Drosophila spindle* -class gene, encodes a protein that colocalizes with Vasa and

RDE1/AGO1 homolog, Aubergine, in nuage. *Development*, *130*(5), 859–871. https://doi.org/10.1242/dev.00310

Finger, D. S., Williams, A. E., Holt, V. V., & Ables, E. T. (2023). Novel roles for RNA binding proteins *squid* , *hephaesteus* , and *Hrb27C* in *Drosophila* oogenesis. *Developmental Dynamics*, *252*(3), 415–428. https://doi.org/10.1002/dvdy.550

Ge, D. T., Wang, W., Tipping, C., Gainetdinov, I., Weng, Z., & Zamore, P. D. (2019). The RNA-Binding ATPase, Armitage, Couples piRNA Amplification in Nuage to Phased piRNA Production on Mitochondria. *Molecular Cell*, *74*(5), 982-995.e6. https://doi.org/10.1016/j.molcel.2019.04.006

Goodrich, J. S., Clouse, K. N., & Schüpbach, T. (2004). Hrb27C, Sqd and Otu cooperatively regulate *gurken* RNA localization and mediate nurse cell chromosome dispersion in *Drosophila* oogenesis. *Development*, *131*(9), 1949–1958. https://doi.org/10.1242/dev.01078

Grieder, N. C., Cuevas, M. de, & Spradling, A. C. (2000). The fusome organizes the microtubule network during oocyte differentiation in *Drosophila*. *Development*, *127*(19), 4253–4264. https://doi.org/10.1242/dev.127.19.4253

Gunawardane, L. S., Saito, K., Nishida, K. M., Miyoshi, K., Kawamura, Y., Nagami, T., Siomi, H., & Siomi, M. C. (2007). A Slicer-Mediated Mechanism for Repeat-Associated siRNA 5' End Formation in Drosophila. *Science*, *315*(5818), 1587–1590. https://doi.org/10.1126/science.1140494

Guo, Y., An, L., Ng, H.-M., Sy, S. M. H., & Huen, M. S. Y. (2017). An E2-guided E3 Screen Identifies the RNF17-UBE2U Pair as Regulator of the Radiosensitivity, Immunodeficiency, Dysmorphic Features, and Learning Difficulties (RIDDLE) Syndrome Protein RNF168. *Journal of Biological Chemistry*, *292*(3), 967–978. https://doi.org/10.1074/jbc.M116.758854

Haase, A. D., Fenoglio, S., Muerdter, F., Guzzardo, P. M., Czech, B., Pappin, D. J., Chen, C., Gordon, A., & Hannon, G. J. (2010). Probing the initiation and effector phases of the somatic piRNA pathway in *Drosophila*. *Genes & Development*, *24*(22), 2499–2504. https://doi.org/10.1101/gad.1968110

Hallson, G., Hollebakken, R. E., Li, T., Syrzycka, M., Kim, I., Cotsworth, S., Fitzpatrick, K. A., Sinclair, D. A. R., & Honda, B. M. (2012). dSet1 Is the Main H3K4 Di- and Tri-Methyltransferase Throughout *Drosophila* Development. *Genetics*, *190*(1), 91–100. https://doi.org/10.1534/genetics.111.135863

Han, B. W., Wang, W., Li, C., Weng, Z., & Zamore, P. D. (2015). piRNA-guided transposon cleavage initiates Zucchini-dependent, phased piRNA production. *Science*, *348*(6236), 817–821. https://doi.org/10.1126/science.aaa1264

Hancks, D. C., & Kazazian, H. H. (2016). Roles for retrotransposon insertions in human disease. *Mobile DNA*, *7*(1), 9. https://doi.org/10.1186/s13100-016-0065-9

Handler, D., Olivieri, D., Novatchkova, M., Gruber, F. S., Meixner, K., Mechtler, K., Stark, A., Sachidanandam, R., & Brennecke, J. (2011). A systematic analysis of *Drosophila* TUDOR domain-containing proteins identifies Vreteno and the Tdrd12 family as essential primary piRNA pathway factors. *The EMBO Journal*, *30*(19), 3977–3993. https://doi.org/10.1038/emboj.2011.308

Harris, R. E., & Ashe, H. L. (2011). Cease and desist: modulating short-range Dpp signalling in the stem-cell niche. *EMBO Reports*, *12*(6), 519–526. https://doi.org/10.1038/embor.2011.80

Hayashi, R., Schnabl, J., Handler, D., Mohn, F., Ameres, S. L., & Brennecke, J. (2016). Genetic and mechanistic diversity of piRNA 3′-end formation. *Nature*, *539*(7630), 588–592. https://doi.org/10.1038/nature20162

Hayward, A., & Gilbert, C. (2022). Transposable elements. *Current Biology*, *32*(17), R904–R909. https://doi.org/10.1016/j.cub.2022.07.044

Hjerpe, R., Aillet, F., Lopitz-Otsoa, F., Lang, V., England, P., & Rodriguez, M. S. (2009). Efficient protection and isolation of ubiquitylated proteins using tandem ubiquitin-binding entities. *EMBO Reports*, *10*(11), 1250–1258. https://doi.org/10.1038/embor.2009.192

Huang, C. R. L., Burns, K. H., & Boeke, J. D. (2012). Active Transposition in Genomes. *Annual Review of Genetics*, *46*(1), 651–675. https://doi.org/10.1146/annurev-genet-110711-155616

Huang, H., Li, Y., Szulwach, K. E., Zhang, G., Jin, P., & Chen, D. (2014). AGO3 Slicer activity regulates mitochondria–nuage localization of Armitage and piRNA amplification. *Journal of Cell Biology*, *206*(2), 217–230. https://doi.org/10.1083/jcb.201401002

Huang, X., Hu, H., Webster, A., Zou, F., Du, J., Patel, D. J., Sachidanandam, R., Toth, K. F., Aravin, A. A., & Li, S. (2021). Binding of guide piRNA triggers methylation of the unstructured N-terminal region of Aub leading to assembly of the piRNA amplification complex. *Nature Communications*, *12*(1), 4061. https://doi.org/10.1038/s41467-021-24351-x

Iki, T., Kawaguchi, S., & Kai, T. (2023). miRNA/siRNA-directed pathway to produce noncoding piRNAs from endogenous protein-coding regions ensures *Drosophila* spermatogenesis. *Science Advances*, *9*(29). https://doi.org/10.1126/sciadv.adh0397

Ipsaro, J. J., Haase, A. D., Knott, S. R., Joshua-Tor, L., & Hannon, G. J. (2012). The structural biochemistry of Zucchini implicates it as a nuclease in piRNA biogenesis. *Nature*, *491*(7423), 279–283. https://doi.org/10.1038/nature11502

Iyer, S. S., Sun, Y., Seyfferth, J., Manjunath, V., Samata, M., Alexiadis, A., Kulkarni, T., Gutierrez, N., Georgiev, P., Shvedunova, M., & Akhtar, A. (2023). The NSL complex is required for piRNA production from telomeric clusters. *Life Science Alliance*, *6*(9), e202302194. https://doi.org/10.26508/lsa.202302194

Jaiswal, D., Jezek, M., Quijote, J., Lum, J., Choi, G., Kulkarni, R., Park, D., & Green, E. M. (2017). Repression of Middle Sporulation Genes in *Saccharomyces cerevisiae* by the Sum1-Rfm1-Hst1 Complex Is Maintained by Set1 and H3K4 Methylation. *G3 Genes|Genomes|Genetics*, *7*(12), 3971–3982. https://doi.org/10.1534/g3.117.300150

Jezek, M., Sun, W., Negesse, M. Y., Smith, Z. M., Orosz, A., & Green, E. M. (2023). Set1 regulates telomere function via H3K4 methylation–dependent and -independent pathways and calibrates the abundance of telomere maintenance factors. *Molecular Biology of the Cell*, *34*(1). https://doi.org/10.1091/mbc.E22-06-0213

Kahney, E. W., Snedeker, J. C., & Chen, X. (2019). Regulation of Drosophila germline stem cells. *Current Opinion in Cell Biology*, *60*, 27–35. https://doi.org/10.1016/j.ceb.2019.03.008

Kawaguchi, S., Isshiki, W., & Kai, T. (2025). Factories without walls: The molecular architecture and functions of non-membrane organelles in small RNA-guided genome protection. *Biochimica et Biophysica Acta (BBA) - General Subjects*, *1869*(7), 130811. https://doi.org/10.1016/j.bbagen.2025.130811

Kawaguchi, S., Xu, X., Soga, T., Yamaguchi, K., Kawasaki, R., Shimouchi, R., Date, S., & Kai, T. (2025). In silico screening by AlphaFold2 program revealed the potential binding partners of nuage-localizing proteins and piRNA-related proteins. *ELife*, *13*. https://doi.org/10.7554/eLife.101967.2

Kazazian, H. H. (2004). Mobile Elements: Drivers of Genome Evolution. *Science*, *303*(5664), 1626–1632. https://doi.org/10.1126/science.1089670

Ketosugbo, K. F., Bushnell, H. L., & Johnson, R. I. (2017). A screen for E3 ubiquitination ligases that genetically interact with the adaptor protein Cindr during Drosophila eye patterning. *PLOS ONE*, *12*(11), e0187571. https://doi.org/10.1371/journal.pone.0187571

Kirino, Y., Vourekas, A., Sayed, N., de Lima Alves, F., Thomson, T., Lasko, P., Rappsilber, J., Jongens, T. A., & Mourelatos, Z. (2010). Arginine methylation of

Aubergine mediates Tudor binding and germ plasm localization. *RNA*, *16*(1), 70–78. https://doi.org/10.1261/rna.1869710

Klattenhoff, C., Xi, H., Li, C., Lee, S., Xu, J., Khurana, J. S., Zhang, F., Schultz, N., Koppetsch, B. S., Nowosielska, A., Seitz, H., Zamore, P. D., Weng, Z., & Theurkauf, W. E. (2009). The Drosophila HP1 Homolog Rhino Is Required for Transposon Silencing and piRNA Production by Dual-Strand Clusters. *Cell*, *138*(6), 1137–1149. https://doi.org/10.1016/j.cell.2009.07.014

Kneuss, E., Munafò, M., Eastwood, E. L., Deumer, U.-S., Preall, J. B., Hannon, G. J., & Czech, B. (2019). Specialization of the *Drosophila* nuclear export family protein Nxf3 for piRNA precursor export. *Genes & Development*, *33*(17–18), 1208–1220. https://doi.org/10.1101/gad.328690.119

Koch, R., Ledermann, R., Urwyler, O., Heller, M., & Suter, B. (2009). Systematic Functional Analysis of Bicaudal-D Serine Phosphorylation and Intragenic Suppression of a Female Sterile Allele of BicD. *PLoS ONE*, *4*(2), e4552. https://doi.org/10.1371/journal.pone.0004552

Koga, Y., Hirakata, S., Negishi, M., Yamazaki, H., Fujisawa, T., & Siomi, M. C. (2024). Dipteran-specific Daedalus controls Zucchini endonucleolysis in piRNA biogenesis independent of exonucleases. *Cell Reports*, *43*(11), 114923. https://doi.org/10.1016/j.celrep.2024.114923

Komander, D., & Rape, M. (2012). The Ubiquitin Code. *Annual Review of Biochemistry*, *81*(1), 203–229. https://doi.org/10.1146/annurev-biochem-060310-170328

Le Thomas, A., Rogers, A. K., Webster, A., Marinov, G. K., Liao, S. E., Perkins, E. M., Hur, J. K., Aravin, A. A., & Tóth, K. F. (2013). Piwi induces piRNA-guided transcriptional silencing and establishment of a repressive chromatin state. *Genes & Development*, *27*(4), 390–399. https://doi.org/10.1101/gad.209841.112

Li, C., Vagin, V. V., Lee, S., Xu, J., Ma, S., Xi, H., Seitz, H., Horwich, M. D., Syrzycka, M., Honda, B. M., Kittler, E. L. W., Zapp, M. L., Klattenhoff, C., Schulz, N., Theurkauf, W. E., Weng, Z., & Zamore, P. D. (2009). Collapse of Germline piRNAs in the Absence of Argonaute3 Reveals Somatic piRNAs in Flies. *Cell*, *137*(3), 509–521. https://doi.org/10.1016/j.cell.2009.04.027

Li, X. Z., Roy, C. K., Dong, X., Bolcun-Filas, E., Wang, J., Han, B. W., Xu, J., Moore, M. J., Schimenti, J. C., Weng, Z., & Zamore, P. D. (2013). An Ancient Transcription Factor Initiates the Burst of piRNA Production during Early Meiosis in Mouse Testes. *Molecular Cell*, *50*(1), 67–81. https://doi.org/10.1016/j.molcel.2013.02.016

Lim, A. K., & Kai, T. (2007). Unique germ-line organelle, nuage, functions to repress selfish genetic elements in *Drosophila melanogaster*. *Proceedings of the National Academy of Sciences*, *104*(16), 6714–6719. https://doi.org/10.1073/pnas.0701920104

Lim, L.-X., Isshiki, W., Iki, T., Kawaguchi, S., & Kai, T. (2022). The Tudor Domain-Containing Protein, Kotsubu (CG9925), Localizes to the Nuage and Functions in piRNA Biogenesis in D. melanogaster. *Frontiers in Molecular Biosciences*, *9*(818302), 1–15. https://doi.org/10.3389/fmolb.2022.818302

Lin, Y., Suyama, R., Kawaguchi, S., Iki, T., & Kai, T. (2023). Tejas functions as a core component in nuage assembly and precursor processing in *Drosophila* piRNA biogenesis. *Journal of Cell Biology*, *222*(10). https://doi.org/10.1083/jcb.202303125

Liu, L., Qi, H., Wang, J., & Lin, H. (2011). PAPI, a novel TUDOR-domain protein, complexes with AGO3, ME31B and TRAL in the nuage to silence transposition. *Development*, *138*(9), 1863–1873. https://doi.org/10.1242/dev.059287

Liu, N., Dansereau, D. A., & Lasko, P. (2003). Fat Facets Interacts with Vasa in the Drosophila Pole Plasm and Protects It from Degradation. *Current Biology*, *13*(21), 1905–1909. https://doi.org/10.1016/j.cub.2003.10.026

Lomoschitz, A., Meyer, J., Guitart, T., Krepl, M., Lapouge, K., Hayn, C., Schweimer, K., Simon, B., Šponer, J., Gebauer, F., & Hennig, J. (2025). The Drosophila RNA binding protein Hrp48 binds a specific RNA sequence of the msl-2 mRNA 3' UTR to regulate translation. *Biophysical Chemistry*, *316*, 107346. https://doi.org/10.1016/j.bpc.2024.107346

Lorenz, D. R., Mikheyeva, I. V., Johansen, P., Meyer, L., Berg, A., Grewal, S. I. S., & Cam, H. P. (2012). CENP-B Cooperates with Set1 in Bidirectional Transcriptional Silencing and Genome Organization of Retrotransposons. *Molecular and Cellular Biology*, *32*(20), 4215–4225. https://doi.org/10.1128/MCB.00395-12

Ma, X., Zhu, X., Han, Y., Story, B., Do, T., Song, X., Wang, S., Zhang, Y., Blanchette, M., Gogol, M., Hall, K., Peak, A., Anoja, P., & Xie, T. (2017). Aubergine Controls Germline Stem Cell Self-Renewal and Progeny Differentiation via Distinct Mechanisms. *Developmental Cell*, *41*(2), 157-169.e5. https://doi.org/10.1016/j.devcel.2017.03.023

Malone, C. D., Brennecke, J., Dus, M., Stark, A., McCombie, W. R., Sachidanandam, R., & Hannon, G. J. (2009). Specialized piRNA Pathways Act in Germline and Somatic Tissues of the Drosophila Ovary. *Cell*, *137*(3), 522–535. https://doi.org/10.1016/j.cell.2009.03.040

McKearin, D. M., & Spradling, A. C. (1990). bag-of-marbles: a Drosophila gene required to initiate both male and female gametogenesis. *Genes & Development*, *4*(12b), 2242–2251. https://doi.org/10.1101/gad.4.12b.2242

Meroni, G., & Diez-Roux, G. (2005). TRIM/RBCC, a novel class of 'single protein RING finger' E3 ubiquitin ligases. *BioEssays*, *27*(11), 1147–1157. https://doi.org/10.1002/bies.20304

Metzger, M. B., Hristova, V. A., & Weissman, A. M. (2012). HECT and RING finger families of E3 ubiquitin ligases at a glance. *Journal of Cell Science*, *125*(3), 531–537. https://doi.org/10.1242/jcs.091777

Miller, T., Krogan, N. J., Dover, J., Erdjument-Bromage, H., Tempst, P., Johnston, M., Greenblatt, J. F., & Shilatifard, A. (2001). COMPASS: a complex of proteins associated with a trithorax-related SET domain protein. *Proceedings of the National Academy of Sciences of the United States of America*, *98*(23), 12902–12907. https://doi.org/10.1073/pnas.231473398

Mohan, M., Herz, H.-M., Smith, E. R., Zhang, Y., Jackson, J., Washburn, M. P., Florens, L., Eissenberg, J. C., & Shilatifard, A. (2011). The COMPASS Family of H3K4 Methylases in Drosophila. *Molecular and Cellular Biology*, *31*(21), 4310–4318. https://doi.org/10.1128/MCB.06092-11

Mohn, F., Handler, D., & Brennecke, J. (2015). piRNA-guided slicing specifies transcripts for Zucchini-dependent, phased piRNA biogenesis. *Science*, *348*(6236), 812–817. https://doi.org/10.1126/science.aaa1039

Mohn, F., Sienski, G., Handler, D., & Brennecke, J. (2014). The Rhino-Deadlock-Cutoff Complex Licenses Noncanonical Transcription of Dual-Strand piRNA Clusters in Drosophila. *Cell*, *157*(6), 1364–1379. https://doi.org/10.1016/j.cell.2014.04.031

Muerdter, F., Guzzardo, P. M., Gillis, J., Luo, Y., Yu, Y., Chen, C., Fekete, R., & Hannon, G. J. (2013). A Genome-wide RNAi Screen Draws a Genetic Framework for Transposon Control and Primary piRNA Biogenesis in Drosophila. *Molecular Cell*, *50*(5), 736–748. https://doi.org/10.1016/j.molcel.2013.04.006

Munafò, M., Manelli, V., Falconio, F. A., Sawle, A., Kneuss, E., Eastwood, E. L., Seah, J. W. E., Czech, B., & Hannon, G. J. (2019). Daedalus and Gasz recruit Armitage to mitochondria, bringing piRNA precursors to the biogenesis machinery. *Genes & Development*, *33*(13–14), 844–856. https://doi.org/10.1101/gad.325662.119

Murano, K., Iwasaki, Y. W., Ishizu, H., Mashiko, A., Shibuya, A., Kondo, S., Adachi, S., Suzuki, S., Saito, K., Natsume, T., Siomi, M. C., & Siomi, H. (2019). Nuclear RNA export factor variant initiates piRNA-guided co-transcriptional silencing. *The EMBO Journal*, *38*(17). https://doi.org/10.15252/embj.2019102870

Murota, Y., Ishizu, H., Nakagawa, S., Iwasaki, Y. W., Shibata, S., Kamatani, M. K., Saito, K., Okano, H., Siomi, H., & Siomi, M. C. (2014). Yb Integrates piRNA Intermediates and Processing Factors into Perinuclear Bodies to Enhance piRISC Assembly. *Cell Reports*, *8*(1), 103–113. https://doi.org/10.1016/j.celrep.2014.05.043

Nakasone, M. A., Buetow, L., Gabrielsen, M., Ahmed, S. F., Majorek, K. A., Sibbet, G. J., Smith, B. O., & Huang, D. T. (2025). Tuning ubiquitin transfer by RING E3 ubiquitin ligases through the linchpin residue. *Life Science Alliance*, *8*(10), e202503394. https://doi.org/10.26508/lsa.202503394

Nezis, I., Stravopodis, D., Papassideri, I., Robert-Nicoud, M., & Margaritis, L. (2002). Dynamics of apoptosis in the ovarian follicle cells during the late stages of Drosophila oogenesis. *Cell and Tissue Research*, *307*(3), 401–409. https://doi.org/10.1007/s00441-001-0498-3

Ninova, M., Chen, Y.-C. A., Godneeva, B., Rogers, A. K., Luo, Y., Fejes Tóth, K., & Aravin, A. A. (2020). Su(var)2-10 and the SUMO Pathway Link piRNA-Guided Target Recognition to Chromatin Silencing. *Molecular Cell*, *77*(3), 556-570.e6. https://doi.org/10.1016/j.molcel.2019.11.012

Ninova, M., Holmes, H., Lomenick, B., Fejes Tóth, K., & Aravin, A. A. (2023). Pervasive SUMOylation of heterochromatin and piRNA pathway proteins. *Cell Genomics*, *3*(7), 100329. https://doi.org/10.1016/j.xgen.2023.100329

Nishida, K. M., Okada, T. N., Kawamura, T., Mituyama, T., Kawamura, Y., Inagaki, S., Huang, H., Chen, D., Kodama, T., Siomi, H., & Siomi, M. C. (2009). Functional involvement of Tudor and dPRMT5 in the piRNA processing pathway in Drosophila germlines. *The EMBO Journal*, *28*(24), 3820–3831. https://doi.org/10.1038/emboj.2009.365

Nystul, T., & Spradling, A. (2007). An Epithelial Niche in the Drosophila Ovary Undergoes Long-Range Stem Cell Replacement. *Cell Stem Cell*, *1*(3), 277–285. https://doi.org/10.1016/j.stem.2007.07.009

Ohtani, H., Iwasaki, Y. W., Shibuya, A., Siomi, H., Siomi, M. C., & Saito, K. (2013). DmGTSF1 is necessary for Piwi–piRISC-mediated transcriptional transposon silencing in the *Drosophila* ovary. *Genes & Development*, *27*(15), 1656–1661. https://doi.org/10.1101/gad.221515.113

Onishi, R., Sato, K., Murano, K., Negishi, L., Siomi, H., & Siomi, M. C. (2020). Piwi suppresses transcription of Brahma-dependent transposons via Maelstrom in ovarian somatic cells. *Science Advances*, *6*(50). https://doi.org/10.1126/sciadv.aaz7420

Page, A. W., & Orr-Weaver, T. L. (1997). Activation of the Meiotic Divisions inDrosophilaOocytes. *Developmental Biology*, *183*(2), 195–207. https://doi.org/10.1006/dbio.1997.8506

Pan, J., Goodheart, M., Chuma, S., Nakatsuji, N., Page, D. C., & Wang, P. J. (2005). RNF17, a component of the mammalian germ cell nuage, is essential for spermiogenesis. *Development*, *132*(18), 4029–4039. https://doi.org/10.1242/dev.02003

Pane, A., Wehr, K., & Schüpbach, T. (2007). zucchini and squash Encode Two Putative Nucleases Required for rasiRNA Production in the Drosophila Germline. *Developmental Cell*, *12*(6), 851–862. https://doi.org/10.1016/j.devcel.2007.03.022

Pardue, M.-L., & DeBaryshe, P. G. (2011). Retrotransposons that maintain chromosome ends. *Proceedings of the National Academy of Sciences*, *108*(51), 20317–20324. https://doi.org/10.1073/pnas.1100278108

Patil, V. S., Anand, A., Chakrabarti, A., & Kai, T. (2014). The Tudor domain protein Tapas, a homolog of the vertebrate Tdrd7, functions in the piRNA pathway to regulate retrotransposons in germline of Drosophila melanogaster. *BMC Biology*, *12*(1), 61. https://doi.org/10.1186/s12915-014-0061-9

Patil, V. S., & Kai, T. (2010). Repression of Retroelements in Drosophila Germline via piRNA Pathway by the Tudor Domain Protein Tejas. *Current Biology*, *20*(8), 724–730. https://doi.org/10.1016/j.cub.2010.02.046

Pelisson, A., Sun Song, U., Prud'homme, N., Smith, P. A., Bucheton, A., & Corces, V. G. (1994). Gypsy transposition correlates with the production of a retroviral envelope-like protein under the tissue-specific control of the Drosophila flamenco gene. *EMBO Journal*, *13*(18), 4401–4411. https://doi.org/10.1002/J.1460-2075.1994.TB06760.X/METRICS

Pickart, C. M. (2001). Mechanisms Underlying Ubiquitination. *Annual Review of Biochemistry*, *70*(1), 503–533. https://doi.org/10.1146/annurev.biochem.70.1.503

Pruneda, J. N., Littlefield, P. J., Soss, S. E., Nordquist, K. A., Chazin, W. J., Brzovic, P. S., & Klevit, R. E. (2012). Structure of an E3:E2~Ub Complex Reveals an Allosteric Mechanism Shared among RING/U-box Ligases. *Molecular Cell*, *47*(6), 933–942. https://doi.org/10.1016/j.molcel.2012.07.001

Qi, H., Watanabe, T., Ku, H.-Y., Liu, N., Zhong, M., & Lin, H. (2011). The Yb Body, a Major Site for Piwi-associated RNA Biogenesis and a Gateway for Piwi Expression and Transport to the Nucleus in Somatic Cells. *Journal of Biological Chemistry*, *286*(5), 3789–3797. https://doi.org/10.1074/jbc.M110.193888

Radion, E., Ryazansky, S., Akulenko, N., Rozovsky, Y., Kwon, D., Morgunova, V., Olovnikov, I., & Kalmykova, A. (2017). Telomeric Retrotransposon HeT-A Contains a Bidirectional Promoter that Initiates Divergent Transcription of piRNA Precursors in Drosophila Germline. *Journal of Molecular Biology*, *429*(21), 3280–3289. https://doi.org/10.1016/j.jmb.2016.12.002

Rivera, A. J., Lee, J.-H. R., Gupta, S., Yang, L., Goel, R. K., Zaia, J., & Lau, N. C. (2025). Traffic Jam activates the Flamenco piRNA cluster locus and the Piwi pathway to ensure transposon silencing and Drosophila fertility. *Cell Reports*, *44*(4), 115354. https://doi.org/10.1016/j.celrep.2025.115354

Rørth, P. (1998). Gal4 in the Drosophila female germline. *Mechanisms of Development*, *78*(1–2), 113–118. https://doi.org/10.1016/S0925-4773(98)00157-9

Roux, K. J., Kim, D. I., Raida, M., & Burke, B. (2012). A promiscuous biotin ligase fusion protein identifies proximal and interacting proteins in mammalian cells. *Journal of Cell Biology*, *196*(6), 801–810. https://doi.org/10.1083/jcb.201112098

Saito, K., Ishizu, H., Komai, M., Kotani, H., Kawamura, Y., Nishida, K. M., Siomi, H., & Siomi, M. C. (2010). Roles for the Yb body components Armitage and Yb in primary piRNA biogenesis in *Drosophila*. *Genes & Development*, *24*(22), 2493–2498. https://doi.org/10.1101/gad.1989510

Saito, K., Nishida, K. M., Mori, T., Kawamura, Y., Miyoshi, K., Nagami, T., Siomi, H., & Siomi, M. C. (2006). Specific association of Piwi with rasiRNAs derived from retrotransposon and heterochromatic regions in the *Drosophila* genome. *Genes & Development*, *20*(16), 2214–2222. https://doi.org/10.1101/gad.1454806

Saito, K., Sakaguchi, Y., Suzuki, T., Suzuki, T., Siomi, H., & Siomi, M. C. (2007). Pimet, the *Drosophila* homolog of HEN1, mediates 2′- *O* -methylation of Piwi-interacting RNAs at their 3′ ends. *Genes & Development*, *21*(13), 1603–1608. https://doi.org/10.1101/gad.1563607

Sato, K., Iwasaki, Y. W., Shibuya, A., Carninci, P., Tsuchizawa, Y., Ishizu, H., Siomi, M. C., & Siomi, H. (2015). Krimper Enforces an Antisense Bias on piRNA Pools by Binding AGO3 in the Drosophila Germline. *Molecular Cell*, *59*(4), 553–563. https://doi.org/10.1016/j.molcel.2015.06.024

Schrader, L., & Schmitz, J. (2019). The impact of transposable elements in adaptive evolution. *Molecular Ecology*, *28*(6), 1537–1549. https://doi.org/10.1111/mec.14794

Shilatifard, A. (2012). The COMPASS Family of Histone H3K4 Methylases: Mechanisms of Regulation in Development and Disease Pathogenesis. *Annual*

*Review of Biochemistry*, *81*(1), 65–95. https://doi.org/10.1146/annurev-biochem-051710-134100

Shpiz, S., Olovnikov, I., Sergeeva, A., Lavrov, S., Abramov, Y., Savitsky, M., & Kalmykova, A. (2011). Mechanism of the piRNA-mediated silencing of Drosophila telomeric retrotransposons. *Nucleic Acids Research*, *39*(20), 8703–8711. https://doi.org/10.1093/nar/gkr552

Sienski, G., Batki, J., Senti, K.-A., Dönertas, D., Tirian, L., Meixner, K., & Brennecke, J. (2015). Silencio/CG9754 connects the Piwi–piRNA complex to the cellular heterochromatin machinery. *Genes & Development*, *29*(21), 2258–2271. https://doi.org/10.1101/gad.271908.115

Sienski, G., Dönertas, D., & Brennecke, J. (2012). Transcriptional Silencing of Transposons by Piwi and Maelstrom and Its Impact on Chromatin State and Gene Expression. *Cell*, *151*(5), 964–980. https://doi.org/10.1016/j.cell.2012.10.040

Spratt, D. E., Walden, H., & Shaw, G. S. (2014). RBR E3 ubiquitin ligases: new structures, new insights, new questions. *Biochemical Journal*, *458*(3), 421–437. https://doi.org/10.1042/BJ20140006

Stein, C. B., Genzor, P., Mitra, S., Elchert, A. R., Ipsaro, J. J., Benner, L., Sobti, S., Su, Y., Hammell, M., Joshua-Tor, L., & Haase, A. D. (2019). Decoding the 5′ nucleotide bias of PIWI-interacting RNAs. *Nature Communications*, *10*(1), 828. https://doi.org/10.1038/s41467-019-08803-z

Sugeedha, J., Gautam, J., & Tyagi, S. (2021). SET1/MLL family of proteins: functions beyond histone methylation. *Epigenetics*, *16*(5), 469–487. https://doi.org/10.1080/15592294.2020.1809873

Swatek, K. N., & Komander, D. (2016). Ubiquitin modifications. *Cell Research 2016 26:4*, *26*(4), 399–422. https://doi.org/10.1038/cr.2016.39

Szakmary, A., Reedy, M., Qi, H., & Lin, H. (2009). The Yb protein defines a novel organelle and regulates male germline stem cell self-renewal in *Drosophila melanogaster*. *Journal of Cell Biology*, *185*(4), 613–627. https://doi.org/10.1083/jcb.200903034

Teixeira, F. K., Okuniewska, M., Malone, C. D., Coux, R.-X., Rio, D. C., & Lehmann, R. (2017). piRNA-mediated regulation of transposon alternative splicing in the soma and germ line. *Nature*, *552*(7684), 268–272. https://doi.org/10.1038/nature25018

Theurkauf, W. E., & Hazelrigg, T. I. (1998). In vivo analyses of cytoplasmic transport and cytoskeletal organization during *Drosophila* oogenesis: characterization of a

multi-step anterior localization pathway. *Development*, *125*(18), 3655–3666. https://doi.org/10.1242/dev.125.18.3655

Touret, F., Guiguen, F., Greenland, T., & Terzian, C. (2014). In between: Gypsy in Drosophila melanogaster Reveals New Insights into Endogenous Retrovirus Evolution. *Viruses*, *6*(12), 4914–4925. https://doi.org/10.3390/v6124914

Vagin, V. V., Yu, Y., Jankowska, A., Luo, Y., Wasik, K. A., Malone, C. D., Harrison, E., Rosebrock, A., Wakimoto, B. T., Fagegaltier, D., Muerdter, F., & Hannon, G. J. (2013). Minotaur is critical for primary piRNA biogenesis. *RNA*, *19*(8), 1064–1077. https://doi.org/10.1261/rna.039669.113

van Lopik, J., Alizada, A., Trapotsi, M. A., Hannon, G. J., Bornelöv, S., & Czech Nicholson, B. (2023). Unistrand piRNA clusters are an evolutionarily conserved mechanism to suppress endogenous retroviruses across the Drosophila genus. *Nature Communications 2023 14:1*, *14*(1), 7337-. https://doi.org/10.1038/s41467-023-42787-1

Vidaurre, V., Song, A., Li, T., Ku, W. L., Zhao, K., Qian, J., & Chen, X. (2024). The *Drosophila* histone methyltransferase SET1 coordinates multiple signaling pathways in regulating male germline stem cell maintenance and differentiation. *Development*, *151*(15). https://doi.org/10.1242/dev.202729

Villasante, A., Abad, J. P., Planelló, R., Méndez-Lago, M., Celniker, S. E., & de Pablos, B. (2007). *Drosophila* telomeric retrotransposons derived from an ancestral element that was recruited to replace telomerase. *Genome Research*, *17*(12), 1909–1918. https://doi.org/10.1101/gr.6365107

Von Stetina, J. R., & Orr-Weaver, T. L. (2011). Developmental Control of Oocyte Maturation and Egg Activation in Metazoan Models. *Cold Spring Harbor Perspectives in Biology*, *3*(10), a005553–a005553. https://doi.org/10.1101/cshperspect.a005553

Wagner, J. M., Roganowicz, M. D., Skorupka, K., Alam, S. L., Christensen, D., Doss, G., Wan, Y., Frank, G. A., Ganser-Pornillos, B. K., Sundquist, W. I., & Pornillos, O. (2016). Mechanism of B-box 2 domain-mediated higher-order assembly of the retroviral restriction factor TRIM5α. *ELife*, *5*(e16309). https://doi.org/10.7554/eLife.16309

Wang, H., Ma, Z., Niu, K., Xiao, Y., Wu, X., Pan, C., Zhao, Y., Wang, K., Zhang, Y., & Liu, N. (2015). Antagonistic roles between Nibbler and Hen1 modulate piRNA 3' ends in *Drosophila*. *Development*, *143*(3), 530–539. https://doi.org/10.1242/dev.128116

Wang, L., Dou, K., Moon, S., Tan, F. J., & Zhang, Z. Z. (2018). Hijacking Oogenesis Enables Massive Propagation of LINE and Retroviral Transposons. *Cell*, *174*(5), 1082-1094.e12. https://doi.org/10.1016/j.cell.2018.06.040

Wang, W., Han, B. W., Tipping, C., Ge, D. T., Zhang, Z., Weng, Z., & Zamore, P. D. (2015). Slicing and Binding by Ago3 or Aub Trigger Piwi-Bound piRNA Production by Distinct Mechanisms. *Molecular Cell*, *59*(5), 819–830. https://doi.org/10.1016/j.molcel.2015.08.007

Wang, X., Ramat, A., Simonelig, M., & Liu, M.-F. (2023). Emerging roles and functional mechanisms of PIWI-interacting RNAs. *Nature Reviews Molecular Cell Biology*, *24*(2), 123–141. https://doi.org/10.1038/s41580-022-00528-0

Wang, Y., Argiles-Castillo, D., Kane, E. I., Zhou, A., & Spratt, D. E. (2020). HECT E3 ubiquitin ligases – emerging insights into their biological roles and disease relevance. *Journal of Cell Science*, *133*(7). https://doi.org/10.1242/jcs.228072

Wasik, K. A., Tam, O. H., Knott, S. R., Falciatori, I., Hammell, M., Vagin, V. V., & Hannon, G. J. (2015). RNF17 blocks promiscuous activity of PIWI proteins in mouse testes. *Genes & Development*, *29*(13), 1403–1415. https://doi.org/10.1101/gad.265215.115

Watanabe, M., Saeki, Y., Takahashi, H., Ohtake, F., Yoshida, Y., Kasuga, Y., Kondo, T., Yaguchi, H., Suzuki, M., Ishida, H., Tanaka, K., & Hatakeyama, S. (2020). A substrate-trapping strategy to find E3 ubiquitin ligase substrates identifies Parkin and TRIM28 targets. *Communications Biology*, *3*(1), 592. https://doi.org/10.1038/s42003-020-01328-y

Webster, A., Li, S., Hur, J. K., Wachsmuth, M., Bois, J. S., Perkins, E. M., Patel, D. J., & Aravin, A. A. (2015). Aub and Ago3 Are Recruited to Nuage through Two Mechanisms to Form a Ping-Pong Complex Assembled by Krimper. *Molecular Cell*, *59*(4), 564–575. https://doi.org/10.1016/j.molcel.2015.07.017

Xie, T., & Spradling, A. C. (2000). A Niche Maintaining Germ Line Stem Cells in the *Drosophila* Ovary. *Science*, *290*(5490), 328–330. https://doi.org/10.1126/science.290.5490.328

Xiol, J., Spinelli, P., Laussmann, M. A., Homolka, D., Yang, Z., Cora, E., Couté, Y., Conn, S., Kadlec, J., Sachidanandam, R., Kaksonen, M., Cusack, S., Ephrussi, A., & Pillai, R. S. (2014). RNA Clamping by Vasa Assembles a piRNA Amplifier Complex on Transposon Transcripts. *Cell*, *157*(7), 1698–1711. https://doi.org/10.1016/j.cell.2014.05.018

Yamaguchi, S., Oe, A., Nishida, K. M., Yamashita, K., Kajiya, A., Hirano, S., Matsumoto, N., Dohmae, N., Ishitani, R., Saito, K., Siomi, H., Nishimasu, H.,

Siomi, M. C., & Nureki, O. (2020). Crystal structure of Drosophila Piwi. *Nature Communications*, *11*(1), 858. https://doi.org/10.1038/s41467-020-14687-1

Yano, T., de Quinto, S. L., Matsui, Y., Shevchenko, A., Shevchenko, A., & Ephrussi, A. (2004). Hrp48, a Drosophila hnRNPA/B Homolog, Binds and Regulates Translation of oskar mRNA. *Developmental Cell*, *6*(5), 637–648. https://doi.org/10.1016/S1534-5807(04)00132-7

Yashiro, R., Murota, Y., Nishida, K. M., Yamashiro, H., Fujii, K., Ogai, A., Yamanaka, S., Negishi, L., Siomi, H., & Siomi, M. C. (2018). Piwi Nuclear Localization and Its Regulatory Mechanism in Drosophila Ovarian Somatic Cells. *Cell Reports*, *23*(12), 3647–3657. https://doi.org/10.1016/j.celrep.2018.05.051

Yoshida, Y., Saeki, Y., Murakami, A., Kawawaki, J., Tsuchiya, H., Yoshihara, H., Shindo, M., & Tanaka, K. (2015). A comprehensive method for detecting ubiquitinated substrates using TR-TUBE. *Proceedings of the National Academy of Sciences*, *112*(15), 4630–4635. https://doi.org/10.1073/pnas.1422313112

Yu, H., & Lesch, B. J. (2024). Functional Roles of H3K4 Methylation in Transcriptional Regulation. *Molecular and Cellular Biology*, *44*(11), 505–515. https://doi.org/10.1080/10985549.2024.2388254

Yu, Y., Gu, J., Jin, Y., Luo, Y., Preall, J. B., Ma, J., Czech, B., & Hannon, G. J. (2015). Panoramix enforces piRNA-dependent cotranscriptional silencing. *Science*, *350*(6258), 339–342. https://doi.org/10.1126/science.aab0700

Zhang, Y., Liu, W., Li, R., Gu, J., Wu, P., Peng, C., Ma, J., Wu, L., Yu, Y., & Huang, Y. (2018). Structural insights into the sequence-specific recognition of Piwi by *Drosophila* Papi. *Proceedings of the National Academy of Sciences*, *115*(13), 3374–3379. https://doi.org/10.1073/pnas.1717116115

Zhang, Z., Xu, J., Koppetsch, B. S., Wang, J., Tipping, C., Ma, S., Weng, Z., Theurkauf, W. E., & Zamore, P. D. (2011). Heterotypic piRNA Ping-Pong Requires Qin, a Protein with Both E3 Ligase and Tudor Domains. *Molecular Cell*, *44*(4), 572–584. https://doi.org/10.1016/j.molcel.2011.10.011

Zhao, K., Cheng, S., Miao, N., Xu, P., Lu, X., Zhang, Y., Wang, M., Ouyang, X., Yuan, X., Liu, W., Lu, X., Zhou, P., Gu, J., Zhang, Y., Qiu, D., Jin, Z., Su, C., Peng, C., Wang, J.-H., … Yu, Y. (2019). A Pandas complex adapted for piRNA-guided transcriptional silencing and heterochromatin formation. *Nature Cell Biology*, *21*(10), 1261–1272. https://doi.org/10.1038/s41556-019-0396-0

Zhou, Y., Zhou, B., Pache, L., Chang, M., Khodabakhshi, A. H., Tanaseichuk, O., Benner, C., & Chanda, S. K. (2019). Metascape provides a biologist-oriented

resource for the analysis of systems-level datasets. *Nature Communications*, *10*(1), 1523. https://doi.org/10.1038/s41467-019-09234-6

# 5. Publication and Contributions

**Publication**

1. Isshiki, W., Kozuka-Hata, H., Oyama, M., Kai, T. and Iki, T. Germline PIWI proximity proteome reveals the cooperative actions of Set1 and Piwi in piRNA-directed silencing of telomeric transposons in *Drosophila*. (Submitting)

2. Lim, L.-X., Isshiki, W., Iki, T., Kawaguchi, S., & Kai, T. (2022). The Tudor Domain-Containing Protein, Kotsubu (CG9925), Localizes to the Nuage and Functions in piRNA Biogenesis in D. melanogaster. *Frontiers in Molecular Biosciences*, 9(818302), 1–15.

3. Kawaguchi, S., Isshiki, W., Kai, T. (2025). Factories without walls: The molecular architecture and functions of non-membrane organelles in small RNA-guided genome protection, *Biochimica et Biophysica Acta (BBA) - General Subjects* 1869 130811.

**Conference presentation**

BioID-based biochemical screening and functional analysis of novel factors involved in piRNA-mediated transposon regulation in *Drosophila melanogaste*r. (1AS-10-03, oral) The 46th Annual Meeting of the Molecular Biology Society of Japan. December 6 - 8, 2023.